GRAVITY AND GEOLOGICAL INVESTIGATIONS OVER THE ZARANDA YOUNGER GRANITE RING COMPLEX OF NORTHERN NIGERIA

by

Kalu Kalu Ibe, B.Sc.(UNN)

Thesis submitted in partial fulfilment of the requirements for the award of the degree of Master of Science, Applied Geophysics.

Department of Physics
Ahmadu Bello University
Zaria

October, 1982

ABSTRACT

Gravity and geological investigations were carried out over the Zaranda hill situated on the Bauchi Sheet (sheet 149 NW) and located between latitudes 10° 9-20' N and 10° 25.00' N and between longitudes 9° 26.00' E and 9° 45.00' E. The investigations were aimed at a detailed analysis of a magnetic low centred on the area on the aeromagnetic total magnetic intensity map of the Bauchi area.

Petrographic, density, structural and chemical analysis based on X-ray fluorescopy were carried out on the samples in addition to field measurements. These analysis show that:

(a) The major structural trend of the units in the complex is NNE - SSW and these dip steeply with values ranging from 75° to 90°.

(b) There are at least five major rock types in the survey area and the Zaranda complex has four recognizable units which intruded the Precambrian crystalline basement made up of gneisses and migmatites. These are:

(i) the precaldera trachyte

(ii) the faylite-bearing hornblende syenite

(iii) the porphyritic granite; and

(iv) basic rocks of intermediate group with some extrusives

In addition, widespread occurrences of muscovite-biotite older granite were observed in the vicinity of the complex. The units are emplaced in a ring-like structure with the older precaldera trachyte at the core and the syenite and granite porphyry emplaced later. The basic rocks form the outermost ring and are emplaced at some distance from the other units.

Analysis of the gravity data shows that Bouguer anomalies ranging from -433 g.u. to - 6l3g.u. with predominant NNE - SSW trending axes lie in the area and that over the complex a residual anomaly of the range from -20 to -106 g.u, exist. The main residual anomaly of -106 g.u. trending NNE - SSW is flanked by relatively positive residual anomalies ranging from -10 to 52 g.u. on the eastern, southern and southwestern margins.

Interpretation of the gravity anomalies using two and three-dimensional models indicate that the Zaranda complex is a tabular 6yenitic body which extends to a depth of about 5.5 km with a central mass of trachytic rock extending to a depth of about 2.5 km. The positive anomalies forming a ring structure were modelled as shallow tabular basic intrusions.

The gravity and geological investigations correlate well. The low gravity anomalies correspond to areas underlain by acid rocks while those areas underlain by the basic rocks have positive anomalies.

The ring-like structure of the Zaranda complex and the emplacement of the basic dykes gave rise to the existence of natural aquifers which could further be investigated. Occurrences of kaolinite pits were found in small amounts, but the existence of large occurrence could also be investigated.

DECLARATION

The work "Gravity and Geological Investigation over the Zaranda Younger granite complex of Northern Nigeria" is the original work of the author. It has not been submitted to any other institution, organization or bodies for any award other than to the Ahmadu Bello University, Zaria, Nigeria.

K.K. Ibe

Dr S.B. Ojo

Prof. D.E. Ajakaiye

DEDICATION

This work is dedicated to my late father, Nna Kalu Ibe Uwa whose last words still inspire me to the service of God and man; to my late brother Ikpo Kalu Ibe for his humility even at death; to my dear mother Madam Afo Kalu Ibe for her patience and love; to all earth scientists who pursue the noble aims of discovering God's blessings to man through the interpretation of nature's writings in rocks.

ACKNOWLEDGEMENTS

I wish to express my profound gratitude to the Head, Department of Physics, Ahmadu Bello University, Professor D.E. Ajakaiye, for her contribution towards the choice, organization and supervision throughout the duration of the project. Her follow-up in all stages of the work has been an immense inspiration source.

I also thank Dr. S.B. Ojo for his concern and kind supervision both before and after the field work. To Mr. S.E. Ananaba, Dr. M.B. Awad, Mr. I.B. Osasuwa, I say thanks for personal contributions made towards the successful completion of this project. Special thanks go to Dr. P.J. Verheijen and the Bauchi Survey Headquarters for their kind provision of benchmarks and their descriptions.

The Director, the Geological Surveys, Kaduna, Mr. Nehikhare, all friends and Technicians of the Surveys, Kaduna, all deserve thanks for their assistance. Mr. A. Ofodum of F.G.G.C Bauchi, provided accommodation during the fieldwork. I am also indebted to the Department of Earth Sciences of the University of Manitoba , the Chief Chemist, Mr. K. Kamlal, for permitting the use of their facilities for the analysis of samples. Professor A. Turnock gave useful suggestions regarding geology.

TABLE OF CONTENTS

		PAGE
TITLE		
ABSTRACT		ii
DECLARATION		iv
DEDICATION		v
ACKNOWLEDGEMENTS		vii
TABLE OF CONTENTS		viii
LIST OF FIGURES		x
LIST OF TABLES		xii
LIST OF PLATES		xiii
LIST OF APPENDICES		xiv
CHAPTER 1 - GENERAL REVIEW		1
1.1	Introduction	1
1.2	Previous Geophysical and Geological work	3
1.3	Location, Accessibility, Aim and Scope of present study	4
CHAPTER 2 - GEOLOGY		6
2.1	Introduction	6
2.2	General geology	6
2.3	Megascopic and petrographic study of rock units	9
2.3.1	Migmatitic gneiss	9
2.3.2	The older muscovite granite	12
2.3.3	Precaldera aphyric trachyte	12
2.3.4	Fayalite-bearing hornblende syenite	12
2.3.5	Granite porphyry	14
2.3.6	Late intrusive rocks	14
2.3.6.1	Introduction	14
2.3.6.2	Olivine basalt	15
2.3.6.3	The Zull dolerite	15
2.3.6.4	Zaranda calcitic basalt	16
2.3.7	The amphibolite	17
2.4	Chemical Analysis	17
2.4.1	Comparison with chemical results from other areas of the Younger Granite province	20
2.5	Structural geology	25
2.5.1	Folds	27
2.5.2	Joints	28
2.6	Hydrogeology	35
2.7	Economic geology	36

PAGE

2.8 Geological history 38

CHAPTER 3 - FIELD PROCEDURES AND INSTRUMENTATION 40

3.1 Bases for the gravity survey 40
3.2 Instrumentation 41
3.3 Field procedure 44
3.4 Base station network 46
3.5 Height determination 49
3.6 Computation of gravity anomalies 50
3.7 Analysis of errors 52

CHAPTER 4 - DENSITY DETERMINATION 54

4.1 Introduction 54
4.2 Density measurements and results 55
4.3 Error in density determination 61

CHAPTER 5 - INTERPRETATION 64

5.1 The Bouguer gravity field 64
5.2 Regional anomaly separation 66
5.3 Residual gravity anomalies and qualitative interpretation 69
5.4 Quantitative interpretation of residual anomalies 72

5.4.1 Introduction 72
5.4.2 Two and three-dimensional models along interpreted profiles 73

5.5 Free-air and bouguer anomaly correlation 77
5.6 Mechanism of intrusion 81

CHAPTER SIX - SUMMARY AND DISCUSSION 86

6.1 Summary 86
6.2 Discussion 88
6.3 Recommendation 88

PLATE 1 92
PLATE 2 93
PLATE 3 94
PLATE 4 95
PLATE 5 96
PLATE 6 97
PLATE 7 98
PLATE 8 99
PLATE 9 100
APPENDIX I 101
APPENDIX II 103

PAGE

APPENDIX III..... 104

REFERENCES 109

LIST OF FIGURES

FIGURE		PAGE
1	Location maps of the survey area	2
2	Total magnetic field intensity map of the Zaranda area	5
3	Geological map of the Zaranda complex and the sections along the interpreted profiles	7
4	Topographic map of the Zaranda ring complex	8
5	A CF diagram of the almandine zone of amphibolite ..... facies of progressive regional metamorphism	10
6	Position of the migmatitic gneiss in the P-T diagram	11
7	Comparison between TiO_2 - SiO_2 plots for Zaranda basic rocks and those from adjoining volcanic areas	24
8	Generalized mineralogical composition of igneous rocks in relation to those of the Zaranda complex ...	26
9	Stereographic polar plots of major and minor joints on the migmatitic gneiss	30
10	Rose diagram of joints on the migmatitic gneiss	32
11	Rose diagram of major joints on the aphyric trachyte	33
12	Stereographic polar plots of joints on the aphyric trachyte	34
13	A schematic section of a suspected aquifer structure south of the complex	37
14	Drift curves for Worden gravimeter No 135	43
15	Base station network	48
16	Density histogram of rock types	58
17	Map of bouguer gravity anomaly	65
18	Map of regional gravity anomaly	68

FIGURE		PAGE
19	Map of residual gravity anomaly	70
20	Residual gravity anomaly and geological map of the Zaranda Younger Granite ring complex	71
21	A two-dimensional polygonal model of the Zaranda complex along Profile A-A^1 (SSW - NNE)	75
22	A three-dimensional cylindrical model of the Zaranda complex along Profile A-A^1 (SSW - NNE)	76
23	A two-dimensional polygonal model of the Zaranda complex along Profile B-B^1 (WNW - ESE)	78
24	A three-dimensional cylindrical model of the Zaranda complex along Profile B-B^1 (WNW - ESE)	79
25	A three-dimensional cylindrical model of the Zaranda complex along Profile C-C^1 (NW - SE)	80
26	Map of free-air anomaly of the Zaranda complex	82
27	Gravity anomalies and subsurface shapes compared with those of the Zaranda complex	84
28	Regional metal zoning in the Younger Granite province	90

LIST OF TABLES

TABLE		PAGE
1	Chemical report on rock types of the Zaranda complex	18
2	Comparison between chemical analysis of biotite and riebeckite granites of the Younger Granite province and the syenites of the Zaranda complex	21
3	Chemical relationship between Zaranda and Filiya trachytes	22
4	Comparison between chemical composition of the Nigerian basalts and those of the Zaranda complex	23
5	Joint readings from the host migmatitic gneiss	29
6	Frequency distribution of joints on the host migmatitic gneiss	31
7	Frequency distribution of major joints on the aphyric trachyte	31
8	Comparison between benchmark values and altimeter readings in height determination	47
9	Comparison of absolute gravity values with respect to Jos and Bauchi primary bases	47
10	Densities of rock types	57
11	Comparison between rock densities in the Younger Granite province and those of the Zaranda complex	59
12	Comparison of rocks of the Zaranda complex with those typical of the Younger Granite province	59

LIST OF PLATES

PLATE		PAGE
1	Photo-micrograph of the migmatitic gneiss	92
2	Photo-micrograph of the older granite	92
3	Photo-micrograph of the trachyte	94
4	Photo-micrograph of the syenite	95
5	Photo-micrograph of the syenite-basalt contact; southern base of the complex	96
6	Photo-micrograph of the olivine basalt	97
7	Photo-micrograph of the Zull dolerite	98
8	Photo-micrograph of the calcite-bearing basalt	99
9	Photo-micrograph of the amphibolitic rock included in the syenite unit	100

LIST OF APPENDICES

APPENDIX

I	Result of megascopic study of rock types .
II	Result of modal analysis of rock units .
III	Principal parameters of gravity stations .
IV	Sum of gravitational attraction of 15 cylinders (3 - D model along Profile A-A^1) .
V	Sum of gravitational attraction of 14 cylinders (3 - D model along Profile B-B^1) .
VI	Sum of gravitational attraction of 5 cylinders (3 - D model along Profile C-C^1) .

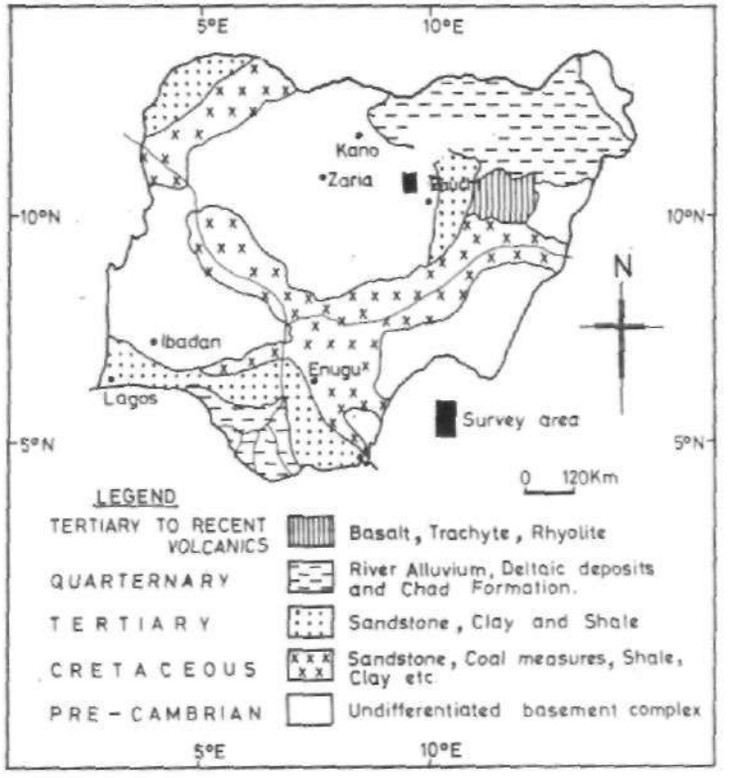
CHAPTER ONE - GENERAL REVIEW

1.1 INTRODUCTION

The Nigerian Younger Granite province (fig. 1) occupies an area of about 22,000 km^2, covers the greater portion of the central region of Northern Nigeria and pinches out into the Niger Republic. The region occupies an enviable position in the history of solid mineral exploration and exploitation. Cassiterite, columbite and a variety of other valuable minerals have been mined in the Jos area (fig. 1) for the past five decades. Minor occurrences of cassiteriteare known throughout the region.

The economic consideration is not the only driving force behind the much geophysical work in the area over the years. The peculiar mechanisms of intrusion of the various individual complexes which has been essentially that of ring-dyke formation, faulting and cauldron subsidence (Ajakaiye, 1974) have added much zeal to the determination by many workers to carry out more detailed investigation in the province.

Since the province, in general, consists of both exposed and buried individual complexes (Ajakaiye, 1981), it offers a lot of potential for more economic minerals yet undiscovered.



(a) Simplified Geological Map of Nigeria.



(b) Geological map of the distribution of the Younger granites of Nigeria.

(Adapted from Olade , 1978)

Fig 1 Location maps of the survey area

1.2 PREVIOUS GEOPHYSICAL AND GEOLOGICAL WORK

The Younger Granite province has, in comparison with other geological provinces of Nigeria, witnessed the greatest amount of geophysical and geological work. The Geological Survey of Nigeria (GSN), in the period 1974 - 1980, carried out airborne magnetic survey covering the whole of Nigeria. Other individuals, organizations and research groups have also contributed a lot in carrying out research in the region. Among these investigations are gravity surveys (Ajakaiye,1968, 1970, 1975, 1976), (Ajakaiye and Burke, 1973), (Ajakaiye and Sweeney, 1974), (Verheijen and Ajakaiye, 1980). Also recent work has been done on the magnetic interpretation of the aeromagnetic data in the region (Ajakaiye, 1981 personal communication).

Most of these geophysical investigations have been supplemented by detailed and systematic geological mapping. Such work includes (Okezie, 1964; Oyawoye, 1968; Turner, 1976; Wright, 1976; Bowden and Turner, 1974; Bowden et al, 1981).

1.3 LOCATION, ACCESSIBILITY, AIM AND SCOPE OF PRESENT STUDY

Most of the individual complexes have been located and although these are not exposed in the majority of cases, further investigations need to be carried out to locate them (Ajakaiye, 1981). Consequently, based on preliminary magnetic interpretation of the G.S.N. aeromagnetic data of 1974 - 1980 (Ajakaiye, 1981, fig. 1) several anomalies were identified. One of these anomalies lies over the Zaranda complex.

The aim of the present work is to carry out a more detailed combination of gravity and geological surveys over and around the Zaranda complex located on the total field aeromagnetic map as a prominent low (fig 2). The field work lasted from August, 1981 until March, 1982.

On the total field aeromagnetic map of Sheet 149 (Bauchi) of GSN and based on 1:100,000 scale, the anomaly occupies the southern portion of the NW quadrant. It is located west of Bauchi and in the eastern corner of the Nigerian Younger granite province (fig 1) and is the only prominent hill in the area which rises over 1,200m above sea level or about 770m above the surrounding landscape. The area investigated lies between latitudes 10° 9.20' N and 10° 25.00' N and between 9° 26.00' E and 9° 45' E. The outcrop of the complex occupies an area of about 100 km^2. The area is moderately accessible by motorable roads and paths run through the entire area (fig 3). On the extreme north of the area is the Ningi-Burra complex; on the east is the Bauchi complex and on the far west is the Kwandonkaya complex (fig 1).

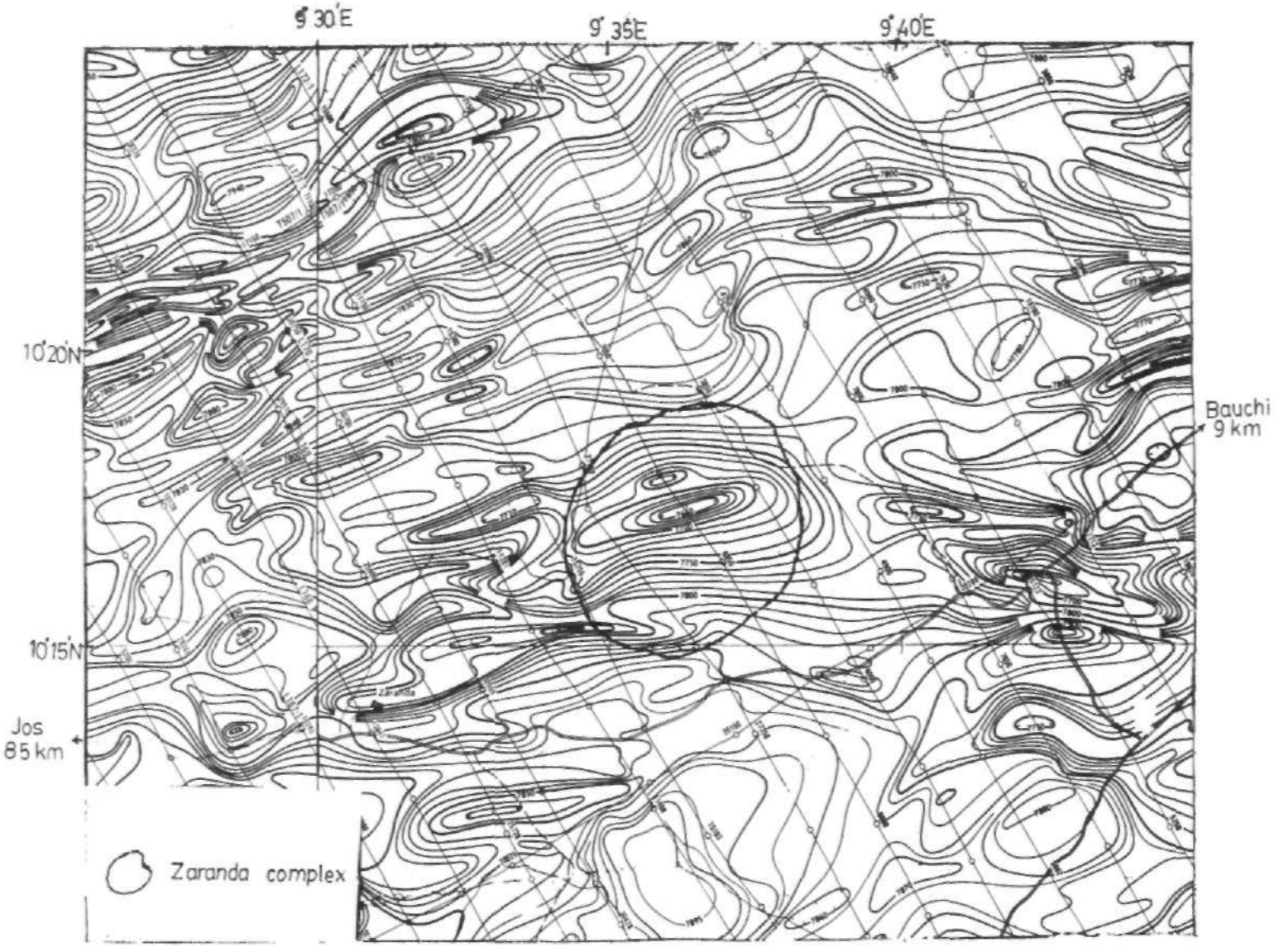


Fig 2 Total magnetic field intensity map of the Zaranda area.
(Adapted from G.S.N aeromagnetic map)

CHAPTER TWO

GEOLOGY

2.1 INTRODUCTION

Gravity anomalies are as a result of density contrast between anomalous bodies and their host rocks. Densities of rocks and other masses, in turn, depend on their chemical and mineralogical composition. This is the basis of the geological investigation.

The Zaranda Younger Granite complex occupies an area of about 100 km^2 and stands out as a topographic high north of Jos-Bauchi road (fig 4).

2.2 GENERAL GEOLOGY

Based on field appearance and density determination of the rock samples, the Zaranda complex is sub-divided into five rock units as shown in fig 3. These are the following, with unit (a) the oldest, and unit (e) the youngest and outermost:

(a) Precaldera aphyric trachyte

(b) Fayalite-bearing hornblende syenite

(c) Porphyritic granite

(d) Olivine basalt

(e) Dolerite

The central and flat top of the hill consists of aphyric trachyte. This is surrounded by the syenite. The syenite is, in turn, fringed on the northern and southern margins of the complex by the porphyritic granite. The complex is bordered on the eastern, western and southern sections by basic units (d) and (e), basalts and dolerites.

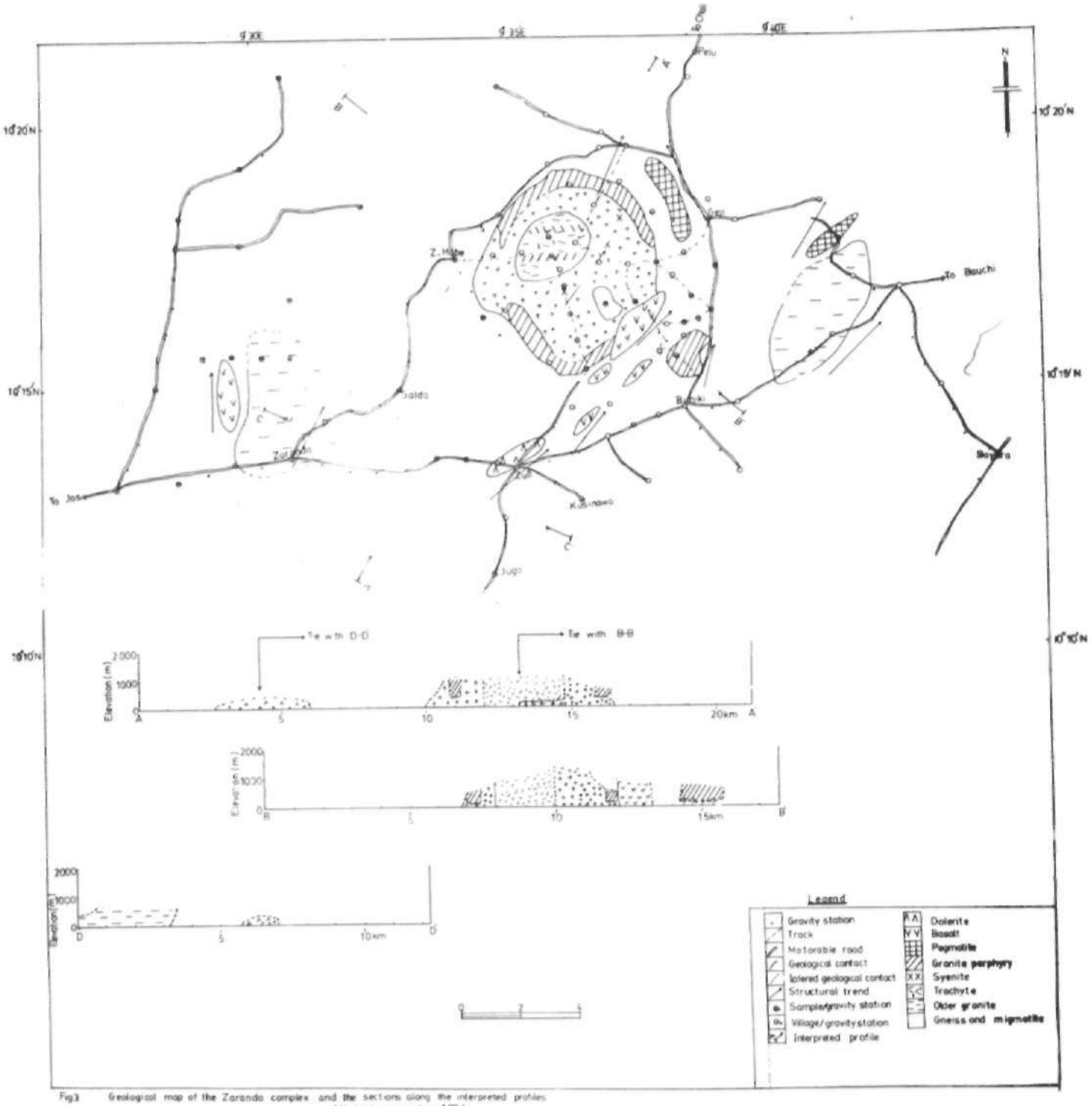


Fig3 Geological map of the Zarando complex and the sections along the interpreted profiles
(Vertical exergeration 1:00)

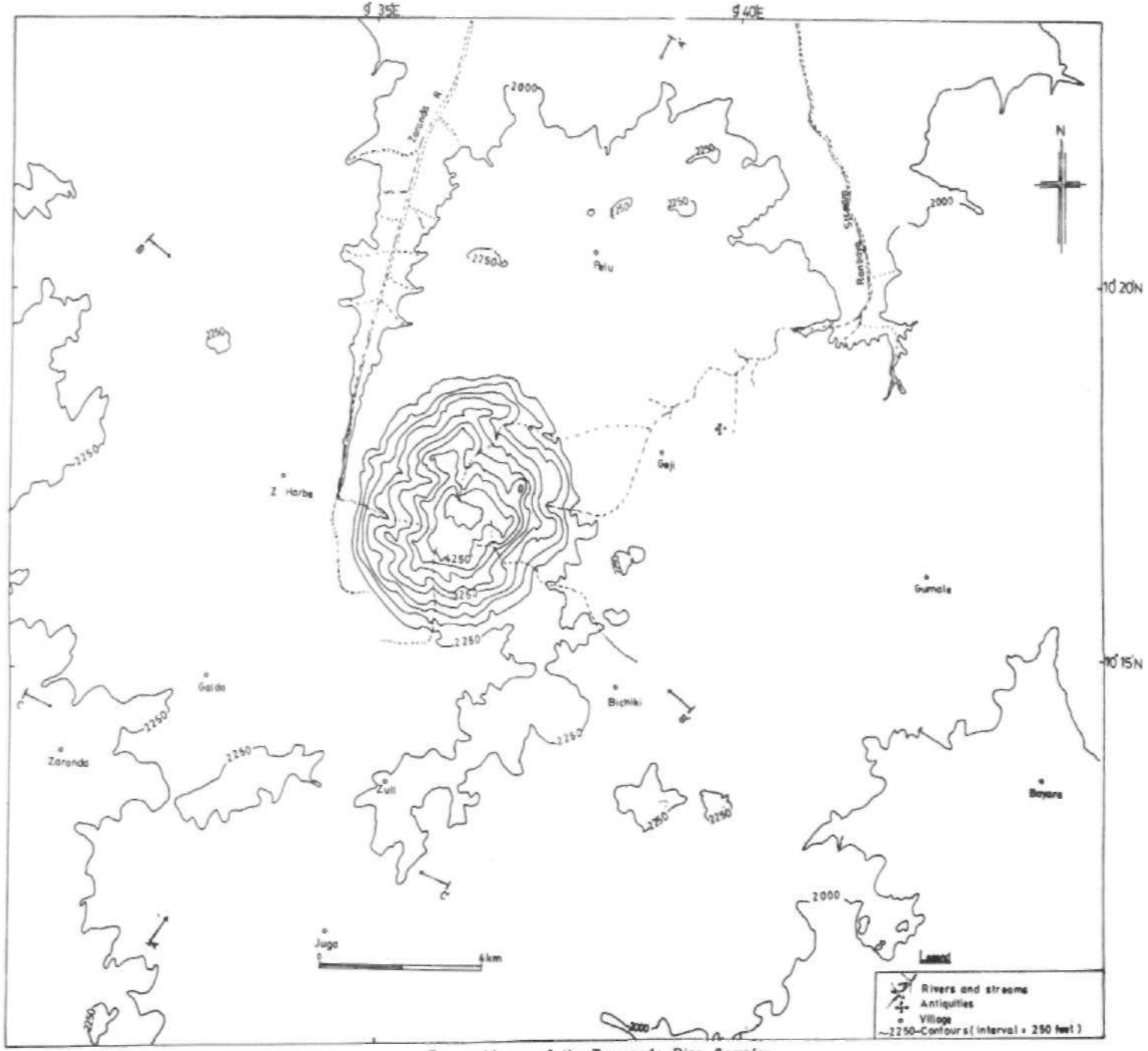


Fig 4

Topographic map of the Zararanda Ring Complex
(Adapted from 1977 Bauchi State photogrametric plot)

Minor occurrences of ultramafic rock were noted throughout the southern parts of the complex border with the host migmatitic gneiss. They stand out as noticeable dark green mounds of about 0.5m high and diameters ranging from 0.2m to 1.0m. They are interpreted as included rocks, not part of the complex.

The host rock into which the Zaranda complex intruded consists of older muscovite-biotite granite, granite and migmatitic gneisses.

2.3 MEGASCOPIC AND PETROGRAPHIC STUDY OF ROCK UNITS

2.3.1 Migmatitic Gneiss

The migmatitic gneiss is the main host rock of the Zaranda complex (Oyawoye, 1968) and occupies about one-half of the survey area (fig 3). Results of a study of 12 sections identified the major mineral phases as shown in appendix III. Also the result of megascopic study is shown in appendix I. The migmatitic gneiss bears the imprint of at least two tectonometamorphic cycles. Firstly, the unit is folded, jointed and banded. Secondly it is metamorphosed to at least medium grade of regional progressive metamorphism. Petrographically, the mineral association shown in appendix II, the structures shown in plate I and plagioclasse ($An_{35} - An_{50}$), indicate that the migmatitic gneiss is of medium grade of regional metamorphism (fig 5). The metamorphism would therefore have had a temperature of at least 450° C and at most 900° C, and a pressure of between 0.35 and 0.65 GPa (Pf). (Turner, 1968; Mason, 1978) (fig 6.)

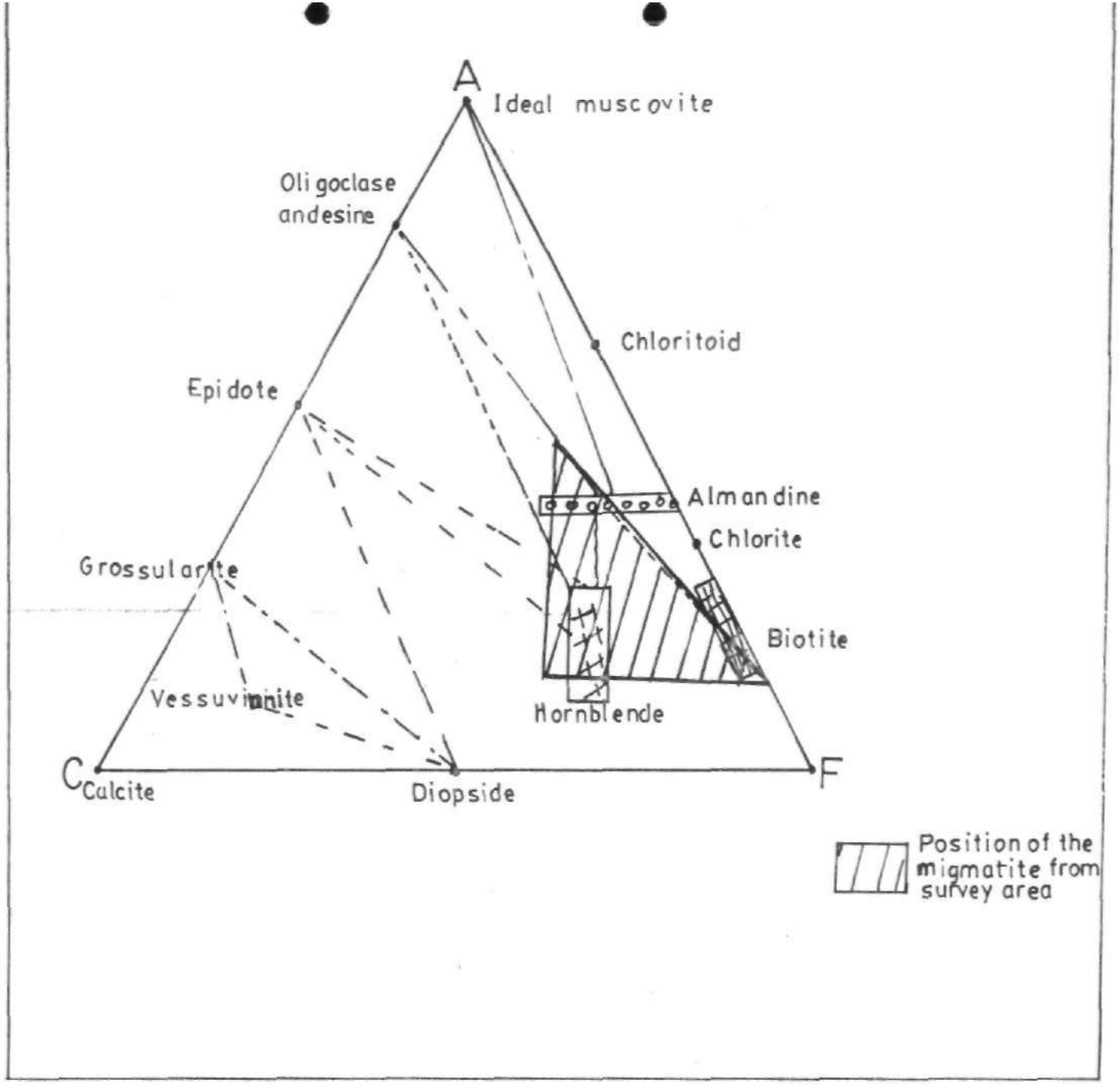


Fig. 5 A C F diagram of the almandine zone of amphibolite facies of progressive regional metamorphism.

(After Turner, 1968)

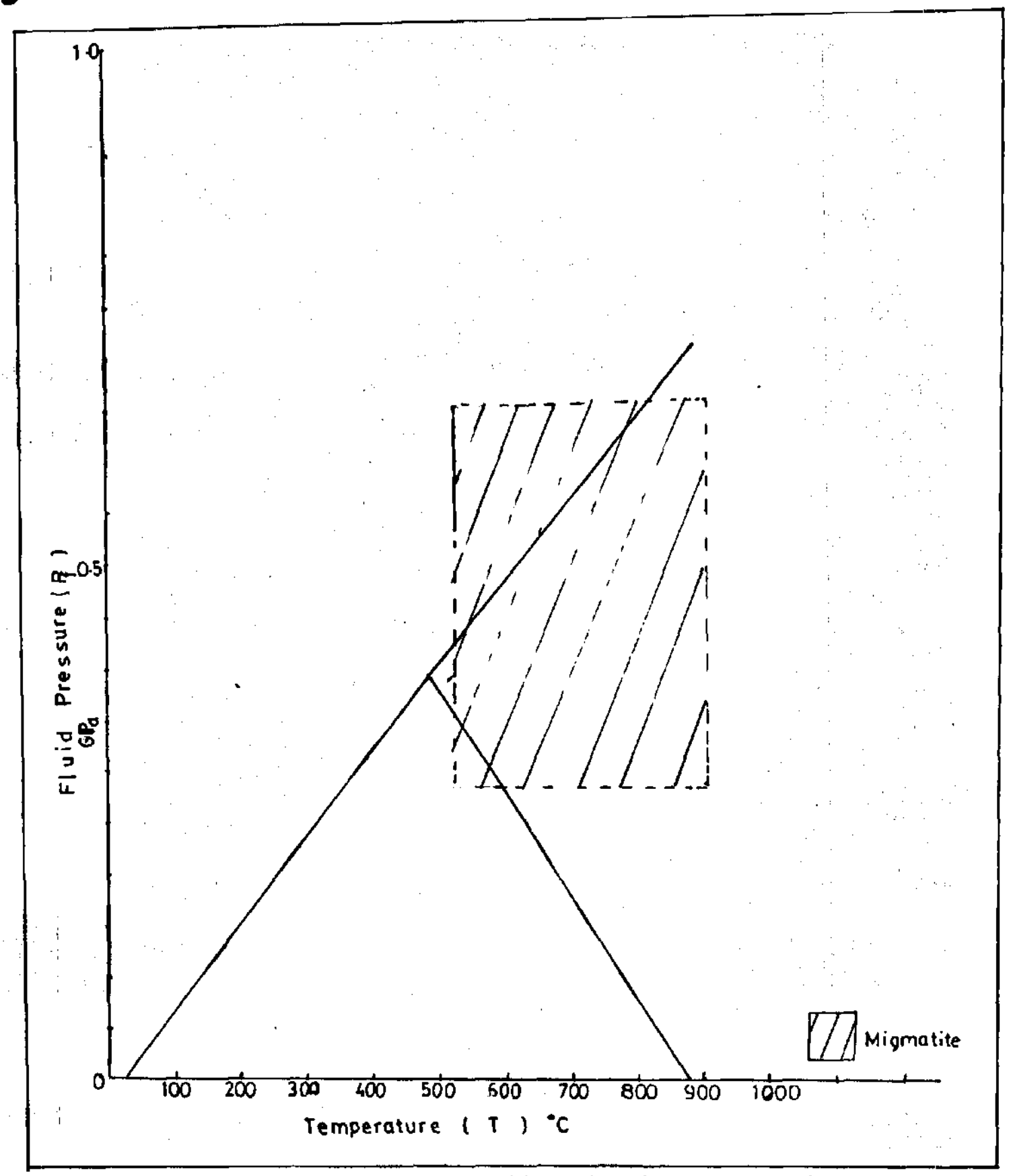


Fig.6 Position of the migmatitic gneiss in the P-T diagram (After Mason, 1978)

2.3.2 The Older Muscovite-biotite Granite

The position of this unit is shown in fig 3. The samples were weathered and a detailed megascopic study was done. However, results of petrographic study is shown in appendix II. Plate 2 shows the photomicrograph of the unit.

2.3.3 Precaldera Anhyric Trachyte

This rock unit occupies the central region of the exposed area of the complex and extends to over 2km in diameter (fig 3). The rock is dark in appearance with lath-shaped sanidine crystals (7mm x 2mm). Under the microscope, it contains prominent growths of sanidine prisms in a ground mass of oxides, feldspar and smaller sanidine crystals in glass (plate 3). Flow structures are delineated by more or less parallel grains of feldspar. Essentially, the texture is glassy-trachytic. A typical section of the trachyte is shown in appendix II and the megascopic result is shown in appendix I.

2.3.4 Fayalite-bearing Hornblende Syenite

This major rock unit (b) is over one-half of the exposed portion of the Zaranda complex (fig 3). It forms a ring-like structure around the older trachyte and contains the moon-shaped porphyry granite. It is light to grey in colour and has variable quartz content noticeable in hand specimen. Results of the megascopic study is shown in appendix I.

Oyawoye (1968) drew attention to the distinction

between fayalite, syenite and hornblende granite in the Zaranda complex on the basis of bimodal quartz content. Moorhouse (1959), Soliman (1982) have also drawn attention to the existence of two types of syenites based on color index. Turner (1976) and Oyawoye (1968) recognized the variation in perthite, quartz, amphibole and dark mineral content in syenites in the Younger Granite province. In leucocratic syenites, quartz (10%) and perthites predominate over mafic minerals. In melanocratic ones, amphiboles and oxides predominate over perthites and quartz (7%).

Turner (1976) also maintained that in quartz-rich syenites, quartz may be present up to 15%, thus having the same composition as granite. Turner (1976) recognized the existence of syenites as marginal facies of biotite granites in the Younger Granite province. Turner (1976) describes the syenite of the Younger Granite province as having a granular texture, and a gradient into porphyritic texture which is typical of the leucocratic syenites. The Zaranda complex syenites with quartz content ranging from 7 - 15% and texture very similar to the leucocratic and melanocratic syenites, thus conform to the syenites from the Younger Granite province. The results of the petrographic study is shown in appendix II and the photo micrograph of the two varieties of syenite are shown in plate 4.

Both the leucocratic and melanocratic syenites contain hornblende and fayalite. Large feldspar grains in some

samples grade some of the syenites towards porphyritic (Rahaman,1976). This is typical of syenites of the province in general and of the Zaranda complex in particular.

The slight difference in mineralogy is reflected in the density values obtained for the two varieties of syenite; (2.64×10^3 kgm^{-3}) and (2.60×10^3 kgm^{-3}) for the melanocratic and leucocratic varieties respectively.

Perthite is common in all samples.

2.3.5 Granite Porphyry

This rock unit is exposed in a ring-like fashion almost around the syenite but in most cases it is included in the latter and has sharp contacts with it. It forms two moon-like structures (fig 3). In hand specimen, the rock is mainly feldspar with some minor quartz intergrowths of size range 1mm to over 3cm. Blades of mica are randomly distributed. Tourmaline is rare and patches of pegmatite are rare.

2.3.6 Late Intrusive Rocks

2.3.6.1 Introduction

The rock units in the Zaranda complex and the host migmatitic gneiss as well as the older granite have been intruded by late basic dykes of varying chemical and mineralogical composition. These basic dykes form more or less ring-like structures which range in size from 1km to 1.5km in outcrop width and stretching to over 7km. Some of these are exposed at distances ranging from 0.0 to 5km from the previous rock units comprising trachyte, syenite

and granite porphyry (fig 3). Differences in colour index, mineralogy and structure indicate three types of basic intrusive rock units as given in fig. 3 and explained below:

2.3.6.2 Olivine Basalt

This rock unit is exposed on the south-eastern and southern portions of the main Zaranda complex (fig 3) at distances ranging 0.0km to 5km from the outline of the complex. The general trend is NNE - SSW and outcrops are made of isolated but parallel strings of dark dykes.

Under the microscope (Plate 5) phenocryts of olivine and laths of laboradoralite are set in a groundmass of smaller olivine grains, augite, feldspar and iron oxide.

One outcrop shows the contact relationship between the dyke and the syenite at the southern end of the complex (Plate 5, fig 3). The unit predominates over the other basic rocks in the survey area and forms a section of the late ring dyke around the complex.

2.3.6.2 The Zull Dolerite

At about 4km south of the complex and near a small village called Zull (fig 3) is a low-lying outcrop of dark rock which trends 260° azimuth. The outcrop is approximately 600m wide and extends in 260° direction for nearly 3km.

Texturally, it is fine to medium grained with faintly visible feldspar laths. Green tints of olivine give the characteristic green colour to the hand specimen.

Under the microscope (Plate 7) laths of andesine and laboradorite are set in a groundmass of augite, olivine, iron oxide and smaller feldspar laths. At the location of the outcrop (Zull), the rock appears to have intruded the host rock (migmatitic gneiss (fig 3). The result of model analysis is given in Appendix II.

2.3.6.4 Zaranda Calcitic Basalt

Right in Zaranda village, a lensoid body of basaltic rock carrying large phenocrysts of calcite (over 3cm in width) trends N - S. (fig 3). The width of the outcrop is over 250m and is approximately 3km in length. The rock is fine-grained and dark in colour with occasional rims of brown material surrounding the calite crystals.

Under the microscope (Plate 8) the phenocrysts are quartz (2%) and calcite (98%). A photo micrograph of a section across one of the calcite-bearing samples is shown in the plate. The groundmass of iron oxide, augite and minor olivine is seen around laths of sanidine and laboradorite. This mineral association suggests a rock of basaltic composition. The presence of calcite is probably due to a carbonate-rich melt which accompanied the crystalization and fractionation of the basaltic magma.

The quartz grain exhibits marked wavy extinction (Plate 8), which is indicative of a possible forceful injection of a carbonate-rich melt of a very hot material (Moorhouse, 1959).

2.3.7 The Amphibolite

All over the border region between the syenite and the host rock, small mounds of dark green rock consisting mainly of green minerals are found. They are not in mappable units.

Under the microscope, large blades of green hornblende (over 90%) are found associated with euhedral grains of sphene (Plate 9). Also prominent strands of serpentine are readily identifiable.

2.4 CHEMICAL ANALYSIS

Chemical analysis was carried out on five samples of the major rocks by X-raying fluorescence analysis (Table I). The analysis shows that:

(a) The trachyte k_3 has over 90% low density oxides, mainly Al_2O_3, SiO_2, K_2O, Na_2O, CaO and P_2O_5 and less than 10% high density oxides; Fe_2O_3+ FeO, MgO, MnO and TiO_2. The preponderance of low density oxides results in a comparatively low density value of the order of 2.56×10^3 kgm^{-3} for the trachyte.

(b) The two varieties of syenite (k_1 and k_2) have nearly the same chemical composition. The values are similar for $(Al_2O_3+SiO_2)$ and (Fe_2O_3+FeO). The slight variation in density between the leuco and melanocratic varieties is probably due to difference of about 0.07% Fe_2O_3+FeO and 0.03% MnO variation (Table 1).

TABLE 1

Chemical report on rock types of the Zaranda complex

Sample No	K_1	K_2	K_3	K_4	K_5	K_6
SiO_2	64.58	67.72	66.88	47.06	44.87	54.15
AL_2O_3	15.04	12.80	14.96	13.89	13.27	13.64
Fe_2O_3 + FeO	6.08	6.01	4.95	10.52	13.00	13.18
MgO	0.05	0.05	0.05	11.23	13.91	1.77
CaO	1.32	0.75	0.26	8.12	7.77	4.95
Na_2O	6.17	5.58	6.12	3.02	1.84	3.52
K_2O	5.50	4.93	4.79	1.53	2.07	3.07
TiO_2	0.40	0.41	0.29	1.57	1.96	1.55
P_2O_5	0.02	0.00	0.00	0.43	0.45	N.D.
MnO	0.18	0.15	0.12	0.16	0.20	0.18
Total	99.32	98.00	98.42	97.53	99.34	96.01

ALL values in % amount.
N.D. not determined
K_1 Leucocratic syenite
K_2 Melanocratic syenite
K_3 Aphyric trachyte
K_4 Dolerite
K_5 Olivine basalt
K_6 Calcite-bearing basalt

Analyst: K. RamLaL
Department of Earth Sciences
University of Manitoba

The variation in the amounts of hornblende and olivine are the main sources of this variation in density of about 0.04×10^{3} kgm^{-3} between k_1 and k_2. $Fe_2O_3+FeO_2$ values for the leucocratic and melanocratic syenites are 6.01% and 6.08% respectively. On the basis of this variation, both varieties were assumed to be one rock unit.

(c) The dolerite and basalts also have only minor differences in some oxide amounts (k_4 and k_5, Table 1). The olivine basalt has slightly more (Fe_2O_3+FeO), but both the olivine basalt and the dolerite have nearly the same CaO content because they have similar amounts of plagioclase. The relatively higher values of (Fe_2O_3+FeO), MgO and TiO_2 and the concentrations of SiO_2, K_2O and Na_2O, contribute to the higher density values of 2.92×10^{3} kgm^{-3} and 2.87×10^{3} kgm^{-3} for the dolerite and olivine basalt respectively. On the other hand, the calcitic basalt of the Zaranda village, (k_6, Table 1) with low MgO content, high SiO_2, Na_2O and K_2O contents, has comparatively lower density value of 2.78×10^{3} kgm^{-3}. The SiO_2 value of 54.15% is considered high for normal basalts. The K_2O+Na_2O value is less compared to the values for k_4 and k_5 but comparable to the figures for k_1 and k_2. These chemical results relate well to both the density values and the gravity anomalies over the trachyte, syenite and the basic rocks as discussed in Chapter 5.

2.4.1. Comparison with chemical results from other areas of the Younger Granite province

Bowden and Turner (1974) presented a geochemical report on the rocks of the Younger Granite province. The result on biotite and riebeckite granites are shown in Table 2. Wright (1976) (Table 3) analyzed the trachyte from the Filia area in the province which has a mean density of 2.47×10^3 kgm^{-3}. The higher density of the Zaranda trachyte is probably due to greater values of TiO_2 and (Fe_2O_3+FeO) (Table 1). However, the values of 2.47×10^3 kgm^{-3} and 2.56×10^3 kgm^{-3} for the Filia and Zaranda trachytes respectively, fall within the range of trachyte densities for the province (Ajakaiye, 1970).

Similar comparisons have been made for the basalts and dolerite. (Table 4). The olivine basalt has the characteristics of the Biu basalt. A TiO_2 - SiO_2 plot (Fig 7) for the basalts and dolerites shows that the basic rocks of the Zaranda complex are subalkaline, but with the olivine basalt tending towards alkaline suite similar to those of Longuda, Biu and Tula areas of the province. Also the plot shows that the calcite-bearing basalt is probably alkaline.

This result was therefore found to be related to the proximity of the basic rocks to the main complex. While the olivine basalt which plots near the alkaline end and outcrop nearer the alkaline Zaranda syenite (Oyawoye, 1968; Bowden and Turner 1974) the dolerite and calcite-basalt which outcrop farther away from the complex plot far away from the alkaline-subalkaline border in

TABLE 2

Comparison between chemical analysis of biotite and riebeckite granites of the Younger Granite province and the syenites of the Zaranda complex

Oxides	A	B	C	D	E	F	K_1	K_2
SiO_2	76.50	74.30	71.60	70.10	75.50	75.90	64.58	67.72
AL_2O_3	11.60	11.47	13.54	16.98	13.62	12.71	15.04	12.80
Fe_2O_3 + FeO	2.43	2.72	2.90	2.43	1.48	1.60	6.08	6.01
MgO	0.01	0.08	0.01	0.01	0.18	0.16	0.05	0.05
CaO	0.25	0.32	0.01	0.72	0.08	0.03	1.32	0.75
Na_2O	3.77	5.28	6.79	3.57	4.57	3.72	6.17	5.58
K_2O	4.97	4.38	3.79	5.56	4.77	4.50	5.50	4.93
H_2O^+	0.28	0.43	0.37	0.26	0.21	0.24	---	---
H_2O^-	0.20	0.08	0.01	0.05	0.05	0.09	---	---
CO_2	---	---	---	---	---	---	---	---
T_1O_2	0.14	0.13	0.23	0.26	0.06	0.10	0.40	0.41
P_2O_5	T_r	0.02	T_r	0.03	T_r	T_r	0.02	T_r
MnO	0.05	0.01	0.07	0.03	0.02	T_r	0.18	0.15
Total % Oxide	100.20	99.14	99.32	99.74	100.14	99.00	99.34	98.20

T_r : trace amount

--- : Not determined

A : Liruei riebeckite granite

B and C: Liruei albite-riebeckite granite

D : Jos biotite granite

E : Pankshin biotite granite

F : Liruei biotite granite

K_1 : Zaranda fayalite-hornblende syenite

K_2 : Zaranda quartz-hornblende syenite

All values in wt. %

(Data A – F from Bowden and Turner, 1974)

TABLE 3

Chemical relationship between Zaranda and Filiya trachytes

Oxide	A*	K_3
SiO_2	58.87	66.88
AL_2O_3	18.77	14.96
Fe_2O_3 + FeO	4.64	4.95
MgO	0.39	0.05
CaO	1.66	0.26
Na_2O	7.68	6.12
K_2O	5.22	4.79
H_2O^+	2.33	—
H_2O^-	0.17	—
CO_2	—	—
TiO_2	0.20	0.29
P_2O_5	0.09	T_r
MnO	0.20	0.12
BaO	0.04	—
Total	100.26	98.42

All values in wt. %

A*: Trachyte plug, 5km north of Filiya (Data from Wright, 1976)

K_3: Trachyte body from Zaranda complex

TABLE 4

Comparison between chemical composition of the Nigerian basalts and those of the Zaranda complex

Oxides	1	2	3	4	5	K_4	K_5	K_6
SiO_2	44.59	45.37	43.85	45.86	44.44	47.06	44.87	54.15
AL_2O_3	15.99	16.58	13.95	16.46	18.45	13.89	13.27	13.64
Fe_2O_3 + FeO	11.34	10.39	11.79	11.12	12.23	10.52	13.00	13.18
MgO	7.00	8.26	10.13	7.90	5.54	11.23	13.91	1.77
CaO	9.83	9.11	10.61	10.22	8.93	8.12	7.77	4.95
Na_2O	4.39	2.50	3.71	3.83	3.87	3.02	1.84	3.52
K_2O	1.84	1.93	1.54	0.56	1.85	1.53	2.07	3.07
H_2O^+	1.94	2.19	0.62	1.22	1.20	---	---	---
H_2O^-	0.27	0.57	0.43	0.40	0.46	---	---	---
CO_2	0.00	Tr	0.15	Tr	Tr	---	---	---
TiO_2	2.43	1.87	2.29	2.61	2.13	1.57	1.96	1.55
P_2O_5	0.83	0.73	0.92	0.28	0.52	0.43	0.45	---
MnO	0.19	0.18	0.21	0.17	0.20	0.16	0.20	0.18
Total Wt %	100.64	100.09	100.20	100.63	99.82			

1 Plug, near Tula junction, Gombe-Numan road

2 Lava, Biu plateau

3 Lava, north of Biu plateau

4 Top of Chikila Lawa, Longuda plateau

5 Basal Lava, Chikila, Longuda plateau

K_4 Dolerite, Zull village, Jos-Bauchi road

K_5 Basal Lava (olivine basalt) base of Zaranda complex

K_6 Calcite-bearing basalt, Zaranda village

---: Not determined

Tr : trace amount

All values in wt %

(Data 1 - 5 from Wright, 1976)

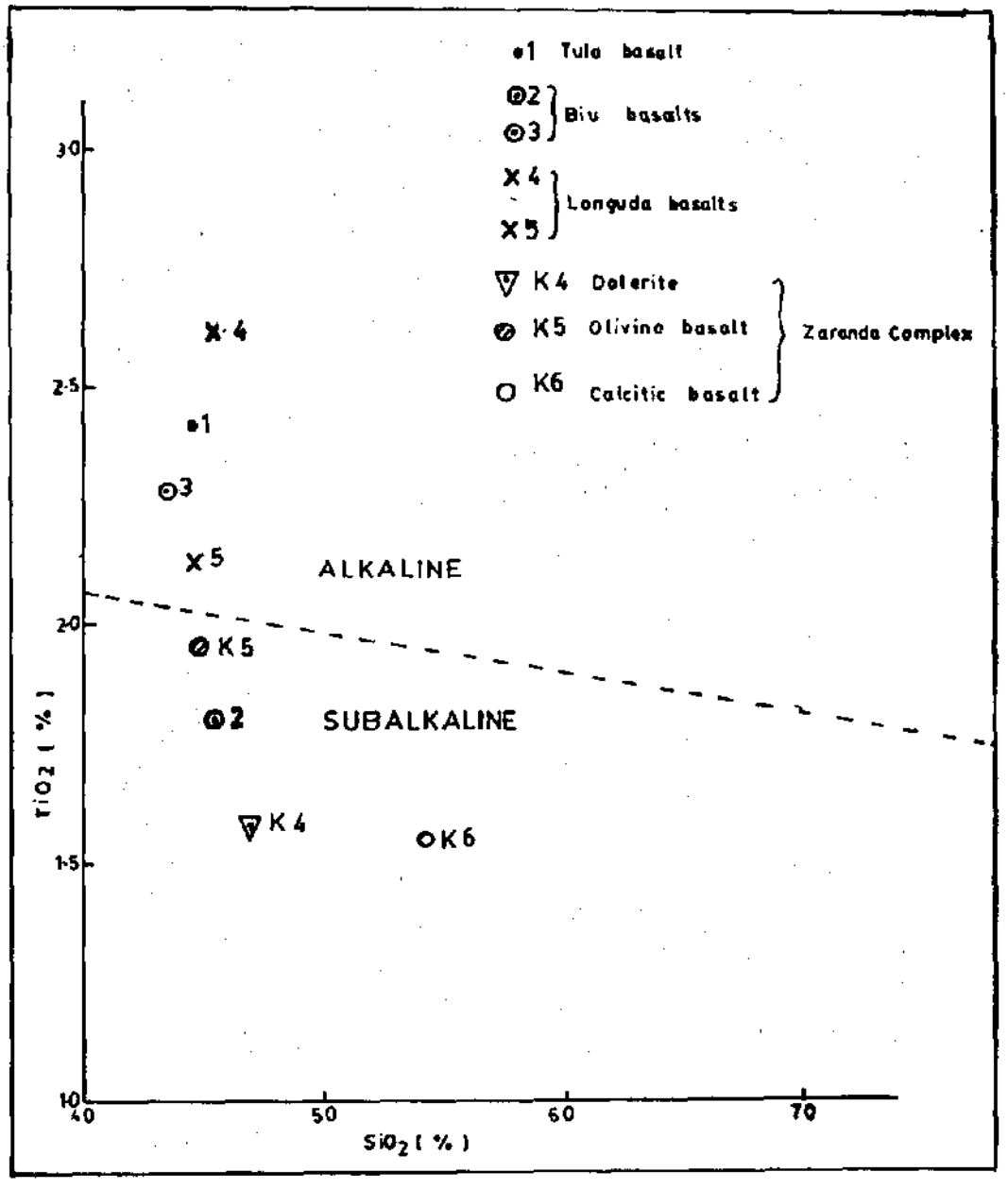


Fig 7 Comparison between $TiO_2 - SiO_2$ plots for Zaranda basic rocks and these from adjoining volcanic areas.

Additional data from Olade (1979), Wright (1976)

the TiO_2 - SiO_2 diagram.

It is thus concluded that the events that led to the emplacement of both the dolerite and calcite-bearing basalt are probably the same as that of the Zaranda complex judging from chemistry of these units, and the nearly equal distance of both the dolerite and the calcite-bearing basalt from the complex (fig 3).

A summary of the mineralogy of igneous rocks shown in fig 8 shows that the rocks of the Zaranda complex can be grouped in two rock families:

(a) the ultramafic-gabbro-basalt

(b) the granite-syenite-trachyte-rhyolite.

Based on mineralogy and chemical analysis, Oyawoye (1968) assigned the name hornblende granite to what Turner (1976) gave quartz syenite. This difference arises from the quartz content and the variation in amount of ferromagnesian minerals. However, a quartz mode of about 15%, olivine and more hornblende than normative amount makes the main rock unit syenite than granite. Hornblende predominates over quartz which is normative and the presence of olivine in nearly all samples grades the syenite out of the granite member.

Based on mineral association, the various rock units have been grouped under definite fields based on volume percent of minerals (fig 8).

These are: (i) Amphibolite-dolerite-basalt

(ii) Syenite-trachyte-porphyry

2.5 STRUCTURAL GEOLOGY

The Zaranda complex intruded the host migmatitic gneiss, gneiss and older muscovite granite in a ring-like

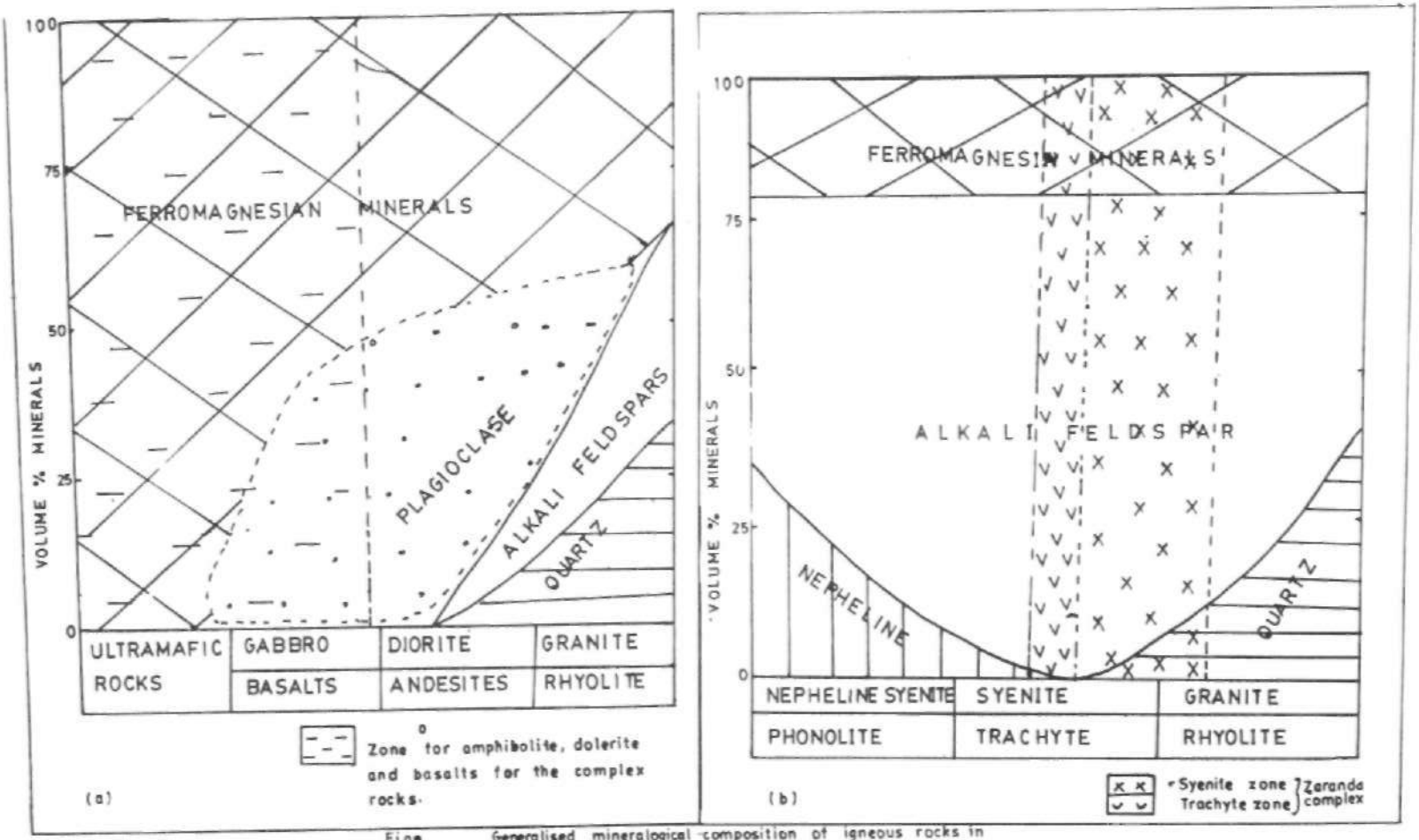


Fig 8 Generalised mineralogical composition of igneous rocks in relation to those of the Zaranda Complex.
(After Cox, 1976)

structure. Consequently, major and minor structural features were observed and their attitudes measured in the field. These features include folds and joints.

2.5.1 Folds

The complex has not been affected by any noticeable folding as the host migmatitic gneiss. Although the late basic intrusions affected the syenite, the effect was only interpreted as minor contact metamorphism due, possibly, to high temperature and to minor folds.

Minor and major joints were observed on the host gneiss and these indicate at least two tectonic events:

(i) the regional movement that led to the emplacement of the older granites must have resulted in folding and low grade metamorphism of pre-existing basic rocks;

(ii) the emplacement of the Zaranda complex led to a higher grade of metamorphism as depicted by the presence of hornblende (plate I). Also the increased metamorphism must have intensified the folding in the host rock, thus upgrading the phase to that of amphibolite (Mason 1978).

2.5.2 Joints

Joints, in general, are evidence of contractive or tensile forces in operation in any geological environment. Major joints trend in the direction of a major rock unit while minor ones trend more or less perpendicularly to the major ones (Ragan, 1973).

Angular relationships of joints and other planar features can be determined more readily if a sphere is constructed centered at some point O (fig. 9a) and whose plane includes the center point O. A given joint observed as a line on the surface but represented as a plane below the surface is projected unto the inner surface of the sphere. This is spherical projection and must be represented in two dimensions.

Practically all points on the lower part of the great circle representing the plane are projected to the horizontal plane of the half sphere by joining them to the zenithal point P. Such projection yields an arc such as abcd (fig. 9b). Thus a series of points and lines are plotted on the horizontal great circle. The method of plotting this great circle is known as the stereographic projection and the figure drawn on this cardinal compass direction is a stereogram. A great circle on the stereogram is a great circle on the sphere thus permitting the construction of any plane representing a structure on an outcrop.

A further advantage of this projection is the representation of a plane by a point thus reducing the dimensions of the plot by one more. For every plane, there is a unique line normal to the plane, called the pole of the plane. This line intersects the hemisphere at a point in the opposite quadrant and is 90° to the plane; therefore from the great circle, a trace count of 90° from the right to the left along the east-west diameter

gives the location of the pole of the plane and thus of the joint measured in the field. For a structure with a strike N 30° E and dip 40° SE, the pole is illustrated in fig.9c.

It is often useful to represent a set of structures measured in the field by plotting their range of values and the corresponding frequencies in a circle. A range of strike values, N--20° , 21°— 40° etc; are chosen and marked on a circle of a suitable radius. Frequencies of joint values in these ranges are plotted along these ranges starting from the center of the circle. The resulting figure is known as the rose diagram. It is useful in estimating the resultant trend of a set of major structures on outcrops. The rose is usually extended in the opposite direction for clarity.

Results of measurements of major joints in the migmatitic gneiss are listed on Table 5 and the polar plots are shown in fig. 9d. Analysis of these data shows that most of the major joints are nearly vertical and trend in the NNE-SSW direction. Similarly, a rose diagram of the major joints in the host rock is also NNW-SSE. Measurements of major joints in the central trachyte body (Table 7) and subsequent polar and rose plots based on these readings (figs. 11 & 12), indicate that the major trend is NNE-SSW. Being the oldest unit in the complex, its emplacement may have been controlled by structures pre-existing in the host migmatitic gneiss.

The observed minor joints in the area probably resulted from later tectonic events that presumably took place in the survey area

TABLE 5

Joint readings from the host migmatitic gneiss

Joint Type	Strike	Dip	Dip Direction	Frequency
Major	N	90°	---	1
	N 20 E	90°	---	15
	N 30 E	75°	330°	15
	N 30 E	90°	---	5
	N 35 E	85°	300°	3
	N 35 E	90°	---	15
	N 40 E	80°	315°	10
	N 40 E	90°	---	15
	N 60 E	75°	295°	1
Minor	S 80 E	90°	---	1
	S 80 E	75°	200°	19
	S 30 E	75°	210°	25
	S 5 E	70°	195°	10
	S 5 E	80°	200°	5

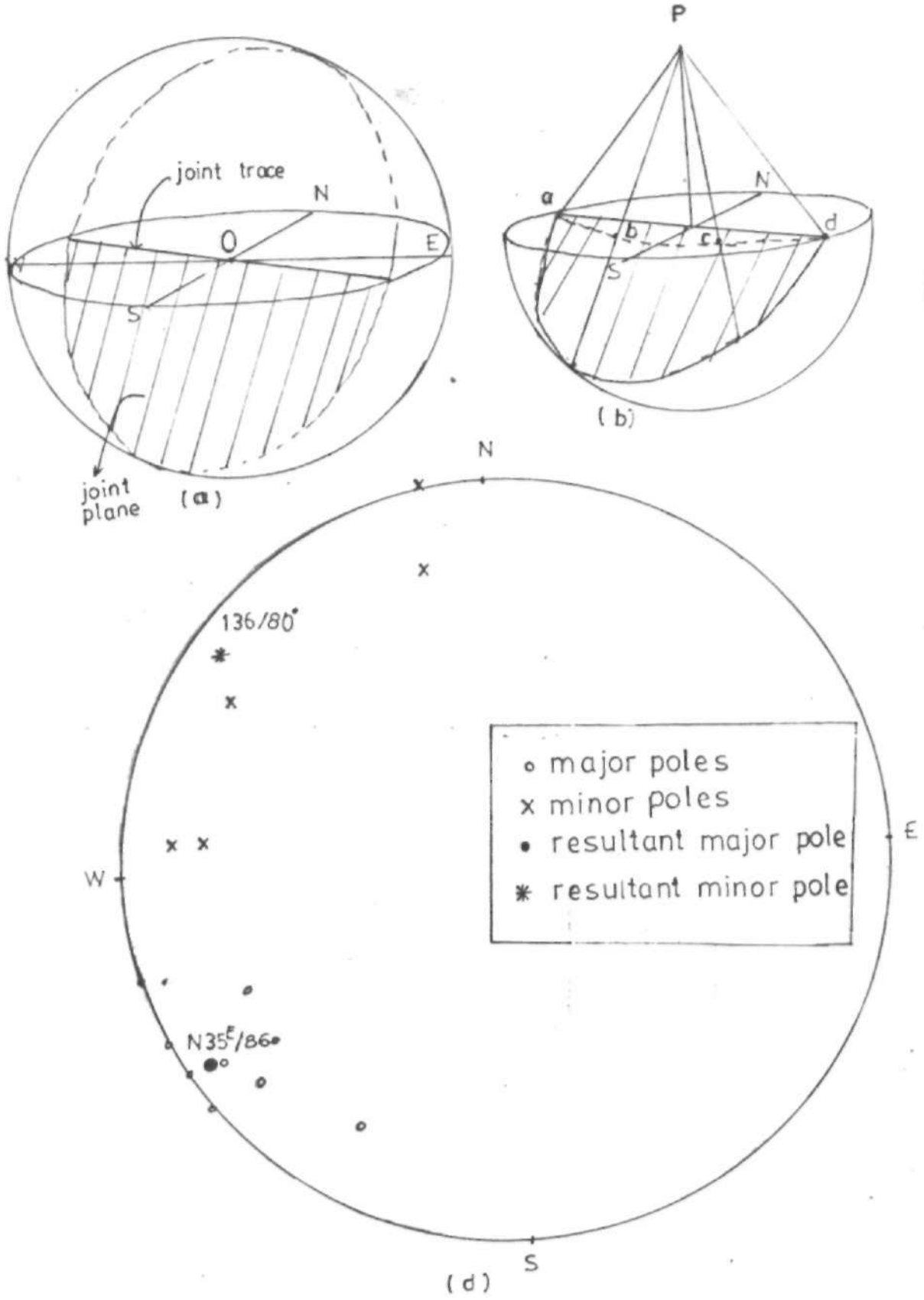


Fig 9 Stereographic polar plots of major and minor joints on the migmatitic gneiss.

TABLE 6

Frequency distribution of joints on the host migmatitic gneiss

Joint Type	Strike Interval	Frequency
Major	N - N 20°E	15
	N 21°E - N 40°E	58
	N 41°E - N 60°E	1
	N 61°E - N 80°E	0
Minor	N 61°E - N 80°E	0
	N 81°E - S 80°E	20
	S 81°E - S 60°E	0
	S 61°E - S 40°E	0
	S 41°E - S 20°E	15
	S 20°E - S	15

TABLE 7

Frequency distribution of major joints on the aphyric trachyte

Strike Interval	Frequency
N - N 20°E	3
N 21°E - N 40°E	29
N 41°E - N 60°E	0
N 61°E - N 80°E	0

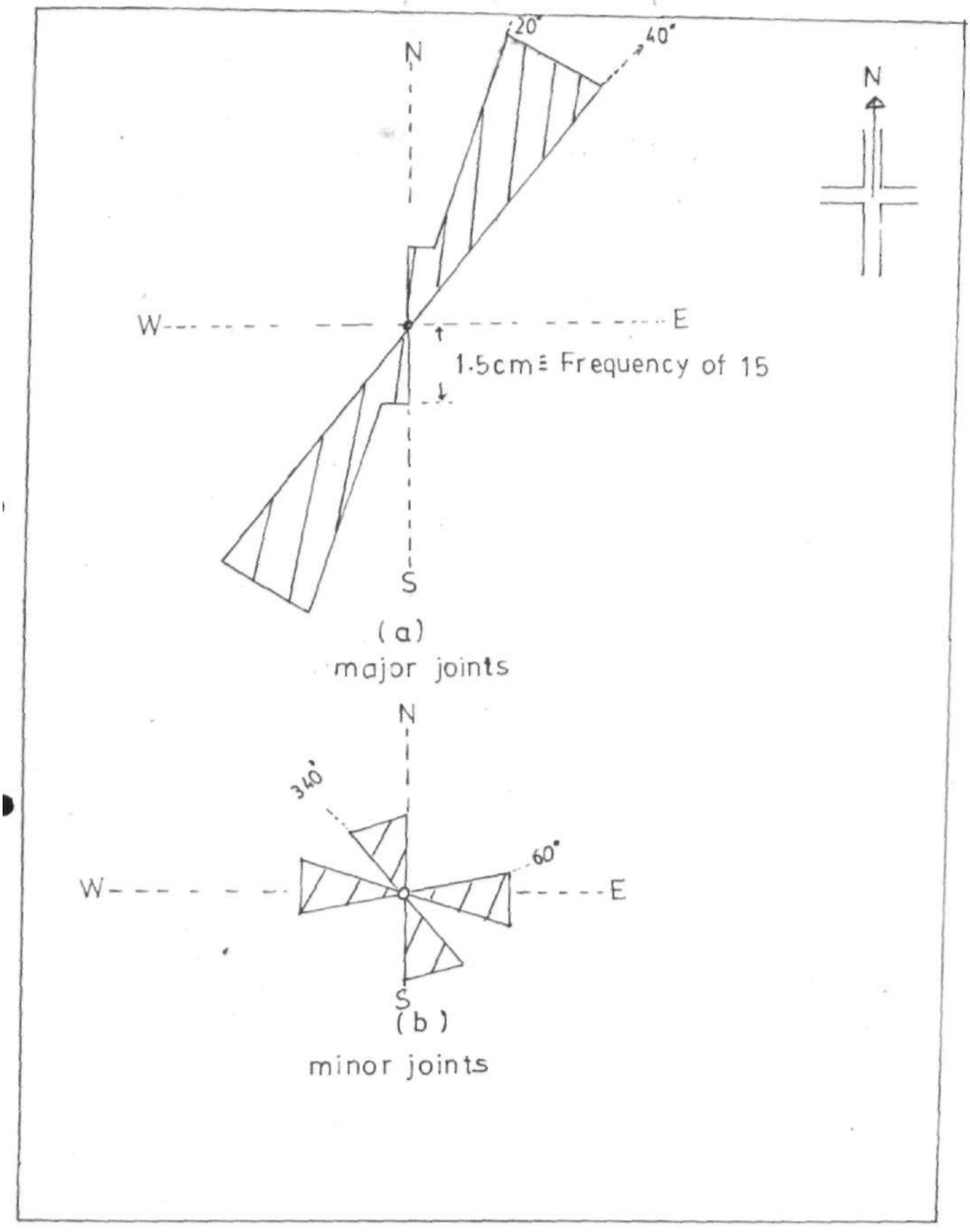


Fig 10 Rose diagrams of joints on the migmatitic gneiss
(Plots of frequency values along strike interval directions)

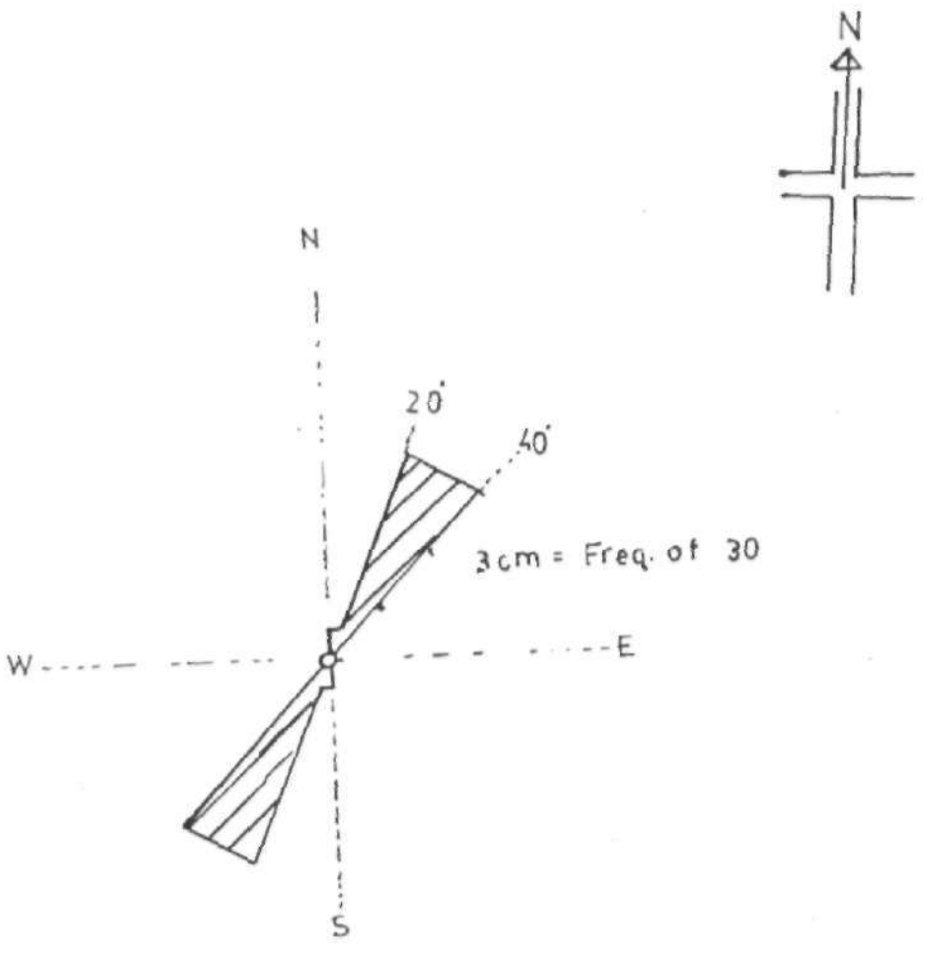


Fig 11 Rose diagram of major joints on the aphyric trachyte.

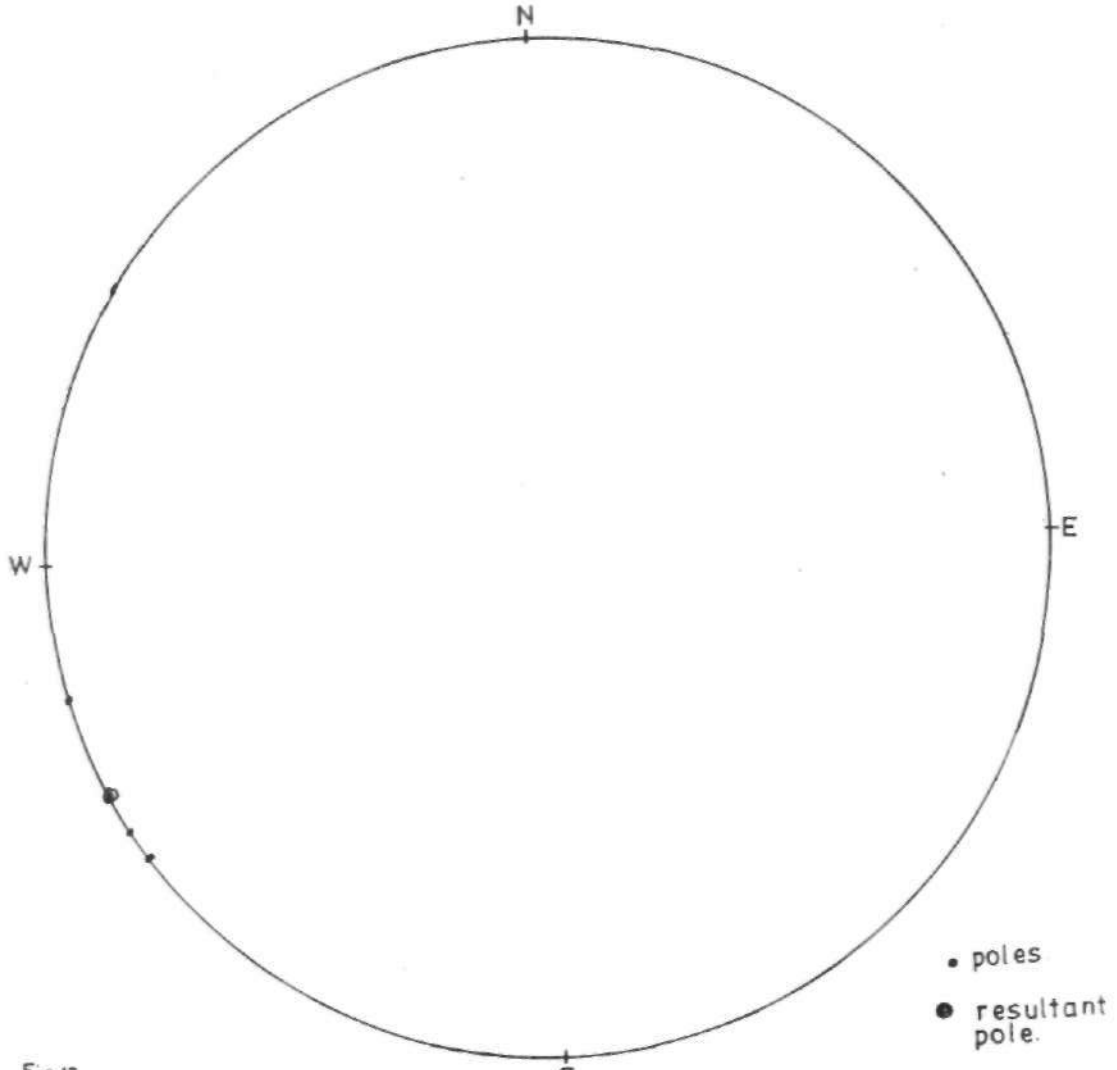


Fig 12

Stereographic polar plots of joints on the aphyric trachyte.

after the emplacement of the complex and other movements that probably resulted from physical processes such as weathering, faulting and minor folding of major structural units in the survey area. In general there is little or no correlation between the observed major and minor joints. In the majority of cases, the trend of the observed minor joints are nearly perpendicular to those of the major ones (fig. 10).

Conclusively, structural plots of data from the Zaranda complex and host migmatitic gneiss show striking similarities in their general trend which can only be interpreted as common structural features to these two major rock units.

2.6 HYDROGEOLOGY

Two major features which control the groundwater potentials of the survey area are:

(a) state of weathering of the various rock types;

(b) structure and location of the basic intrusive dykes.

From existing hand-dug wells in the area, the weathered portions of the migmatitic gneiss constitute the main water-bearing zones. In the vicinity of Zull, Geji and Hadam-balamba (fig. 3), the weathering depth is as much as 18m.

In general, the rocks in these areas are porous and greatly weathered. Wherever the Zaranda complex rock units

outcrop over seemingly flat region such as in Bolu and Zaranda Harbe areas, there are always water problems. A good example of the structure of the aquifers in the vicinity of the complex is shown in fig. 13. The basic dyke exposed at Zull (fig. 3) confines the run-off from the complex and the migmatitic gneiss. Consequently, underground water is abundant on both the northern and southern sections of the exposed rock.

Data from the well at Zull shows that water level is 8m below the surface in a well that is 25m deep. North of Zull, perenial ponds exist due also to the impervious action of the dolerite at Zull.

The presence of abundant and good water in the area south of the complex and north of Zull and in few other areas such as Zaranda, places them as possible areas for further water investigation.

2.7 ECONOMIC GEOLOGY

Mineral associations in any rock units have been used as indices for predicting economic mineral deposits and their trends. Syenites and granites in the Younger Granite series often contain intergrowths of quartz and associated wolframite, cassiterite and beryl (Ajakaiye, 1974); (Soliman 1982). Banke and Liruei complexes are examples of such associations (Ajakaiye, 1970, 1974). In W. Australia, tin deposits and iron ore are associated with syenites and granites, although the chemistry of such association is not clear (Blockley, 1980). Also the occurrence of basic or ultra-

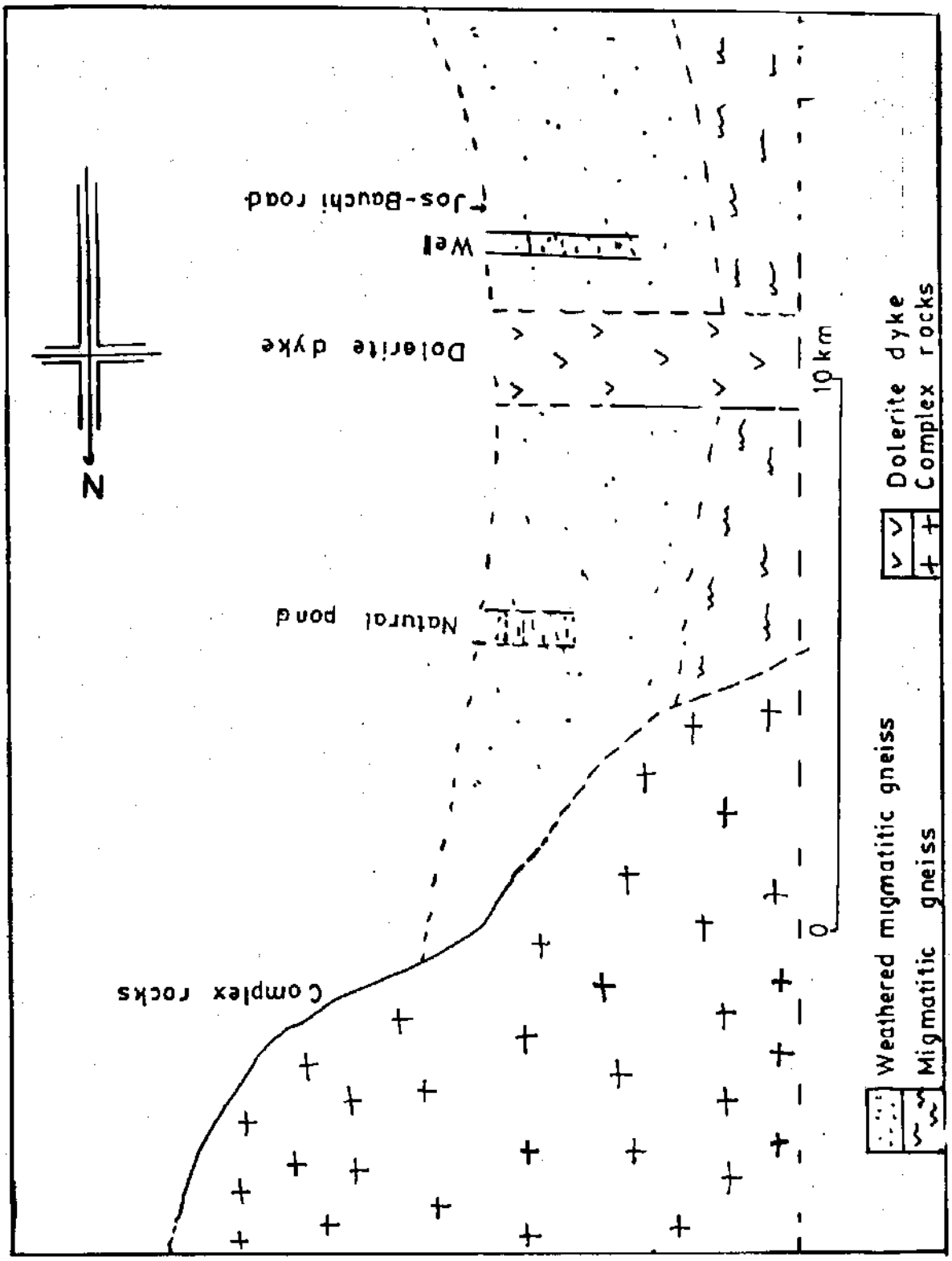


Fig 13 A schematic section of a suspected aquifer structure south of the Complex.

basic rocks is a guide to the integrated exploration for asbestos (Blockley,1980; Onyeagocha, 1979). These observations could be applied to the rock and mineral associations of the Zaranda complex where syenites, basic and ultrabasic rocks co-exist.

In Hadambalamba and Chali, minor occurrences of kaolinite pits were noticed; some have dimensions ranging from 1 - 5m and 10m wide. The existence of such pits and widespread occurrence of potassium pegmatite dykes sustains some local potteries in these villages.

A much more extensive occurrence of koalinite and potasium pegmatite may exist but needs further investigation.

2.8 GEOLOGICAL HISTORY

Rocks of the survey area have been considered under two main divisions:

(i) the Pre-Cambrian crystalline basement comprising the migmatitic gneiss, older granite and granite gneiss;

(ii) the Jurassic Younger Granite rocks made up of syenite, trachyte, basic rocks granite porphyry and minor occurrences of amphibolitic rock.

It would appear that at least two major tectonic events have taken place in the area. Turner (1976) maintained that older rocks of probable basic origin were

subjected to low-grade metamorphism during the emplacement of older granites. These low grade metamorphosed rocks were probably re-mobilized during the Pan African and Jurassic periods. The imprints of such episodes are often manifested as folded bands, microfaulting and the presence of amphibolitic material (Bowden and Turner, 1974)

In the survey area, an unmappable rock unit containing over 80% amphibole exist which indicates that the complex is probably underlain by ultrabasic rock. The amphibole's presence may also indicate metamorphism of a parent basic rock (Turner, 1976; Mason, 1978).

CHAPTER THREE

FIELD PROCEDURES AND INSTRUMENTATION

3.1 Bases For The Gravity Survey

All geophysical survey techniques are based on the fact that exist exist some spatial variation of physical parameters between areas of interest and that of non-interest. However, the size or magnitude of such contrast evidently determines the suitability and success achieved in employing a given method. Some of these contrasts include density contrast, susceptibility contrast, etc., which are used in conventional geophysical techniques.

Gravity surveys have been used to locate both buried and exposed Younger Granite bodies, clay deposits, buried water channels and disseminated ores because of pronounced density contrasts existing between these bodies and their host rocks. A recent interpretation of the magnetic anomalies over the Nigerian Younger Granite complexes (Ajakaiye, 1981), has pinpointed various exposed and buried anomalies suitable for further detailed groundwork. A careful study of the density measurements over the Younger Granite province (Ajakaiye, 1970) also indicate that the intrusions in the region have distinct density contrast of the order of about 0.06×10^{3} kgm^{-3} in relation to the host crystalline basement. The result of gravity survey carried out by Ajakaiye (1968, 1970, 1974, 1975, 1981) correlate with the magnetic interpretation in the province.

Bott (1953) suggested that buried and exposed acid intrusions have negative gravity anomalies because of their low density in comparison with the denser host rocks (basement or metasedimentary). Also, Gustaf (1967) confirmed that negative Bougver anomaly over granite intrusions is interpreted as being caused by low density rock compared to the denser country rock. He found that a density contrast of about 0.07×10^{3} kgm^{-3} existed between such bodies. These values of density contrast are very comparable to a value of 0.06×10^{3} kgm^{-3} obtained by Ajakaiye (1970) over the Younger Granite province of Northern Nigeria.

The Zaranda complex is believed to be one of the exposed Younger Granite intrusions of Nigeria (Okezie, 1964; Oyawoye, 1968; Ajakaiye and Burke 1973; Turner 1976). Thus the choice of gravity survey as one of the prime methods in this investigation is in line with earlier gravity surveys over exposed and unexposed acid intrusions.

Surface features of most of the Younger Granite complexes, chemical composition, mineralogical and petrographic significance are best documented through systematic and comprehensive geological mapping and analysis of results. Consequently, the gravity survey has been accompanied by background geological investigation to aid in the quantitative interpretation of the gravity survey.

3.2 Instrumentation

In the survey, a standard Worden gravity meter model No. 135 was used. The instrument has a scale constant of 0.92 6.g.u./div.

and an accuracy of ± 1.0 g.u. for readings less than 25,000 g.u. Prior to the fieldwork, the gravity meter was mounted on a solid slab and observed for three consecutive days at 15-minute intervals lasting between 06.30 hours and 19.30 hours (normal fieldwork period). During the actual fieldwork, the instrument was similarly observed and drift curves were plotted (fig. 14).

Prior to the fieldwork, a maximum drift of 0.09 g.u./hour was recorded, but this increased to 0.11 g.u./hour during the fieldwork. The manufacturer's estimated drift of ± 3.0 g.u./hour is higher than the drift values obtained during the survey. Gravimeter drifts result from creep in the spring elements, temperature fluctuation, sudden jarring and vibration and the observed diurnal drift is a combination of these factors. The main cause of gradual increase in scale reading for a given station is often due to vibration. The observed daily drift curves for the duration of the survey show striking similarities (figs. 14a and b).

In normal gravity surveys, the elevations of gravity stations are usually determined by geodetic levelling but due to the constraints posed by equipment, time and crew, two Wallace and Tiernan altimeters Model No. FA 181 with scale factors of 3.05m/division were used to determine the elevations of gravity stations. Essentially, an altimeter is an aneroid barometer which usually measures pressure, but because a normal barometer operates on the principle of pressure variation with elevation, it is calibrated by the manufacturers to give relative elevations. Also the pressure variation depends on gravity effect according to the relation:

$$P = \rho g h \quad \ldots\ldots\ldots\ldots\ldots\ldots\ldots\ldots\ldots\ldots \quad 3.1$$

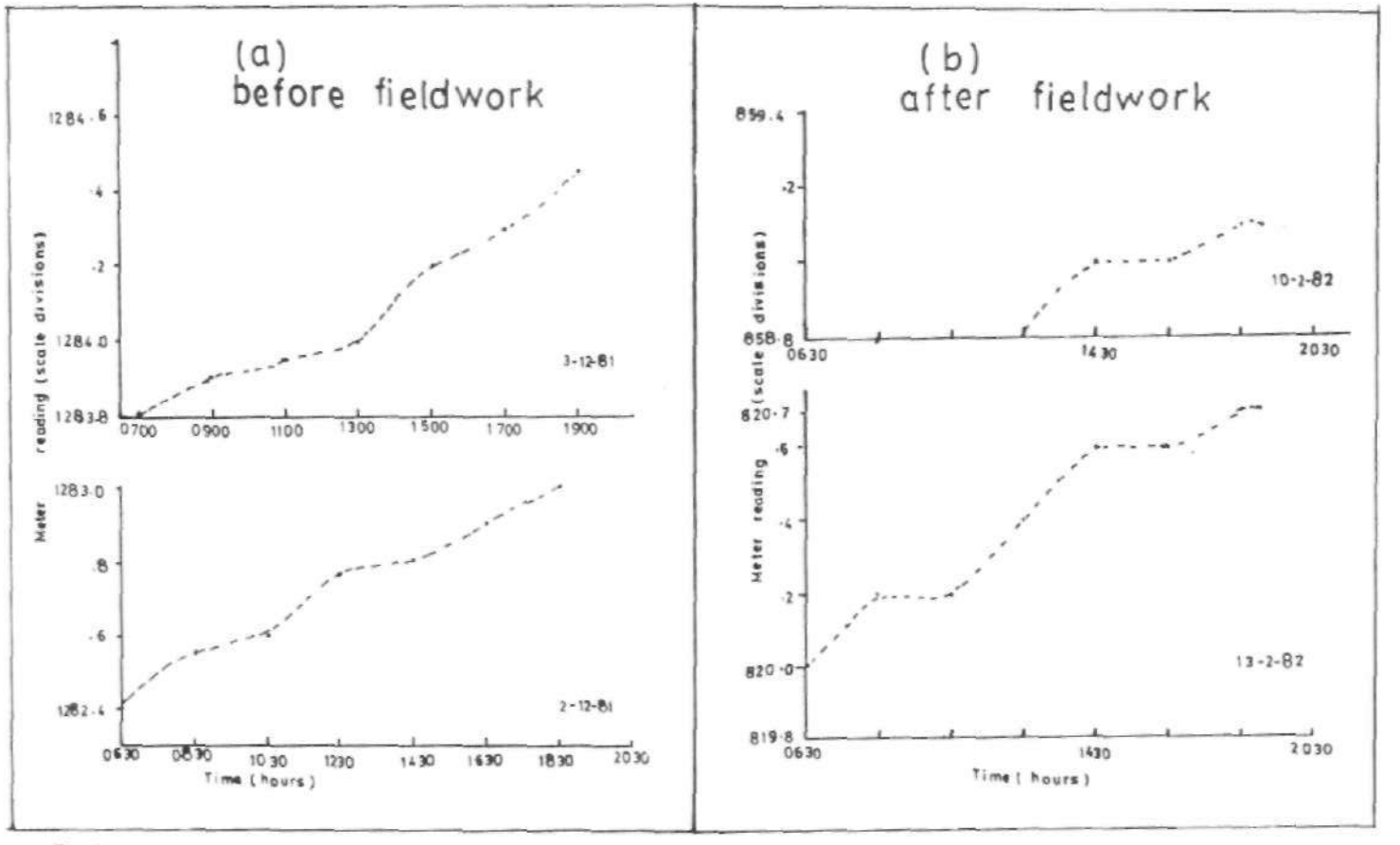


Fig 14

Drift curves for Worden gravimeter No 135

where P, ρ , g and h are pressure, dry air density, acceleration due to gravity and elevation (height) of air column above the barometer respectively.

Allan et al (1971) indicated that the relationship in equation 3.1 is too simple to explain the behaviour of aneroid barometer. This is so because in normal field conditions, the air is not completely dry and there is marked fluctuation in temperature gradient as elevation varies. During the fieldwork, these conditions were found not to be true because temperature variations with altitude and relative humidity of the survey area of the order of about 60 - 75% suggested that the altimeter readings be corrected for temperature and relative humidity.

Apart from the error that would be associated with the elevation values if the altimeter readings were not corrected for humidity and temperature, reading error, hysteresis as a result of imperfection in the spring mechanism, introduced errors of $\pm$ 0.4m and $\pm$ 3m respectively (Verheijen and Ajakaiye, 1980). These workers also found out that the instrument can have an accuracy of the order of $\pm$ 1.2m for a survey carried out during the stable periods in the area of survey. Altimeter drifts were assumed to be linear when loops were established in less than three hours between two gravity base stations.

A brunton compass was used to take structural readings and to align profiles across the complex.

3.3 FIELD PROCEDURE

Prior to the actual fieldwork, reconnaissance surveys were carried out in August, 1981 and the actual survey was carried out

between November 1981 and April 1982. The reconnaissance survey was aimed at determining traverse lines and location of elevation bench marks. Also, few samples of rocks were collected, and topographic maps of the survey area were compiled from the Bauchi survey headquarters. During the actual fieldwork, 45 base stations and 148 detail gravity stations were established at distance intervals ranging from 0.5km to 4km, most of the stations being established at 1km interval.

Mode of transportation between stations was principally by means of a Landrover supplied by the Geological Survey Department, Jos and a pick-up van belonging to the Physics Department of Ahmadu Bello University. A few stations which were inaccessible by a motor vehicle were occupied on foot. For the motor vehicle mode of transportation, distances were read out from their odometers with an accuracy of $\pm$ 0.1km, and steel tape was used to estimate distances between stations that were occupied on foot with an estimated error of $\pm$ 1.5m in 1km. This is the error in positioning of the instrument. Assuming an accuracy of $\pm$1.5m for the map, then an estimated error in latitude correction is of the order of about $\pm$ 3.3×10^{-5} g.u. per 27km. For easy recognition of station locations, all gravity stations were established along rivers, road junctions, schools and near monuments such as Geji rock paintings (1100 A.D.) east of Geji village (fig. 3).

Altimeter readings were tied to several elevation bench marks in order to improve the accuracy of elevations of detail gravity stations. Height values determined with the altimeters were compared

with known bench mark values (Table 8). A maximum error of -2.012m and a minimum of -0.96m were estimated.

3.4 BASE STATION NETWORK

Two primary base stations located at Jos and Bauchi were used as control for the base stations established. The problem of re-setting the gravity meter at very short distances between base and detail stations because of the large gradient, made it impracticable to carry out the base network before the detail gravity observations. Thus both base and detail gravity stations were established simultaneously and loops established in the process using the ABABCBC technique (Nettleton, 1971). Gravity differences of the order of 1386 g.u. were recorded within a distance of 4km. The base network is shown in fig. 15. A maximum error of closure of 4.00 g.u. and a minimum of 0.0 g.u. were estimated for all the loops established on foot and by motor vehicles respectively.

Drift corrections were applied to all the observed readings. Assuming a linear drift in both the gravity meter and the altimeter at bases observed at intervals of less than three hours, using the relation below, the gravity difference G is computed as:

$$G = \pm \frac{(R_{G1} + R_{G2})\ K_G}{2} \quad \cdots\cdots \quad 3.2$$

where G = change in gravity value between two base stations A and B, RG_1 and RG_2 are changes in scale readings of the meter between the base stations (obtained from the drift curve), K_G is the instrument constant; and

TABLE 8

Comparison between benchmark values and altimeter readings in height determination

Benchmark No.	Altimetric Height (m)	Geodetic Height (m)	Error in Height (m)	Error in Bouguer Value (g.u.)
BM 10	652.27	653.23	-0.96	- 1.89
BM 31	726.80	727.42	-0.62	- 1.22
CSYP 612	667.48	669.49	-2.01	- 3.97

Compare with:

± 1.2m for stable periods and

± 2.5m for unstable periods
(Verheijen & Ajakaiye, 1980)

TABLE 9

Comparison of absolute gravity values obtained with respect to Jos and Bauchi primary bases

Base Station in Survey Area	Gravity Value w.r.t. Jos Value of 9778620.41 g.u.	Gravity value w.r.t. Bauchi Value of 9780285.90 g.u.	Error in absolute value (g.u.)
Galda	9780051.4	9780057.1	± 5.7
Zaranda Harbe	9780119.3	9780115.5	± 3.8
Zull	9780059.2	9780060.7	± 1.5
Bichiki	9780116.1	9780119.6	± 3.5
Geji	9780177.2	9780180.5	± 3.3
Hadambalamba	9780180.1	9780182.1	± 2.0

Why ±

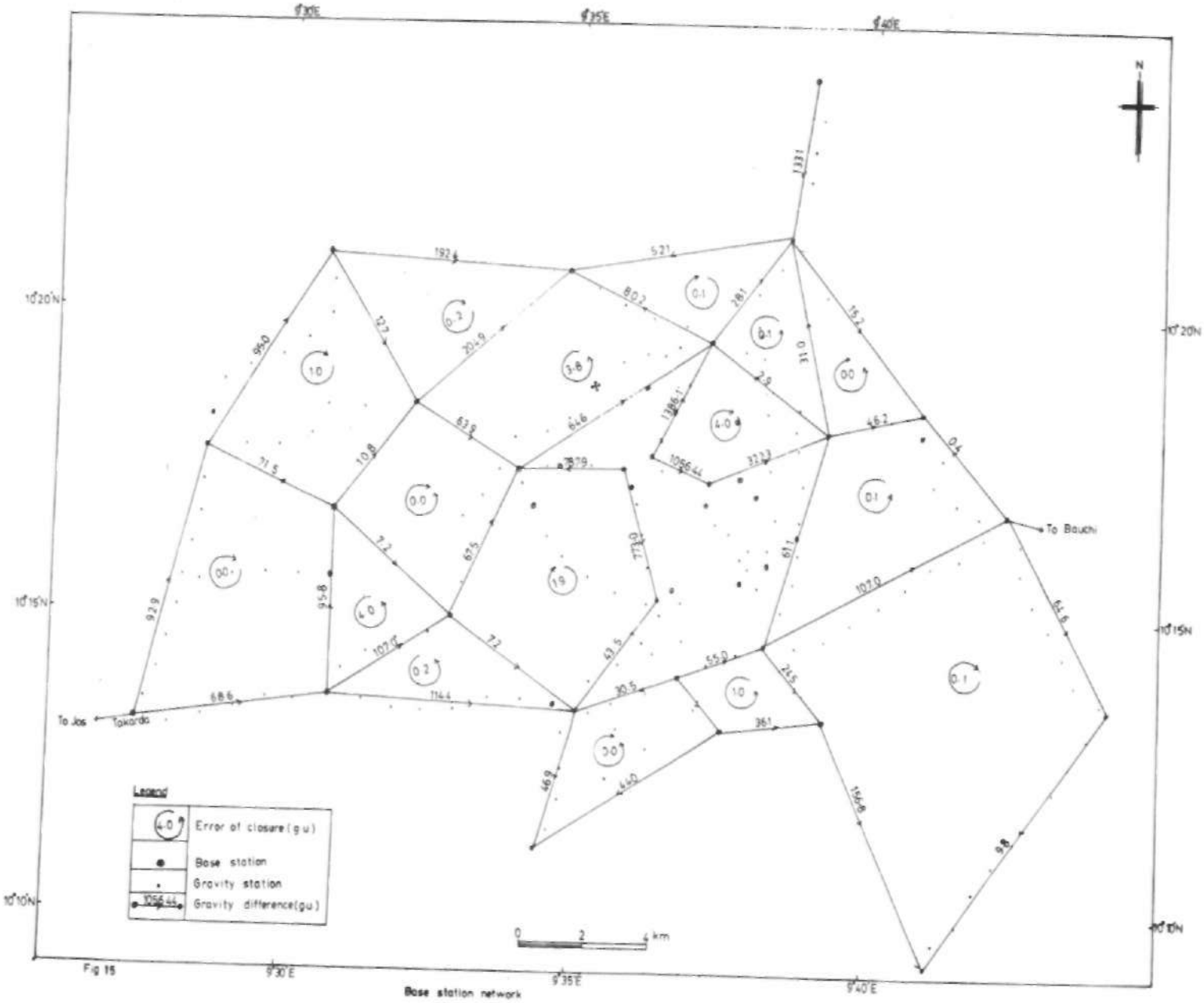


Fig 15

Base station network

$$u = \frac{(\bar{g}_B - \bar{g}_A) - (R_B - R_A) K_G}{t_B - t_A} \quad \ldots\ldots\ldots\ldots\ldots\ldots 3.3$$

where u is the drift rate between base stations A and B and $\bar{g}_B$ and $\bar{g}_A$; t_B and t_A and R_B and R_A are the absolute gravity values, times of observation and instrument readings at B and A respectively.

The absolute gravity values at detail gravity stations were computed from the relation:

$$\bar{g}_d = \bar{g}_A + u\,(t_D - t_A) + (R_D - R_A) K_G \quad \ldots\ldots\ldots 3.4$$

where $\bar{g}_d$ = absolute gravity value at an intermediate station D; R_D, t_D are scale reading and time of observation at detail Station D respectively.

3.5 HEIGHT DETERMINATION

In gravity surveys, height determination is very important because the gravitational potential depends on the distance between the element of the gravity meter and the attracting mass. This distance is measured in terms of the height between the plane of the gravity station and the sea level. Since the altimeters used in the survey give only relative height values, the readings were tied to known heights determined geodetically and located on several benchmarks along Jos - Bauchi road (Verheijen, Personnel communication). All altimeter readings were corrected for drift, relative humidity and temperature(Allan et al,1971). A procedure similar

to that used for the gravimeter was adopted in the determination of absolute heights of stations in which the difference in elevation between stations B_1 and B_2 is given by H

where:

$$H = \mp [(R_{B2} - R_{B1}) K_A H_F] \mp T_c \quad \ldots\ldots 3.5$$

and R_{B2}, R_{B1}, are scale readings at bases B_2 and B_1 respectively, K_A is scale constant, H_F and T_c are humidity factor and temperature correction respectively.

The mean of the elevations obtained from the two altimeters at each station was adopted as the elevation of the station.

3.6 COMPUTATION OF GRAVITY ANOMALIES

The gravity data were corrected for drift, latitude, free-air, Bouguer and terrain effects. It was necessary to apply terrain correction due to the rugged topography of the area where the complex outcrop. Sandberg (1958) proposed that where gravity stations are located near a high land mass, an inclined plane approximation represents more accurately the terrain near such stations than does the conventional block cylinder model, that is:

$$T_R = 2\gamma\varrho R [\pi - 2 \cos\theta K (\sin\theta)] \quad \ldots\ldots 3.6$$

where:

T_R = total terrain correction in mgals

R = radius in (cm) from the gravity station to the top of such an inclined plane

θ = slope angle

γ = gravitational constant

ρ = crustal density in gm cm^{-3}

$K(\sin\theta)$ = complete first order elliptic integral.

Based on the above relation, the terrain corrections covering Hammer (1939) zones A through H were calculated. The Hammer chart from zones I through M was used to compute the terrain corrections. A maximum terrain correction of the order of 78 g.u. was obtained at a station near the central part of the complex while values obtained for stations at distances of 3km from the complex have values not greater than 2 g.u. It was also noted that this maximum value was obtained at a station near the central and highest point in the complex.

The free-air anomaly was computed from the expression:

$$g_{FA} = g_{ob} - g_{th} + \frac{dg}{dz}(h) \quad \ldots\ldots\ldots \quad 3.7$$

while the Bouguer anomaly was computed from the relation expression:

$$g_{BA} = g_{FA} - 2\pi\rho G(h) + T_R \quad \ldots\ldots\ldots \quad 3.8$$

where:

g_{FA} = free-air anomaly

g_{ob} = observed gravity at a station

g_{th} = theoretical gravity value at a station

h = station elevation (m) above sea level

ρ = assumed crustal density of 2.67×10^{3} kgm^{-3}

$\frac{dg}{dz}$ = vertical gravity gradient given by -3.085963 $g.u.m.^{-1}$

G = universal gravitational constant

T_R = terrain correction at a station

$$2\pi\rho G(h) = 1.1154873 \text{ g.u.m}^{-1}$$

The theoretical gravity value at a given station of latitude θ was computed from the 1967 International Gravity Formula (IGF) given by:

$$g_{th} = g_o [1 + 0.005278895\sin^2\theta + 0.000023462 \sin^4\theta] \quad .....3.9$$

where: g_{th} is defined as in equation

g_o = equatorial gravity value based on the 1967 Gravity Reference System and given by 9780318.46g.u.

θ = latitude of a given station. Latitudes of stations were determined to the nearest hundredth of a minute, from four 1:50,000 topographic maps. The absolute values at base stations were used to determine the closure error in the loops (fig. 15) covering the area of survey. The adjusted values were used to determine the Bouguer anomaly at each station. The resulting anomalies were contoured manually (fig. 17) to give the map of Bouguer gravity anomaly.

3.7 ANALYSIS OF ERRORS

In gravity surveys error in Bouguer anomaly in a station result from the cummulative errors due to assumed density of the crust, latitude, elevation and terrain effect.

Error in elevation amounted to ±2.012m. Assuming this value to be the maximum error, then the maximum error in Bouguer correction is ± 3.965 g.u. and the error in free-air correction is 6.21 g.u.

This error of - 2.012m was considered reasonable since Verheijen and Ajakaiye (1980) determined a maximum error of - 1.20m in height for the province. This error of - 2.012m was obtained by using standard elevation bench marks located throughout the survey area as has been explained in the section for height determination.

The error in latitude was estimated by using the accuracy factor of ±11m for the topographic maps used in the survey, assumed earth radius of 6,400km, determining the change in latitude as a result and making use of equation 3.9. Thus the error in latitude was estimated as contributing only $\pm$ 3.3 x 10^{-5} g.u. per station and was considered negligible.

The error contributed due to the assumed mean crustal density of 2.67 x 10^3 kg m^{-3} was ignored because the mean density for the host migmatitic gneiss was estimated to be 2.68 x 10^3kg m^{-3}, while the mean density for all the rock samples in the survey area was estimated to be 2.686 x 10^3 kg m^{-3}. Thus the mean density for the rocks of the survey area was considered very close to the mean crustal density.

The use of Jos and Bauchi as primary base stations for the survey gave nearly the same absolute gravity value for one of the base stations. With only a difference of 5.7 g.u. when the absolute value was tied to Jos and Bauchi respectively, it was assumed that the values for the estimated absolute gravity in the area of survey were reasonable(Table 9).

However the errors that would have been contributed from drifts and terrain effects were reduced to the barest minimum as a result of application of drift and terrain corrections as explained in the preceeding section.

CHAPTER FOUR

DENSITY DETERMINATION

4.1 INTRODUCTION

In principle, interpretation of gravity data depends directly on the density contrast between adjacent rock units. The accuracy of Bouguer anomalies in any gravity survey depends greatly on the accuracy of assumed rock densities where such rocks do not outcrop and more precisely on the accurate density determinations of the rock units where either the rocks outcrop or borehole data are available. Gustaf (1967) proposed that the emplacement of acid intrusions depends on the density of the intruding rocks. The flow structures often observed on metamorphic terrains result from direct density contrast between low density leucocratic minerals and high density melanocratic ones. Hot spotism and emplacement of upper mantle material in continental drift areas have much to do with the contrast in density between peridotites and lower crustal material such as granites which have lower density value than the former.

A density contrast of the order of $\pm$ 0.06×10^{3} kgm^{-3} is sufficient to cause appreciable Bouguer anomaly (Gustaf, 1967; Ajakaiye, 1970).

It was not possible to carry out insitu density determination due to lack of borehole data and equipment at the time of the survey. Therefore rock samples were systematically collected as described by Lahee (1931) during the field trip. On analysis and identification, it was found out that out of the 122 fresh samples collected, 37 were syenite, 10 were porphyritic granite, 12 were

aphyric trachyte, 18 were migmatitic gneiss, 30 were muscovite biotite older granite, 11 were basalt and four were dolerite. The rock association presented above clearly shows that the area surveyed is a metamorphic terrain with acid and basic intrusions.

4.2 DENSITY MEASUREMENTS AND RESULTS

Due to inavailability of borehole data and inability to carry out insitu density determination, laboratory method which employs the principle of Archimedes was used. Samples were first dried in air for seven days and both dry and saturated densities of the individual rock samples were determined with an electronic digital balance model No. PS 15.

Firstly the samples were weighed in air and then weighed while in water of density $1x10^3$ kgm^{-3}. The samples were then soaked in water for 48 hours and their wet densities determined using the following relation:

$$\rho_D = \frac{Wa}{Wa - Ww} \qquad \ldots\ldots\ldots 4.1$$

$$\rho_W = \frac{Wa}{Wa - Ww} \qquad \ldots\ldots\ldots 4.2$$

where:

ρ_D = dry density of a given sample

ρ_w = saturated density of the same samples

Wa = weight of sample (dry or saturated) in air

Ww = weight of sample (dry or saturated) in water

the value $\frac{\rho_D + \rho_w}{2}$ was taken as the mean density of the sample of a given rock unit.

Two main rock types, metamorphic host rock and igneous rocks were deduced from the measurements and analysis. The igneous rock unit is subdivided into acid igneous and basic igneous rocks. The calculated mean density for the migmatitic gneiss is $(2.68 \pm 0.03) \times 10^3$ kgm^{-3} form a total of 18 samples (Table 10). The histogram for the gneiss shows a bimodal distribution which is consistent with the two types of gneiss encountered in the field(fig.16c) The density of the 30 samples of muscovite-biotite granite $(2.57 \pm 0.02) \times 10^3$ kgm^{-3} and the histogram for these show a different distribution from that of the gneiss(fig 16f)

The histogram of the syenite samples show near normal distribution. The modes are probably due to sampling or errors in measurements of densities. These modes indicate values of mean densities of $(2.62 \pm 0.03) \times 10^3$ kgm^{-3}, $(2.65 \pm 0.03) \times 10^3$ kgm^{-3} and $(2.68 \pm 0.03) \times 10^3$ kgm^{-3} respectively (fig.16a). A mean value of $(2.62 \pm 0.03) \times 10^3$ kgm^{-3} was obtained and the histogram shows a near normal distribution about this value.

The more or less bimodal distribution in the histogram is indicative of probably two varieties of syenite. These two varieties are the olivine-hornblende-rich and the olivine-hornblende poor and the distribution in their densities is related to their mineralogical and chemical differences (Tables 1, 10, Appendix II).

A comparison of the density distribution $(2.55 - 2.69) \times 10^3$ kgm^{-3} of the syenite from the Zaranda complex and the values of $(2.65 - 2.89) \times 10^3$ kgm^{-3} got by Ajakaiye (1970) from the Younger Granite province (Table 11) shows that the syenites of the

TABLE 10

Densities of Rock Types

Rock Type	Number of Samples	Range in Densities x $10^{3}kgm^{-3}$	Average Density x$10^{3}kgm^{-3}$	Difference Between Dry and Saturated Densities x $10^{3}kgm^{-3}$	Standard Deviation x $10^{3}kgm^{-3}$
Dolerite	4	2.91 - 2.92	2.92	0.01	0.01
Calcitic Basalt	11	2.73 - 2.79	2.76	0.01	0.02
Olivine Basalt	6	2.83 - 2.93	2.87	0.01	0.01
Porphyritic Granite	10	2.49 - 2.55	2.51	0.01	0.01
Syenite	37	2.56 - 2.69	2.62	0.02	0.03
Trachyte	12	2.48 - 2.59	2.56	0.02	0.04
Muscovite-Biotite Older Granite	30	2.54 - 2.63	2.57	0.02	0.02
Migmatitic Gneiss	18	2.64 - 2.75	2.68	0.01	0.03

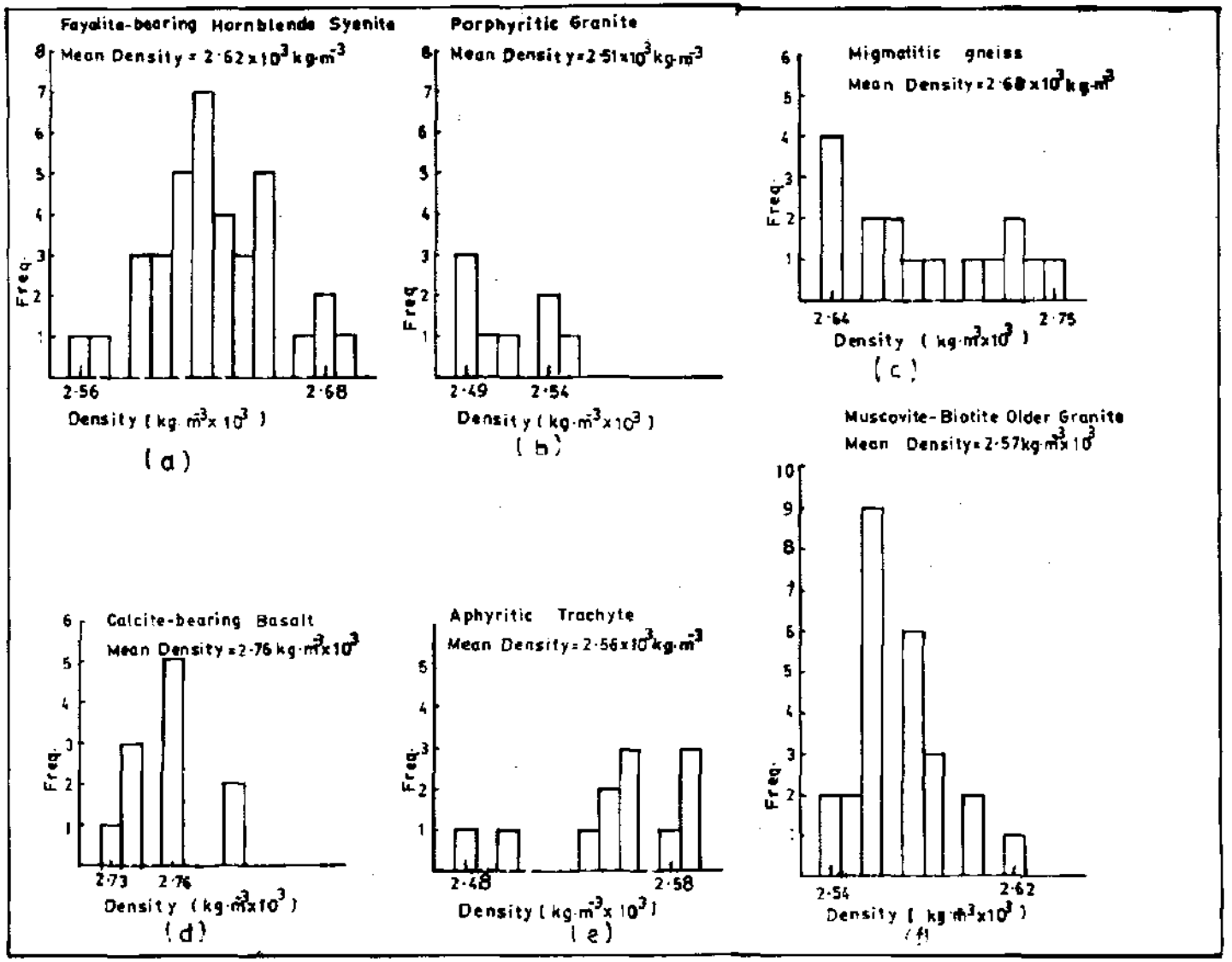


Fig 16 Density histograms of rock types

TABLE 11

Comparison between rock densities in the Younger Granite Province and those of the Zaranda complex

Rock Type	Younger Granite Province*		Zaranda Complex	
	Range x 10^3 kgm^{-3}	[Mean ± std dev	Range x 10^3 kgm^{-3}	[Mean ± std dev
Dolerite	2.88 - 3.04	2.97 ± 0.05	2.91 - 2.92	2.92 ± 0.01
Basalt (a) Calcitic	2.59 - 3.02	2.85 ± 0. 1	(a) 2.73 - 2.79	2.76 ± 0.02
" (b) Olivine	----	----	(b) 2.83 - 2.93	2.87 ± 0.01
Granite Porphyry	2.53 - 2.70	2.61 ± 0.04	2.49 - 2.54	2.51 ± 0.01
Syenite	2.65 - 2.87	2.70 ± 0.05	2.55 - 2.67	2.62 ± 0.03
Older Granite	2.59 - 2.82	2.66 ± 0.05	2.54 - 2.62	2.57 ± 0.02
Migmatitic Gneiss	2.57 - 2.96	2.69 ± 0.06	2.64 - 2.74	2.68 ± 0.03

* (After Ajakaiye, 1970)

TABLE 12

Comparison of rocks of the Zaranda complex with those typical of of the Younger Granite province

Phase	Rock types in the Younger Granite province *	Equivalent rock types in the Zaranda complex
Acid	Basalts and dolerites. Fine grained granite. Granite porphyry. Microgranite.	Dolerite and olivine basalt, porphyritic granite and pegmatite.
Intermediate	Andesite Quartz monzonite Augite dunite Hornblende granite Augite syenite Quartz syenite	Quartz syenite Hornblende - faylite syenite
	Olivine gabbro Olivine dolerite Olivine basalt	Precaldera aphyric trachyte

* Data for the Younger Granite province adapted from (Falconer et al, 1923)

Zaranda complex are less dense than those from the other parts of the province. This difference is possibly due to the fact that the Zaranda syenites contain a fair amount of quartz (5 - 10%) and more perthites.

The 10 samples of porphyritic granite have a mean density of $(2.51 \pm 0.01) \times 10^3$ kgm^{-3} (fig. 16). The apparentlylow density is probably due to the presence of two predominant minerals, quartz and feldspar which have identical density value of $(2.5 - 2.6) \times 10^3$ kgm^{-3}. (Telford, 1976).

From a total of 12 samples, a mean density of $(2.56 \pm 0.04) \times 10^3$ kgm^{-3} was obtained for the aphyric trachyte. The high standard deviation is a result of mineralogical variations in the samples collected and the highly fractured nature of the samples; for example, some of the samples have large prisms of sanidine (density = 2.5×10^3 kgm^{-3}) but others have little or no such large phenocrysts at all.

Two varieties of basalts were recorded in the survey. The calcite variety has a mean density of $(2.76 \pm 0.02) \times 10^3$ kgm^{-3} while the olivine variety has a mean value of $(2.87 \pm 0.03) \times 10^3$ kgm^{-3}. The low density of the calcitic basalt results from the presence of large calcite crystals (Plate 8) of density 2.58×10^3 kgm^{-3} that are evenly distributed over any given sample. The slightly higher density of the olivine variety results from the widely distributed grains of olivine of density 3.0×10^3 kgm^{-3} in each sample. The four samples of dolerite gave a mean density of $(2.92 \pm 0.01) \times 10^3$ kgm^{-3}. This is a basic rock and the preponderance of olivine and iron material in the samples with uniform

mineralogy contribute to its high mean density.

A comparison between the densities of rocks determined by Ajakaiye (1970) in the Younger Granite province (Table 11) and those determined in the present survey over the Zaranda complex shows that the density values for the rock units in the area fall within the range of values for similar rock types in the Younger Granite province.

4.3 ERROR IN DENSITY DETERMINATION

Errors in density determination are grouped under the following categories:

(a) instrument error and

(b) error due to weathering and porosity of the rock samples.

Instrument Error

The digital balance used in the determination of the densities of the rock samples has an accuracy of 1.0×10^{-3} kg for any given sample. Most of the samples used for the density determination weighed between 3.0 kg and 4.0 kg. Thus for a particular dolerite sample which weighed 3.5kg in air and 2.301 kg when immersed in water, using equation 4.1, a density value of $(2.92 \pm .004) \times 10^{3}$ kg m^{-3} was obtained.

Weathering and Porosity

Error in density values may arise due to weathering which leads to a change in the chemical composition of the samples from outcrops. The state of weathering of the selected samples was found to be within the tolerable limit for density determination. This was determined by considering both in hand specimen and under microscope

the alteration products of some minerals; e.g. augite, which weathers to iron oxide and lends brown colour to the rock in which it occurs. This was found to be the case with a few dolerite and syenite samples before the final selection of samples was done for density determination.

Porosity of samples may be increased by increasing the cracks in them. Such cracks can only result when samples are strained by hammering. This process was minimized by avoiding repeated and severe hammering on samples. When the porosity of rocks is reduced by compaction as in deep burial, then density increases, but this is only noticeable to a greater extent in sedimentary rocks. Pettijohn (1975) gave an expression relating the porosity (P) of rocks in terms of depth of burial as given below:

$$P = pe^{-bx} \qquad \ldots\ldots\ldots\ldots 4.3$$

where: P = porosity of a given rock sample at a depth of X units of depth.

p = average porosity of surface clays

b = constant

Compaction due to depth of burial is usually negligible in igneous rocks and is much more negligible when only fresh samples are considered. Thus errors arising from compaction were deemed negligible since fresh samples were collected at the surface and the problem of burial for the Zaranda rocks was neglected more so when all the samples were identified as being igneous rocks.

Densities of the same rock type may vary appreciably from province to province due to differences in mineralogy, chemistry, rate of metamorphism and intensity of tectonic forces. The greater the area covered in a given petrological or [igneous province], the greater the range in density values as reflected in the standard deviation values. A careful study of Table 10 reveals that the standard deviation values obtained in the Zaranda complex are quite less than those of Ajakaiye (1970) that covered a wider igneous province. Even from a small area of survey as the Zaranda, complexity in mineralogy leads to higher standard deviation values. This fact is evident from a study of the trachyte (Appendix II and Plates 3 and 8) where low density zenolith of calcite or sanidine are enclosed in a basalt of higher density and the distribution over various samples is not uniform. The various rock types and their density values are given in Tables 11&12 and the values obtained for the various rocks in the complex (trachyte, basalts, syenite, granite and dolerite) are typical for these rock types in the Younger Granite province as determined by Ajakaiye (1970).

In the Zaranda complex, mineralogical differences among rock samples of the same rock unit were considered to be the main causes of density variation in such samples.

CHAPTER FIVE

INTERPRETATION

5.1 THE BOUGUER GRAVITY FIELD

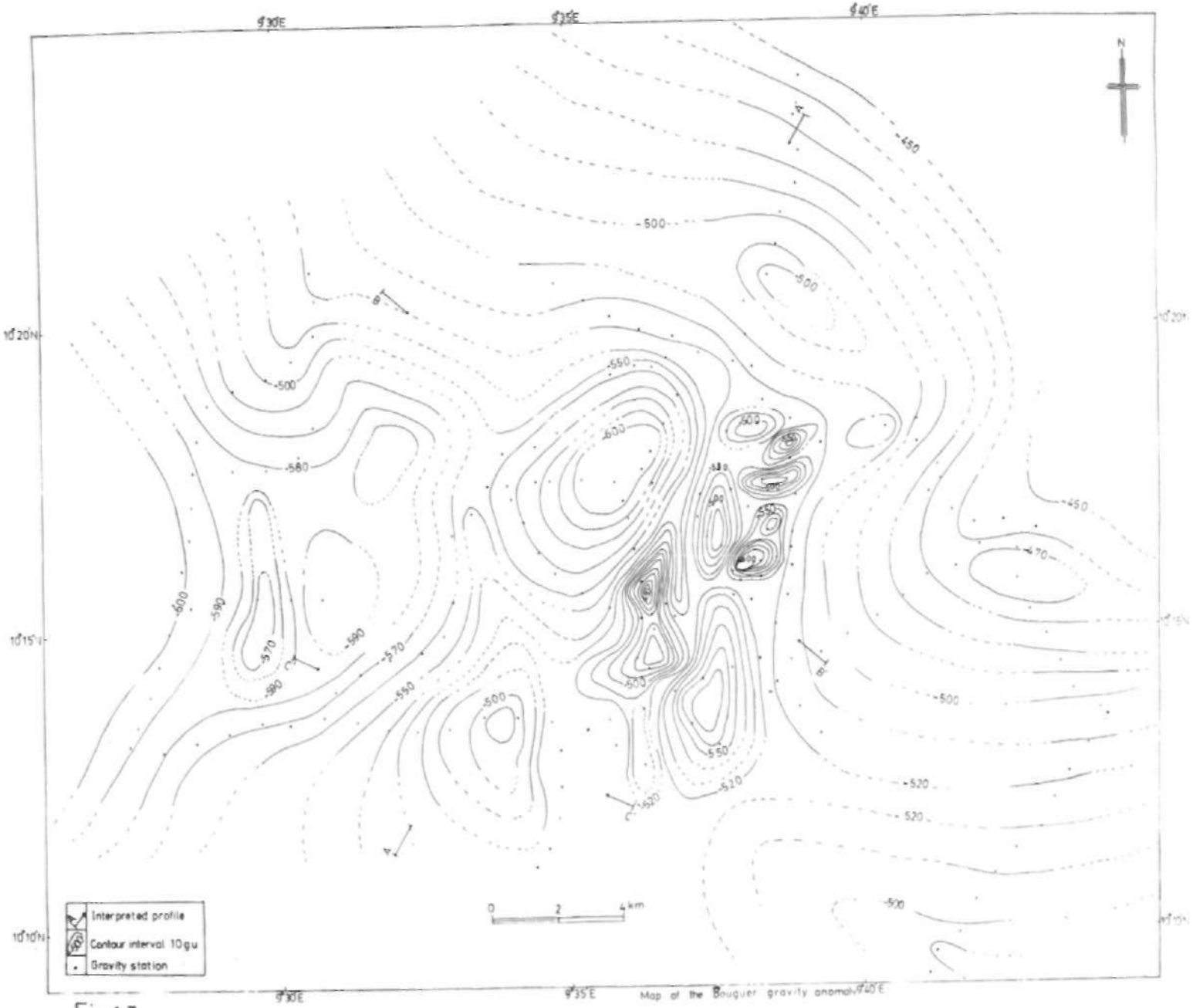
The main features of the Bouguer gravity anomaly shown in Fig. 17 are:

(a) A broad negative anomaly of over -600 g.u. trending NNE - SSW in the centre of the complex. The magnitude of this field along an ESE - WNW is also over -600 g.u. but the size is smaller. While the size in an ESE - WNW profile is 5km, this is increased to about 8km in the NNE - SSW profile.

(b) A relatively smaller anomaly of approximately -480 g.u. located at about 2km SE of the -600 g.u. anomaly and also trending in the NNE - SSW.

(c) At some 4km east of the -600 g.u. anomaly, a series of negative Bouguer anomalies ranging from -570 to -600 g.u. are separated from the main anomaly of -600 g.u. by the smaller anomalies of -480 g.u. These series also trend as the main anomaly.

(d) At some 6km west of the main anomaly there is a broad negative anomaly of over -600 g.u. separated from the main anomaly over the complex by a -570 g.u. N-S trending anomaly. This -570 g.u. anomaly lies over the Zaranda village.



Map of the Bouguer gravity anomaly

Fig 17

(e) The trends of these anomalies have about 90% correlation with surface geology (Fig.20) and also correlate with the observed Bouguer gravity and geological map (Ajakaiye,1970; Fig. 1).

5.2 REGIONAL ANOMALY SEPARATION

In gravity surveys, deep-seated and large scale structures of non-interest uaually mask the shallow-seated ones of interest to the investigator (Telford, 1976; Dobrin, 1976). The process of removal of the effects of these large scale anamalies of non-immediate interest is still a great problem in gravity interpretation. Usually the process of removal of these regional anomalies, as they are called, involves filtering whereby the effect of these large scale features are removed. Some of these processes include visual smoothening, analytical methods, second derivatives, upward and downward continuation. The choice of a particular method depends on factors like size of anomaly, data acquisition method, purpose of the survey and the availability of additional geological control. The choice of any method also depends on the experience of the investigator. In the analytical method where the residual anomalies are assumed to be random errors of some degree, polynomial fitting of low order (first and second) may not apply. This is particularly so in a survey where the gravity data

was not collected on a regular grid and in an attempt to digitize, a lot of extrapolation error is introduced. In this survey, the area investigated was small in comparison to the Younger Granite province where definite regional gravity values were adopted in some cases (Ajakaiye, 1970).

The geology of the area under the present investigation is complex and as such using a definite order of polynomial in the analytical method may not be adequate to remove the regional anomalies.

The graphical method was therefore used because:

(a) the regional trends were evident from both the geological gravity map of Ajakaiye (1970,fig. 1) which covers the present area of investigation and from the observed Bouguer gravity anomalies in the survey area shown in fig. 17. Thus a comparison between the trends of these regionals suggests the use of the graphical method of regional-residual anomaly separation which the author has adopted in the area of survey.

(b) due to the complex geology of the area, local closures were randomly distributed, thus making the estimation of regional trends easier. Eight random profiles were chosen to cover the entire area. The values of the regionals along these profiles were plotted, contoured and smoothened to generate the regional map (Fig. 18). The residual anomalies were then obtained by subtracting the regional trend from the observed bouguer gravity anomalies (Fig. 19). Although the method of regional anomaly separation is biased, the additional information deduced from the supplementary geological mapping carried out by the author helped minimize errors.

The maximum range of anomalies in the bouguer gravity field is about 180 g.u; the highest and lowest observed bouguer values being -613 g.u. and -433 g.u. respectively. Thus a regional gradient of -180 g.u. in about 40km distance (4.5 g.u. km^{-1}) was estimated in the area. The average observed bouguer value in the survey area was estimated at about -525 g.u. This value was found to be close to the value of -500 g.u. for the Younger Granite province. The average trend of the regional field was estimated as N45°W. This trend was also found to be consistent with that of Ajakaiye (1970) in the Younger Granite province and estimated at N50°W. This trend is parallel to the Quartenary basalt flows in the Jos area (Wright, 1976).

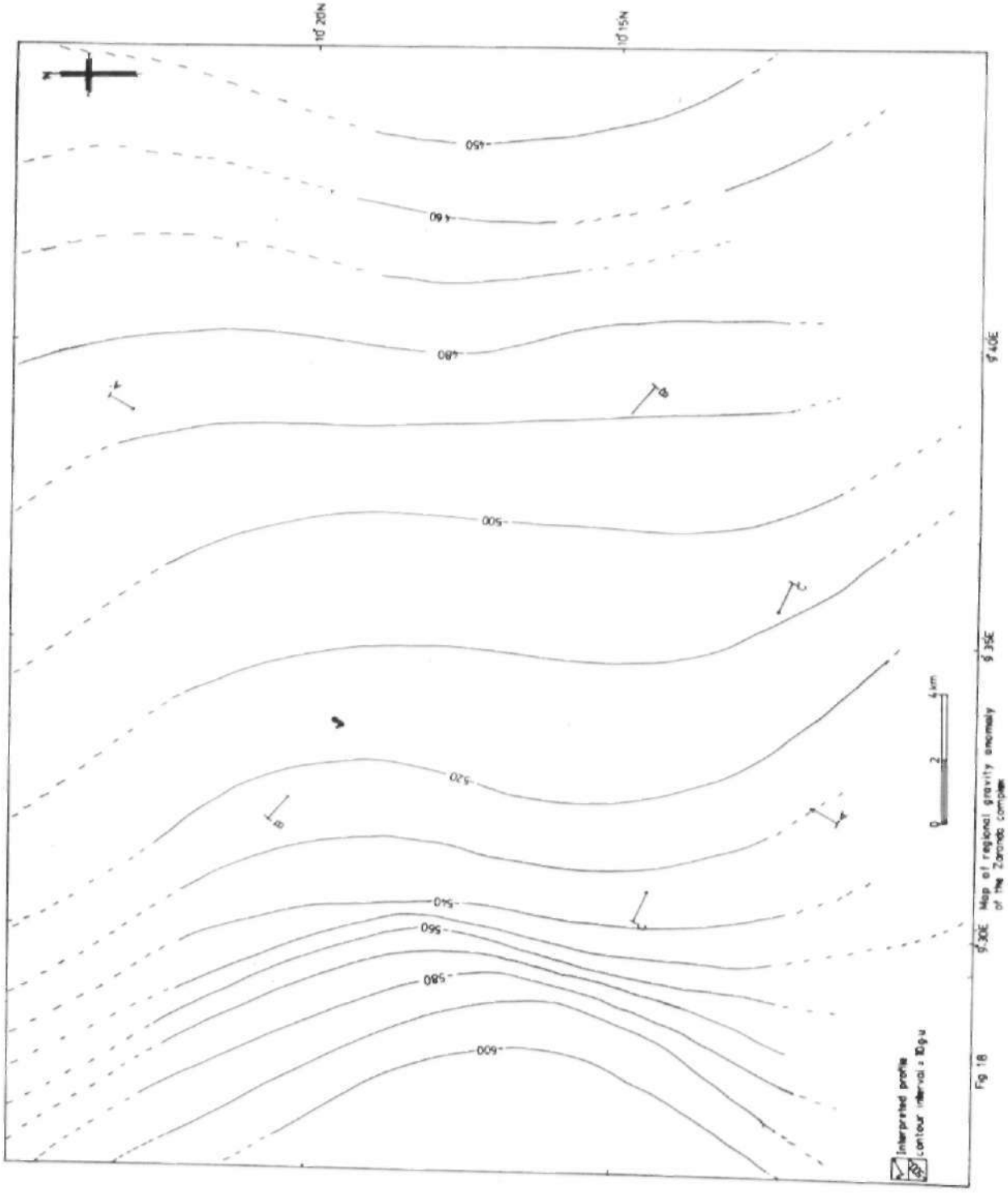


Fig 18 Map of regional gravity anomaly of the Zarand complex

5.3 RESIDUAL GRAVITY ANOMALIES AND QUALITATIVE INTERPRETATION

The main features of the residual anomaly shown in Fig. 19 are:

(a) A large central, fairly symme trical low gravity anomaly with an amplitude of about 106 g.u. and centred on the aphyric trachyte (Fig. 20).

(b) Anomaly size of about 5km in the WNW direction (profile $B-B^1$) and about 7km in the NNE direction (profile $A-A^1$).

(c) About 3km SE of the larger central anomaly a relatively low anomaly of amplitude -80 g.u. and size of about 1km is located near an outcrop of porphyritic granite (Durji Hill).

(d) The 106 g.u. and -80 gu anomalies are separated by isolated positive residual anomalies of amplitude ranging from 17 g.u. to 52 g.u. which correlate with mapped basic intrusions of basalts and dolerite rocks.

(e) About5km west of the main central anomaly a small positive anomaly of about 10 gu which correlates with the calcite-bearing basalt is located over the Zaranda village (Fig. 3 & 20).

Thus the main negative anomaly of acidic rock is flanked on the east, west and south mainly by positive anomalies caused by intrusive basic rocks. These features are the basis on which the three profiles $A-A^1$, $B-B^1$ and $C-C^1$ were selected for interpretation.

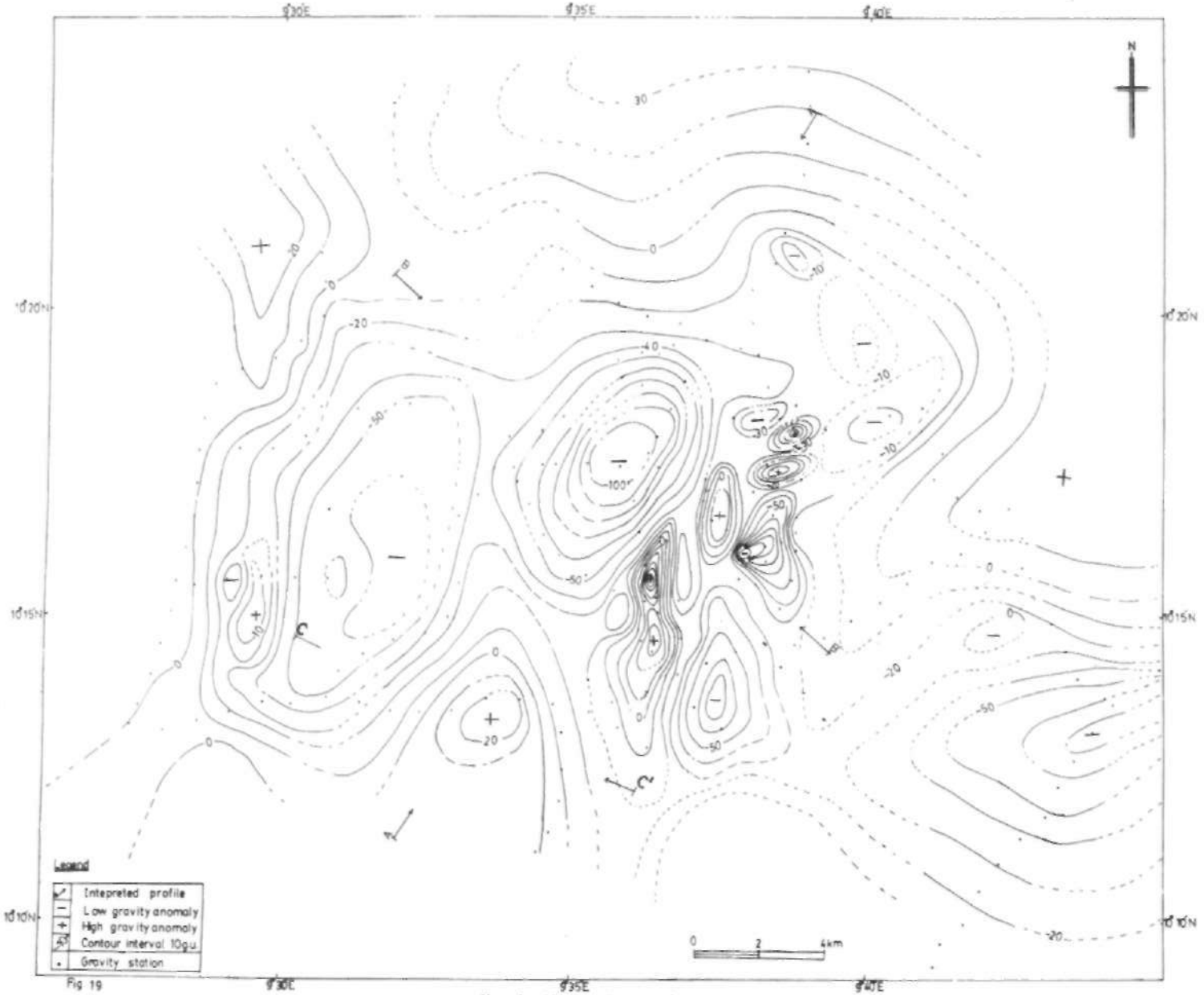


Fig 19

Map of residual gravity anomaly

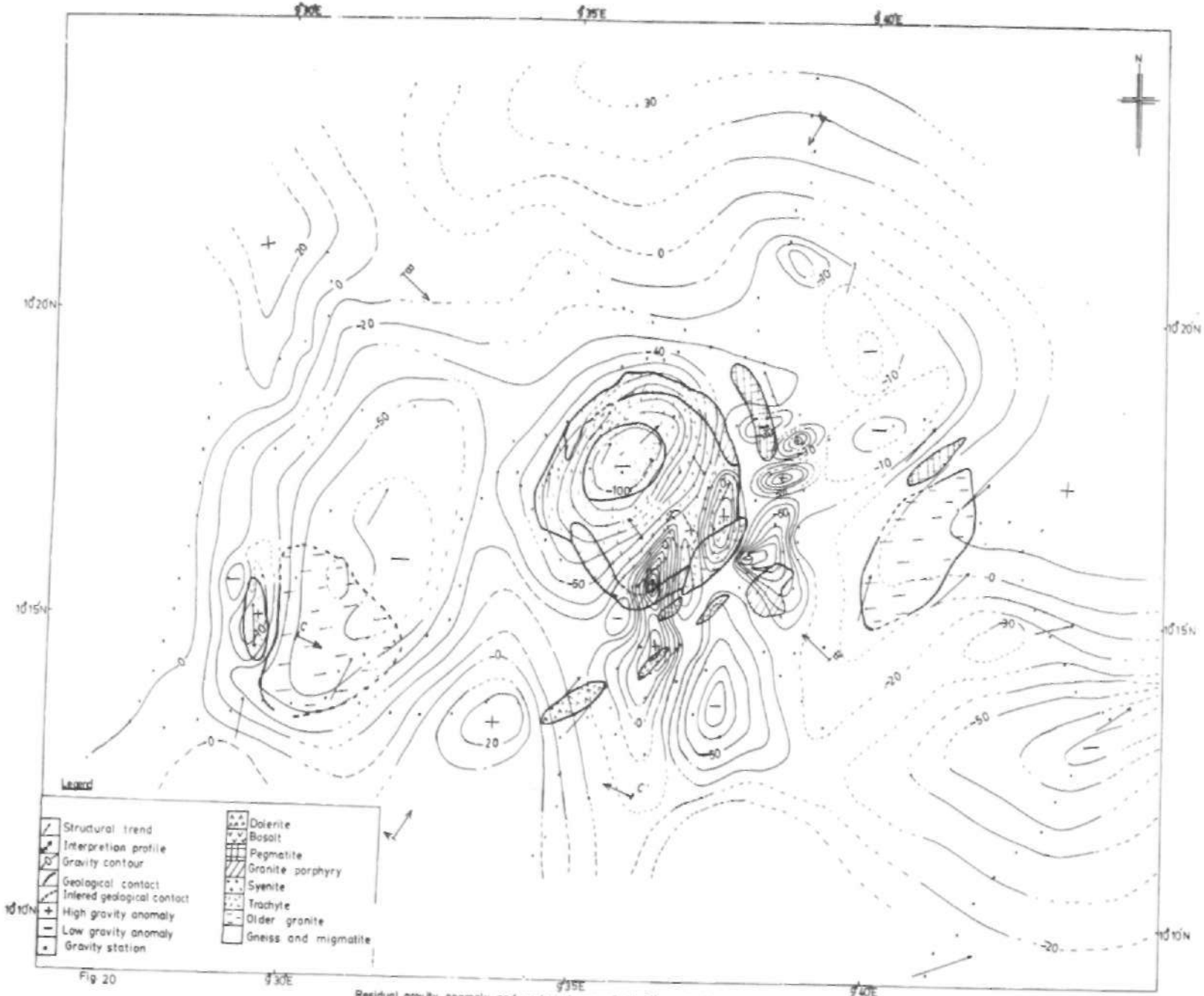


Fig 20

Residual gravity anomaly and geological map of the Zaranda Younger Granite ring complex.

Profile A-A^1 is approximately 30km, trends SSW - NNE and cuts across main residual anomaly discussed above. Along this profile, the maximum anomaly does not appear to be centred on the outcrops. This may indicate the subsurface trend and extent of the rocks which outcrop in the area.

Profile B-B^1 is about 20km long trends WNW - ESE and is perpendicular to Profile A-A^1 (Fig. 20). It cuts across the major rock units and the basalt outcrop some 3km SE of the complex discussed earlier.

Profile C-C^1 is about 9km long and cuts across the positive closure that exist south of the complex (Fig. 19). The main features are shown. Two rock types are shown with only the older granite outcroping along this profile. A residual anomaly of 10 g.u. observed over the basic rock location while a value of about -65 g.u. is centred on the older granite. The densities of these rocks are (2.92 and 2.58) x 10^3 kgm^{-3} respectively.

5.4 QUANTITATIVE INTERPRETATION OF RESIDUAL ANOMALIES

5.4.1 Introduction

Basically, the aim of any quantitative interpretation of gravity data is to present an acceptable model of the anomalous body suspected to be the cause of the residual field. Simple geometric shapes are assumed and the gravity effects of such shapes representing the anomalous mass calculated. Although it is possible to obtain a particular solution to a set of potential data displayed by the

anomaly field, there is no unique solution to such potential field data. This is because gravity effect of any body depends on many parameters which cannot easily be determined (Telford et al, 1976 ; Dobrin, 1976). These parameters include:

(a) depth of burial

(b) thickness of the anomalous mass

(c) lateral extent

(d) density contrast between the body and the host rock

(e) complexity in geology

(f) shape of the body

The number of these unknown parameters can greatly be reduced from density profiling, additional geological control relating to lithology, structural data and supplementary as discussed earlier.

5.4.2 Two and Three Dimensional Models Along Interpreted Profiles

Both two and three dimensional model interpretations were carried along Profiles A-A^1, B-B^1 and C-C^1 and were qualitatively described in the preceding section. However, the two-dimensional model interpretation served as a control for the subsequent three-dimensional models. Right vertical cylinders were used as the three-dimensional models based on:

(i) closure patterns of the bouguer and residual fields;

(ii) results of structural data analysis which yielded dip values ranging from 75% to 90% and thus assumed to be due to near vertical intrusions;

(iii) circular outcrop; and

(iv) models used by previous workers (Ajakaiye, 1974)

Three different rock types, in addition to the host migmatitic gneiss, have been identified and chosen for modelling along Profile $A-A^1$. These include:

(a) the Zull dolerite ($\varrho = 2.92 \times 10^3$ kgm^{-3}) with a density contrast of 0.24×10^3 kgm^{-3};

(b) the fayalite-hornblende syenite ($\varrho = 2.62 \times 10^3$ kgm^{-3}) with a density contrast of -0.06×10^3 kgm^{-3} ;

(c) the precaldera aphyric trachyte ($\varrho = 2.56 \times 10^3$ kgm^{-3}) with a density contrast of -0.12×10^3 kgm^{-3}. The values of the above density contrasts were similar to those of Ajakaiye (1970).

A two-dimensional program (Nagy, 1964) modified by Ojo (Personal communication) which calculates the gravitational attraction of polygonal bodies of arbitrary shapes and a three-dimensional program for a right vertical cylinder (Osazuwa, personal communication) were used for the models. The models with the best fit show that the syenite is tabular (Fig 21) with a maximum depth of 5.5km to its base while the depth to the bottom of the trachyte body is 2.5km. These two bodies were mapped as outcroping over a profile length of 6km with the trachyte occupying the central region (Figs. 21 & 22). The dolerite body located at about 3km south of the complex outcroped at a distance of 500m from the profile and along the profile $A-A^1$ was modelled as a domed structure (Lopolith) of thickness 1km and extending towards the syenite body. It is buried at a depth of 500m below the surface.

A density contrast of -0.10×10^3 kgm^{-3} between the porphyry granite and the host rock was used in the two and three-dimensional interpretation. Along Profile $B-B^1$, the main anomalous body appears

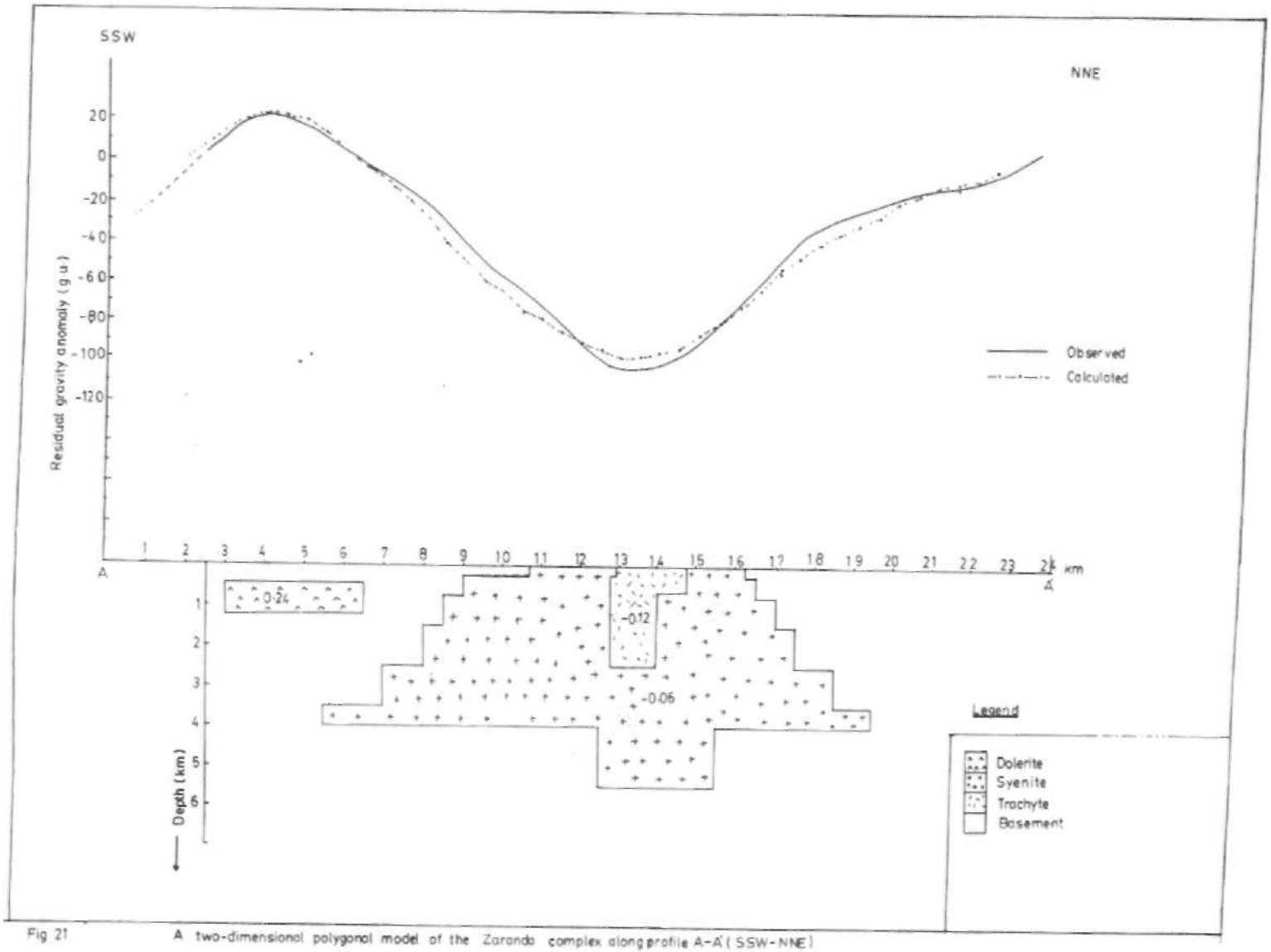


Fig 21 A two-dimensional polygonal model of the Zaranda complex along profile A-A' (SSW-NNE)

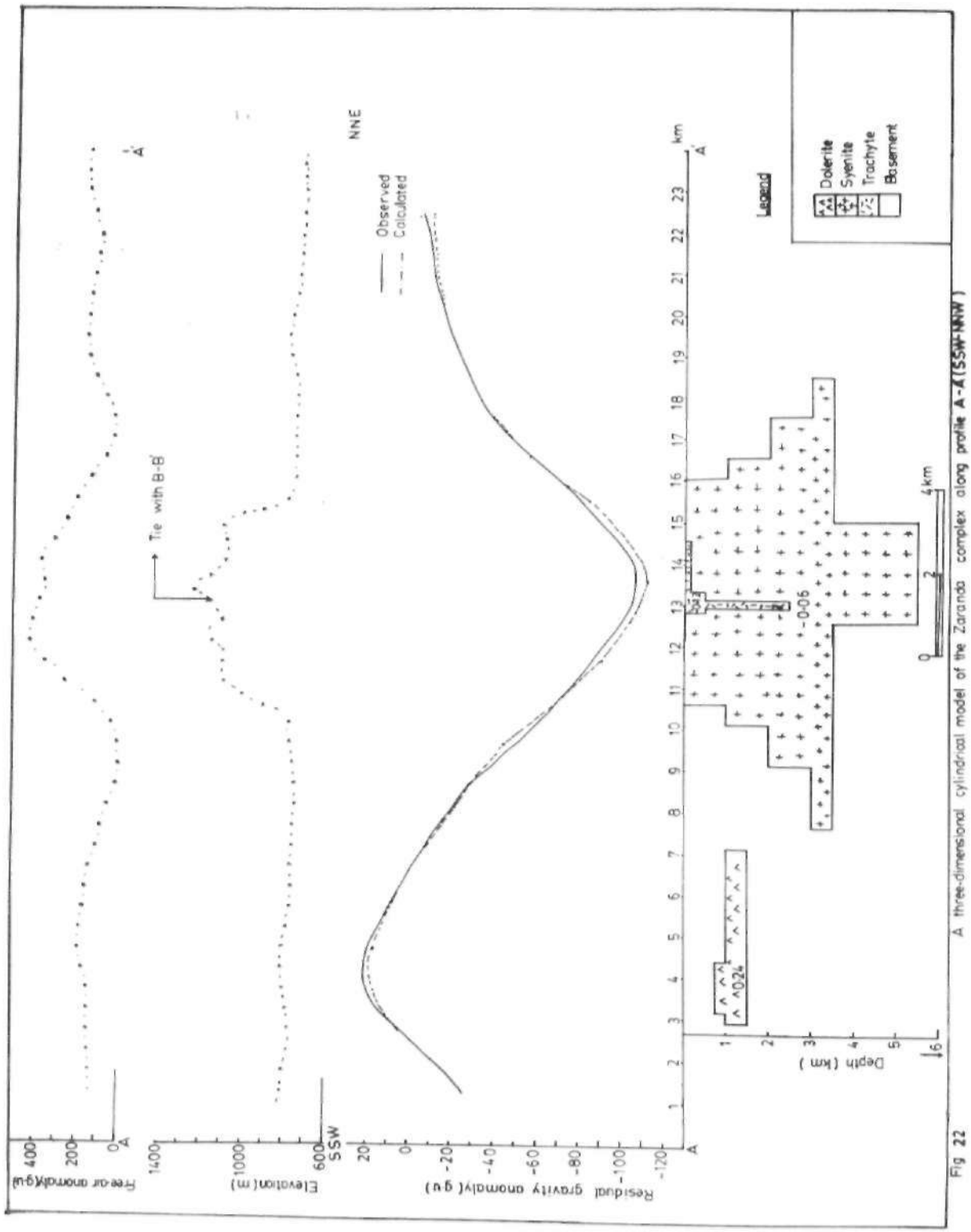


Fig 22 A three-dimensional cylindrical model of the Zarando complex along profile A-A'(SSW-NNW)

to be circular while the granite porphyry was modelled as a vertical intrusion outcroping and extending to depth of about 2km (Figs. 23 & 24).

It is interesting to note that along Profile B-B^1, the modelled width of the syenite body compares very well with the outcrop distance on this same profile of about 6km. It is observed that the thickness modelled for the porphyritic granite along Profile B-B^1 is not the true thickness because the profile does not cut across the centre of the closed residual anomaly.

A three-dimensional interpretation along Profile C-C^1 indicated the following:

(a) a section of the syenite unit underlies the dolerite. This section was assumed to be reasonably located because Profile A-A^1 ties with C-C^1 nearer the west of C-C^1 than to the east (Fig. 25), and the behaviour of the syenite mass beyond the end A could not be determined. The presence of this rock unit generated a better fit to the observed anomaly;

(b) at the central part of the profile a dolerite body, possibly a lopolith rather than a dyke corresponding to a gravity anomaly of about 20 g.u. is buried at a depth of 500m;

(c) at some 11km east of Profile C-C^1 is an older granite body buried at a depth of 250m and modelled as a thin body along this profile with an amplitude of about -32 g.u. in the residual gravity anomaly.

5.5 FREE-AIR AND BOUGUER ANOMALY CORRELATION

There is an inverse relationship between the Bouguer and free-air anomalies in the Zaranda area. The Bouguer and free-air anomaly maps

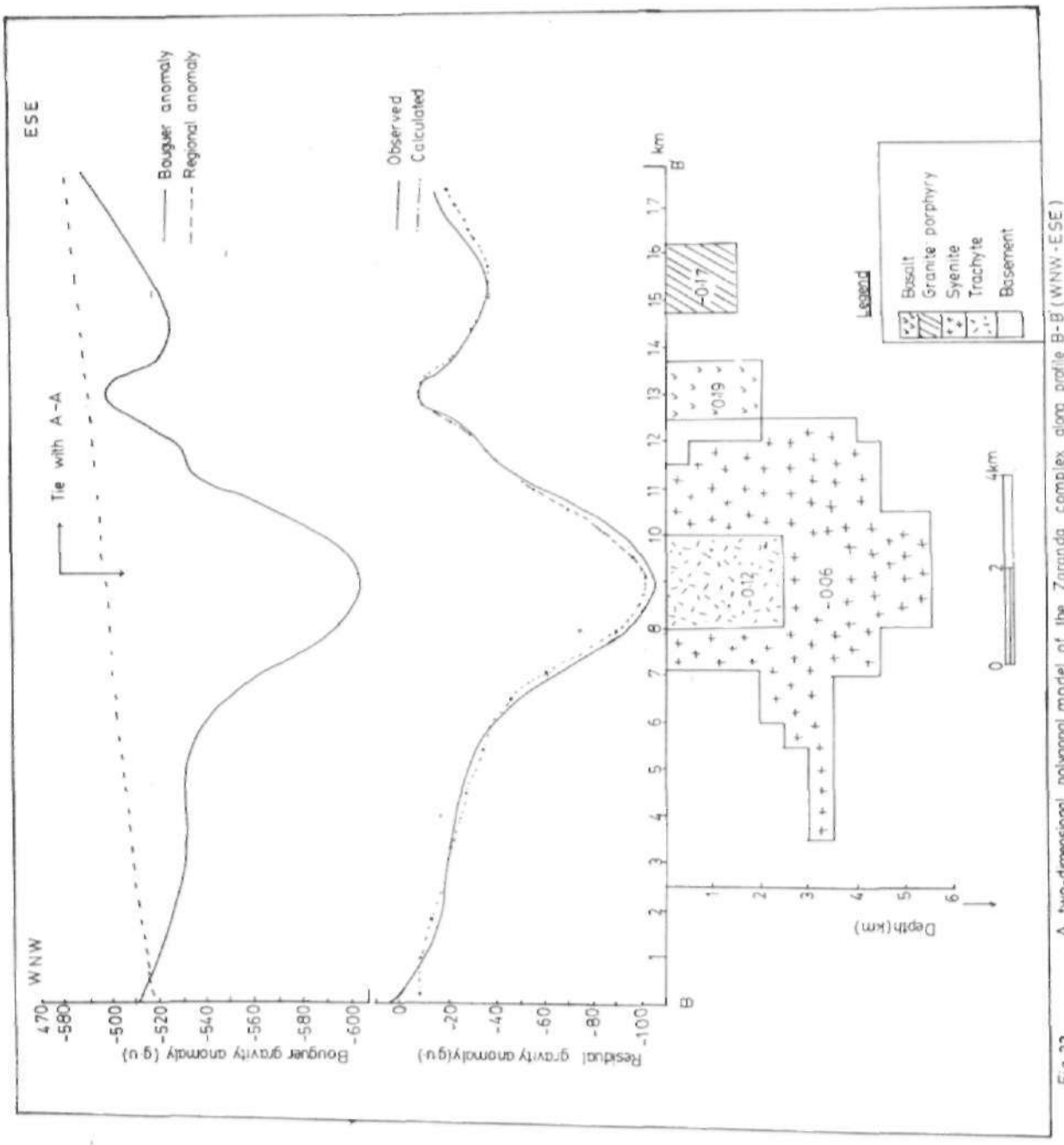


Fig 23 A two-dimensional polygonal model of the Zaranda complex along profile B-B' (WNW-ESE)

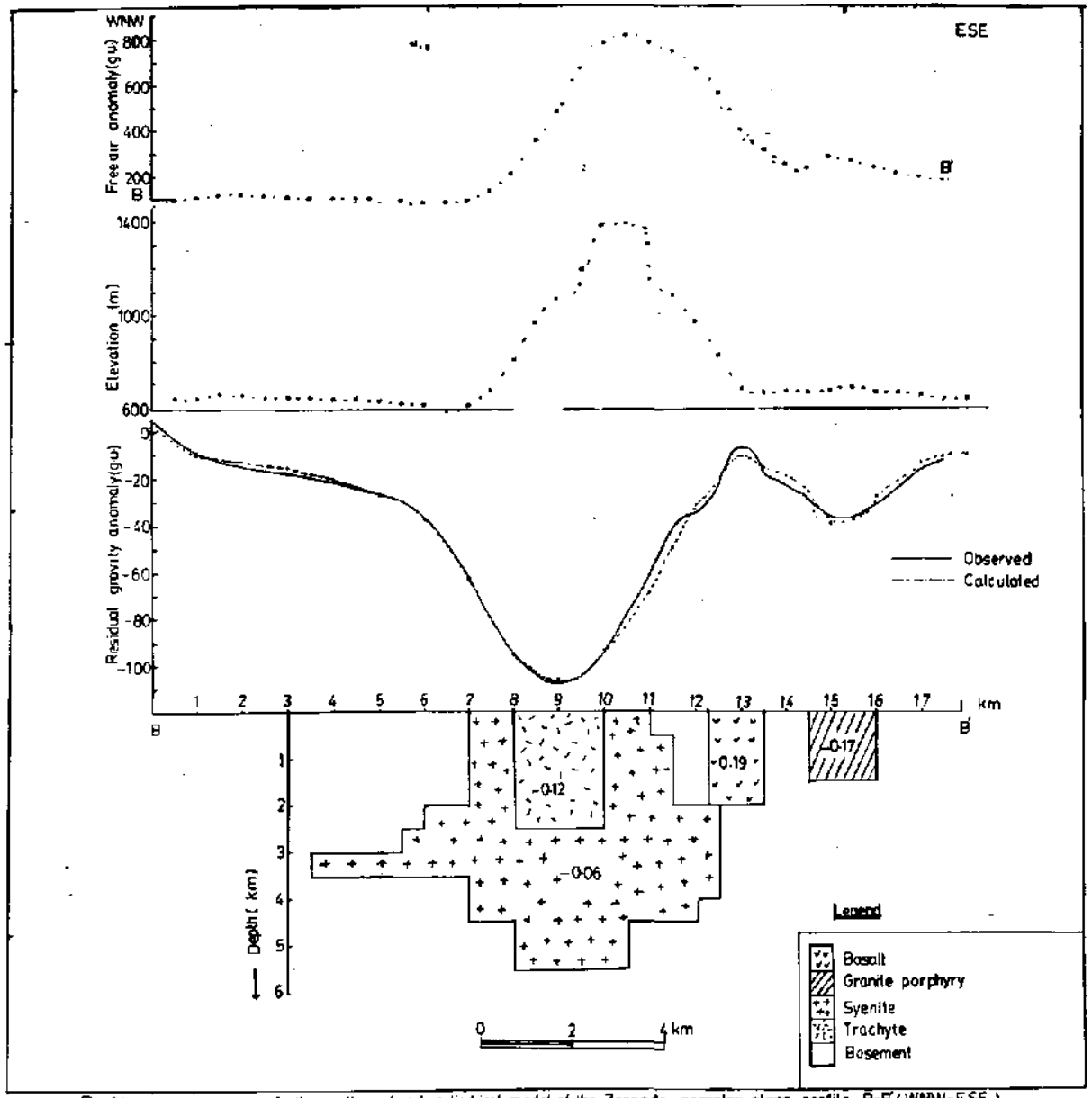


Fig 24 A three-dimensional cylindrical model of the Zarandа complex along profile B-B' (WNW-ESE)

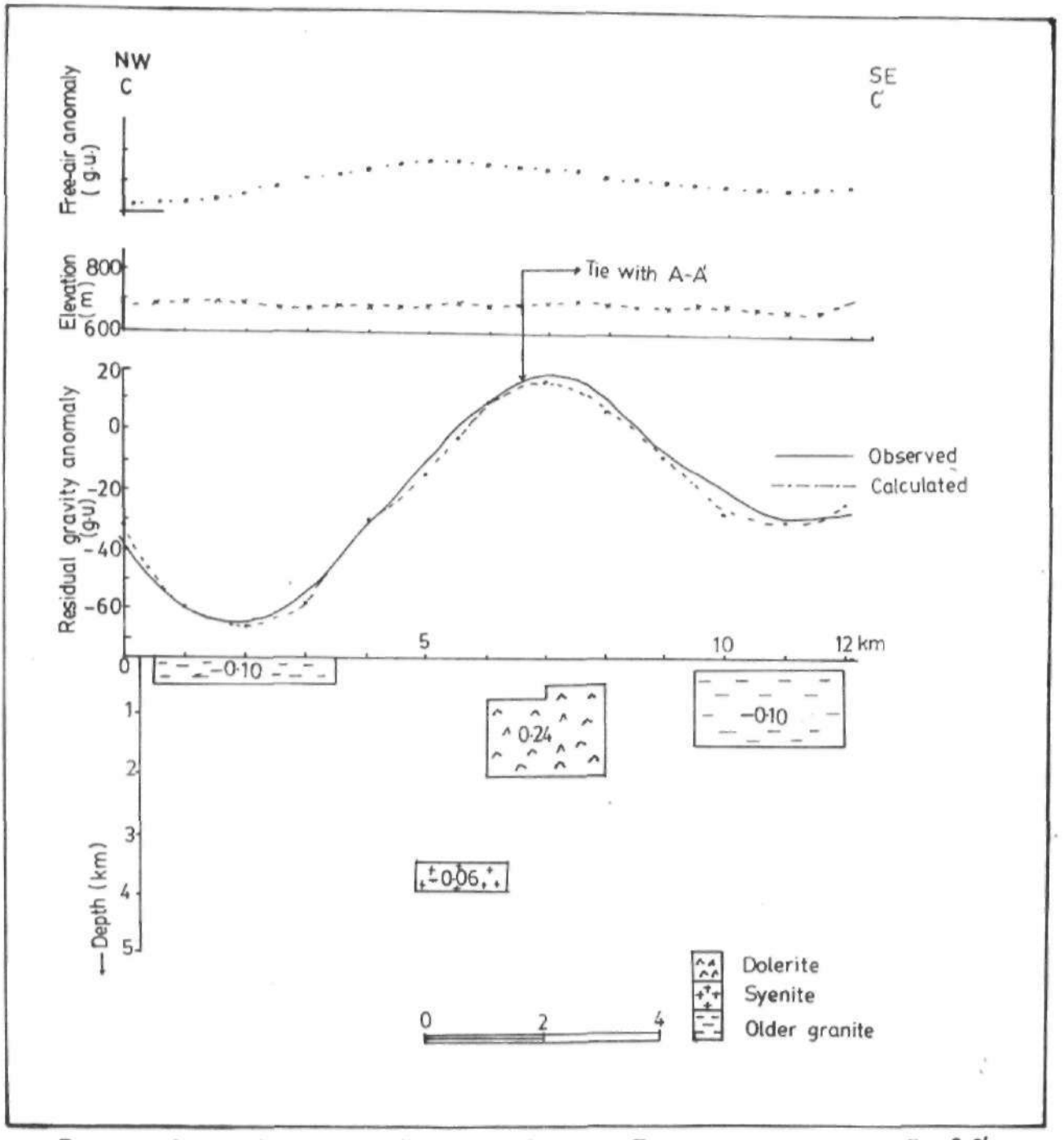


Fig 25 A three-dimensional cylindrical model of the Zaranda complex along profile C-C'

(Figs. 17 & 26 show this). Also the elevation seems to be directly related to free-air anomaly as revealed on the topographic map (Fig. 3).

Plots of elevation and free-air anomaly values along the interpreted profiles show this relationship (Figs. 22, 24 & 25).

In the survey area, the maximum observed free-air anomaly for a station was 790 g.u. and this value was obtained at a station whose elevation was 1317.33m above sea level. This value compares very well with a value of 800 g.u. near Jos at an elevation of 1,400m above sea level.

Generally, the free-air anomaly increases with elevation in a positive manner while the reverse is the case with the Bouguer anomaly (Figs. 22, 24 & 25).

5.6 MECHANISM OF INTRUSION

In well over 50 individual exposed and buried Younger Granite complexes of Nigeria, the main mode of emplacement has been that of fracturing, ring dyke formation, faulting, cauldron subsidence and subsequent upliftment of earlier rock units (Ajakaiye, 1974; 1981; Turner, 1976; Oyawoye, 1968).

Anderson, 1936, Billings, 1945 are of the opinion that in any region of ringed intrusions, inhomogeneity of the parent magma give rise to ringed intrusions and cones. They also suggested that there must be enough pressure under confinement so any process that initiates relaxation through fracturing or faulting is accompanied by a rise of low density material to the surface. Chapman (1935) also indicated that syenites and biotite granites always intrude the crystalline basement



Fig 26 Map of Free-air anomaly of the Zaranda complex

through cauldron subsidence. Bott (1953) also suggested that stopping of country rock and magmatic intrusion, forceful injection of magma that thrusts aside the country rock with or without their compression, leads to the formation of magmatic Younger Granites. Anderson (1936) attributes the late ring dykes that succeed magmatic acid intrusion to those that follow pre-existing structures in the host rock. He made comparison between such late ring dykes and the Kudaru complex of Nigeria and found that the complex and most other Nigerian Younger Granite complexes intruded through pre-existing weak zones in the crystalline basement.

Bott (1953) maintained that deep and acid intrusions could probably be associated with mafic rocks. The occurrence of rock bodies of seemingly mafic suite in the Zaranda complex probably indicates that the complex is a large and deep acid intrusion or that the complex is made up of moderately deep acid intrusions underlain by the mafic rock. Bott's (1973) guidelines for determining approximate mode of emplacement of acid intrusions are illustrated in Fig. 27.

A comparison of these anomalies with those of Profiles A-A^1, B-B^1 and C-C^1 shows that the Zaranda complex was probably not emplaced through cauldron subsidence, rather through forceful injection through seemingly weak zones still shown by the structural trend.

Based purely on field evidence, the trachyte body probably is the oldest rock unit in the Zaranda complex. Turner (1976) maintained that in most ringed intrusions in the province, the basic rocks herald the emplacement of the bodies and also that these basic rocks mark the end of the intrusion. In the Zaranda complex, subsequent rock units

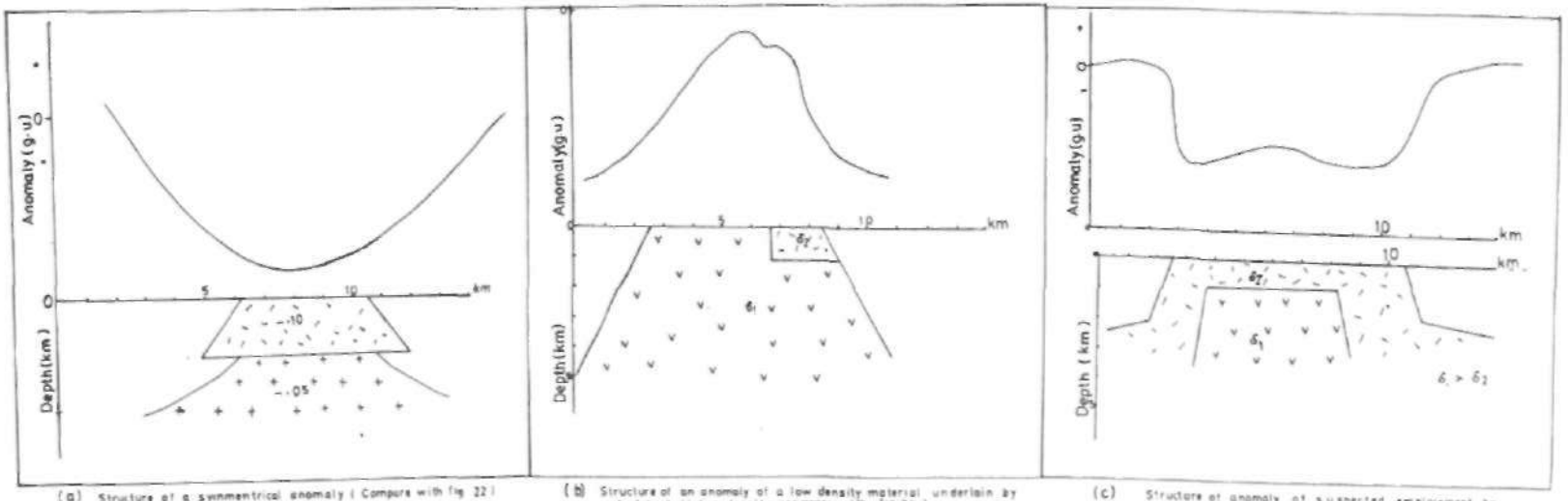


Fig 27

Gravity anomalies and subsurface shapes compared with those of the Zarunda complex

(Adapted from Bott, 1973)

emplaced after the trachyte did so in a ringed manner and successively emplaced in rings of increasing radius from the centre. (Fig. 3). Based on Bott (1973) model, it is suggested that the pre-caldera trachyte is surrounded and underlain by the syenite.

In most ringed intrusions, the individual units are emplaced successively towards the centre from the early basic dykes, but in the Zaranda complex, the location and attitude of the early and late basic rocks represented by trachyte and basalts respectively, suggest a probable progressive outward emplacement. Falconer and Raeburn(1923) grouped the emplacement of the Younger Granite complexes into rock phases which are all present in the survey area (Table 12). Thus the trachyte represents the early basic rocks; the syenite and porphyry are the units of the intermediate phase while the dolerite and basalt represent the late basic phase.

CHAPTER SIX

SUMMARY AND DISCUSSION

6.1 Summary

Qualitative and quantitative analysis of Bouguer and residual gravity fields over the Zaranda complex reveal the following:

(a) There is a maximum Bouguer gravity value of about -613 g.u. and a minimum of -433 g.u. characterizing the area with the value of -605 g.u. centred on the complex itself. A residual gravity field of the order of -106 g.u. was observed to be centred also on the complex and relatively positive residual fields of amplitude in the range of -10 g.u. to 52 g.u. were seen to flank the central value of -106 g.u.

(b) The trends of these anomalies are conspiciously NNE - SSW. This trend was also evident from the structural data analysis of the survey area (Figs. 9, 10 & 11).

(c) Comparison made between residual and Bouguer gravity fields reveals that the central negative gravity anomaly of amplitude -106 g.u. is centred on a central trachyte body mapped during the survey. Also surrounding the trachyte of density 2.56×10^3 kgm^{-3} is a relatively denser rock unit - syenite - with a mean density of 2.62×10^3 kgm^{-3}. The central anomaly made up of trachyte and syenite is flanked by basic rocks made up of basalts and dolerite

which were assumed to be the cause of the positive residual anomalies.

(d) Both two and three-dimensional models along and perpendicular to the major trend show that the Zaranda complex is a tabular body made up of syenite and extending to a depth of about 5.5km. However, the main rock unit comprising the syenite carries another tabular body essentially trachytic which has a thickness of about 2.5km. Both units outcrop. The model along the profile perpendicular to the trend of the anomaly has an outcrop width comparable to the depth of 5.5km, the outcrop width being 6km. The models also show that the units have steep outward dipping contacts up to a depth of about 3.5km. This model was deemed reasonable because the structural data shows that dips in the range of 75° to 90° were typical of all the foliations and joints.

(e) Analysis of structural data from both the host migmatitic rock and the complex show similar trends in the NNE - SSW which were observed to correlate with the trends of both the residual and Bouguer fields and that of the magnetic anomaly on the total magnetic intensity map (Fig. 2).

It should be noted that the causes of the gravity anomalies as being the different rock types in the survey area have been substantiated with a chemical analysis of the various rock units which correlate with the observed anomalies (Appendix 1).

6.2 Discussion

The shape of the gravity anomaly over the Zaranda complex which essentially displays a prominent closure, the trend of the anomalies, the result of the structural and chemical analyses suggest the following probable deductions on the Zaranda complex:

(i) The complex probably must have intruded the host migmatic gneiss through pre-existing structures judging from the trend of the gravity anomalies, which correlate with those of the major structures in the host rock.

(ii) The Zaranda complex is a ring-like intrusion judging from the geological setting of the individual rock units which were observed to have probable distinct time lapse between their emplacements. This deduction is in view of the structure of the outer basic rock units which form nearly a ring structure around the main complex and located at a distance of about 3km from the prominent hill representing the Zaranda complex.

(iii) Mineralogy and chemistry of the rock units that were observed as being the cause of the gravity anomalies suggest that the Zaranda complex is probably underlain by rocks of ultramafic origin as shown by the field occurrence of mafic and hornblende-rich rocks as large but unmappable units in the complex.

6.3 Recommendations

Most geophysical investigations are aimed at identifying the optimum structures or conditions that favour concentration of valuable

economic minerals rather than the direct exploration for these minerals. Other non-economic minerals but essential like water may be located in such structures. Since the presence of these structures and materials cause appreciable contrast in density and resistivity, it is recommended that the area under survey in general be investigated in detail for economic minerals such as asbestos using the gravity method as primary geophysical method and followed up with detailed resistivity survey. Water-bearing formations, where they occur, usually are characterized by low gravity anomalies. The area lying between Zull village and the complex which has been intruded by the dolerite dyke could further be investigated for apossible potential water-bearing zone.

The occurrence of small pits of kaolinite in Hadambalamba located on the northern part of the complex (Fig. 3) needs more detail gravity survey to estimate the extent and economic viability of such deposits.

Although the Zaranda complex is located just outside the barren zone of the regional metal zoning in the Younger Granite province (Olade, 1978; Fig. 28), much of the zoning has been based purely on surface geological mapping and chemical analysis. Since most geophysical techniques, which include gravity surveys, give the most likely structure of exposed bodies, at depth, it is therefore suggested that zoning based on geophysical surveys be given priority when evaluating economic mineral potentials of outcropping bodies like the Zaranda complex. Thus the Zaranda complex as a barren zone can be re-assessed through detail gravity, magnetic, seismic or resistivity surveys. Most gravity work of Ajakaiye(1968,1974) have confirmed the use of gravity methods in the search for economic minerals in the Younger

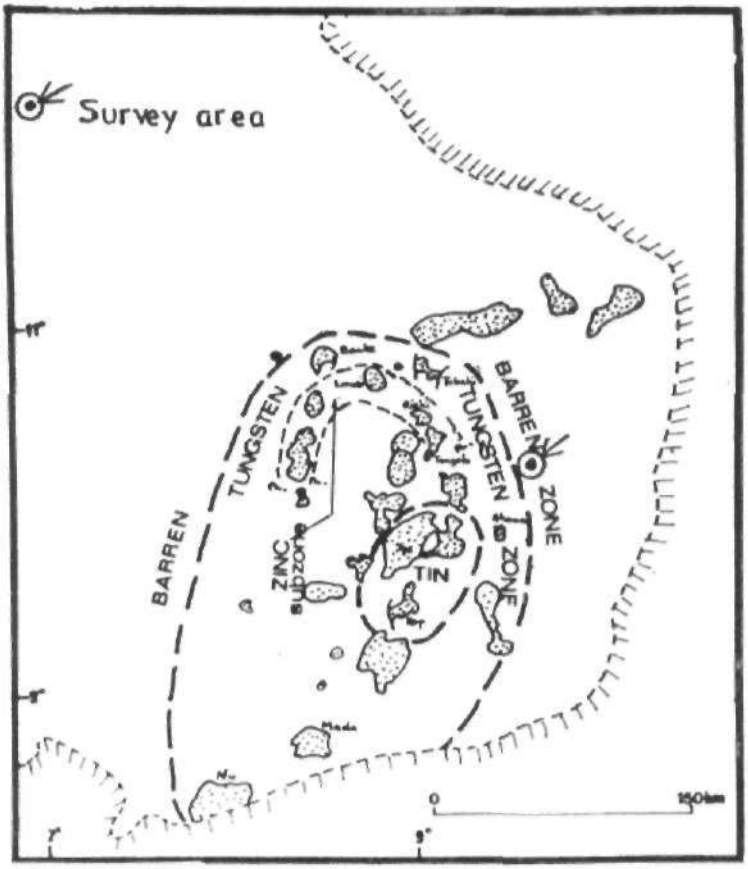


Fig 28 · Regional metal zoning in the Younger Granite province

(After Olade. 1978)

Granite province in particular, and in other geological provinces in Nigeria in general.



Plate 1

Photomicrograph of the migmatitic gneiss (X-nicols)
x 64

Blades of biotite, feldspar, quartz and garnet coexist.

Note also strained quartz (q).



(a)
X nicols

(b)
Plane light

Plate 2

Photomicrograph of the older granite
x 64

Weathered feldspar, biotite and quartz are visible.



a
X nicols



b
Plane light

Plate 3

Photomicrograph of the trachyte
x 160
Large prism of sanidine in glassy to ophitic groundmass

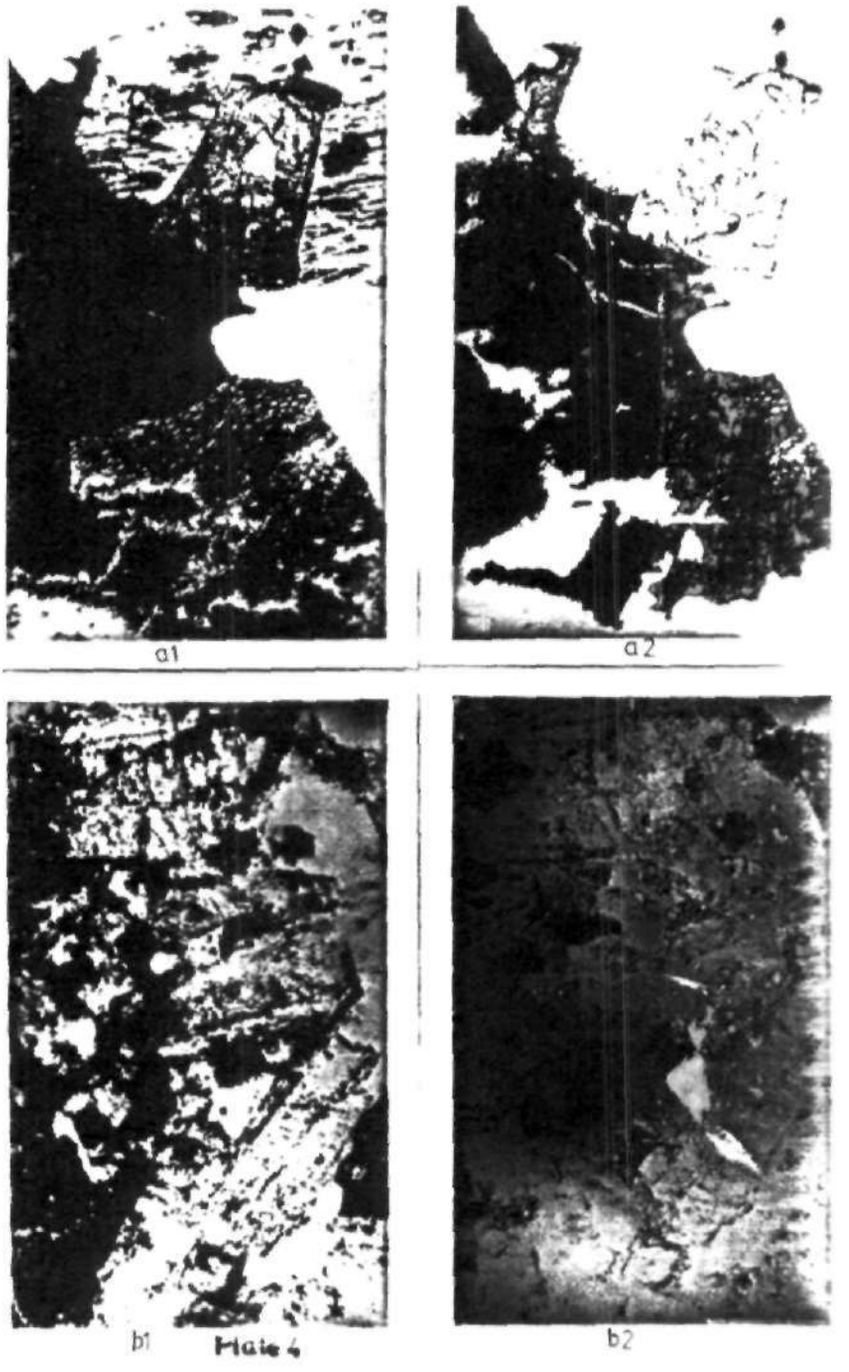


Plate 4

Photomicrograph of the syenite

×42

a melanocratic variety (a1 X nicols, a2 plane light)

b leucocratic variety (b1 X nicols b2 plane light)

Note the blades of hornblende in both varieties and the depleted amount of hornblende in (b); riebeckite in (b) and euhedral olivine grains in (a).



X nicols



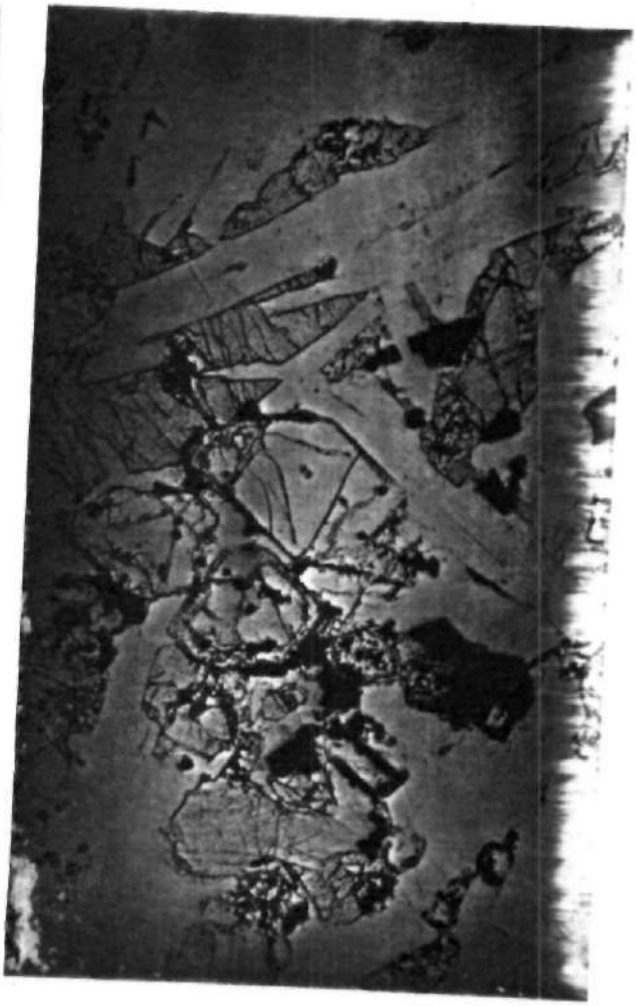
Plane light

Plate 5

Photomicrograph of the syenite-basalt contact, southern base of the complex. Note dark ophitic basalt (b) and the granitic texture of the leucocratic syenite (s)

X 28





(a)
X nicols

Plate 6

(b)
Plane light

Photomicrograph of the olivine basalt.

Ophitic texture similar to that of plate 7. less iron but more plagioclase.

x 100



X nicols

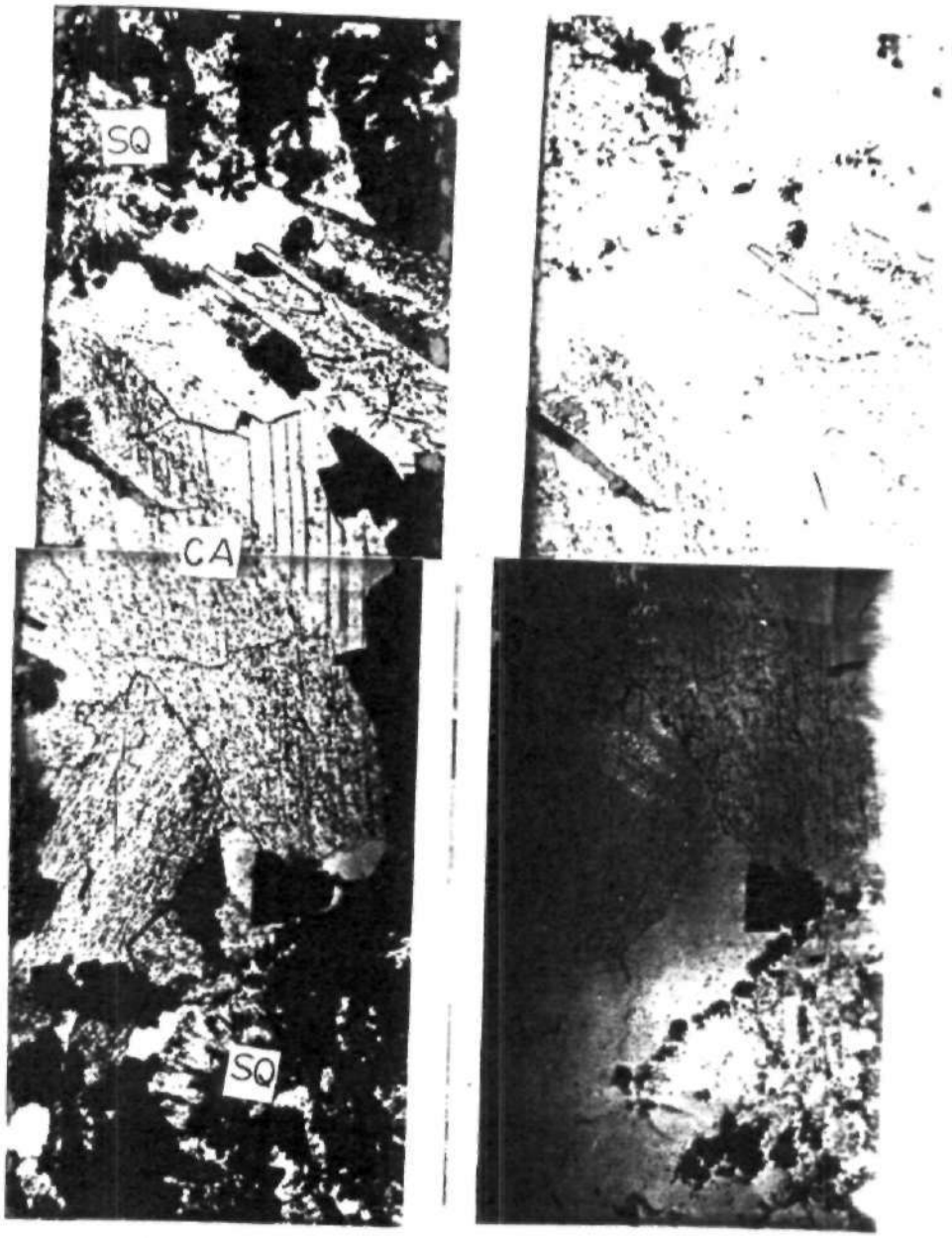


Plane light

Plate 7

Photomicrograph of the Zull dolerite.
x 100

A typical ophitic texture. Augite and iron oxide + olivine form the groundmass around laboradorite/andesine laths.



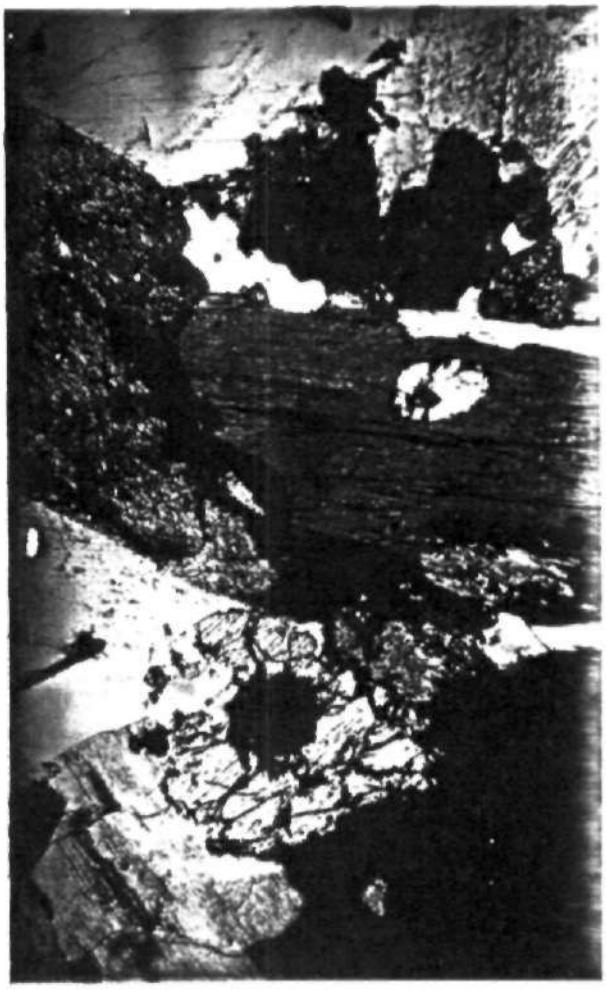
(a)
X nicols

(b)
Plane light

Plate 8

Photomicrograph of the calcite-bearing basalt.
x 75

Large calcite grain (CA) surrounded by strained quartz (SQ) set in an ophitic groundmass of iron ore augite olivine and plagioclase.



X nicols



Plane light

Plate 9

Photomicrograph of the amphibolitic rock included in the syenite unit

x 64.

Mainly hornblende but sphene (top right corner of plate) and occasional plagioclase.

APPENDIX I

Results of megascopic study of rock units

Rock Unit	Texture, Structure & Color	Minerals Observed	Field Name
A Migmatite	Dark with leuco and melanocratic bands. Medium to coarse-grained. Highly jointed and micro-faults exist.	Quartz, biotite, feldspar, amphibole. Feldspar is in form of augens in some samples.	Migmatite
B Muscovite-biotite Older granite	Light-coloured, weathered, medium-grained with prominent blades of light-coloured muscovite.	Quartz, muscovite, biotite, feldspar, garnet.	Granite
C Aphyric trachyte	Grey, fine-grained with prisms of light-coloured minerals suspected to be feldspar. Jointed.	Ferromagnesian minerals, feldspar.	Trachyte
D Syenite	Light to grey in colour; medium to coarse-grained.	Quartz, feldspar, amphibole, biotite.	Granite
E Porphyritic granite	Very coarse-grained with mostly inter-growth of minerals.	Quartz, potasium, feldspar	Granite porphyry
F Olivine-basalt	Dark, fine-grained	Feldspar, olivine and ferromagnesian minerals	Basalt

APPENDIX I

(cont'd)

Rock Unit	Texture, Structure and Colour	Minerals Observed	Field Name
G Dolerite	Dark with visible light prisms of feldspar. Medium to fine-grained.	Feldspar, ferro-magnesian Olivine	Dolerite
H Calcite-bearing basalt	Dark with prominent patches of light-coloured crystals; fine-grained with some brown tints in circular form.	Feldspar, large calcite crystals, Olivine ferro-magnesian minerals.	Andesite
I	Dark-green with visible flakes of green minerals. Medium-grained and weathers to reddish brown.	Mainly amphibole and other green minerals.	Hornblendite (?)

APPENDIX II

Result of modal anaysis of rock units

Minerals	Rock Units and Modal Amounts (%)								
	A	B	C	D	E	F	G	H	I
Quartz	20	20	5	10	10	--	--	--	--
Feldspar	40	55	65	55	80	--	----	--	5
Plagioclase	5 An35-An50	-- --	5 --	-- --	-- --	60 An_{45} - An_{60}	66 An_{35} - An_{70}	55 An_{30} - An_{50}	--
Muscovite	5	12	--	--	--	--	--	--	--
Biotite	15	5	--	5	10	--	--	--	--
Olivine	--	--	2	2	--	5	5	--	--
Garnet	2	5	--	--	--	--	--	--	--
Iron Oxide	3	--	5	5	--	10	10	10	2
Augite	--	--	5	--	--	10	20	10	--
Sphene	2	--	--	--	--	--	--	--	2
Riebeckite	--	--	--	2	--	--	--	--	--
Hornblende	5	--	--	20	--	--	--	--	90
Calcite	--	--	--	--	--	--	--	15	--
Opaque minerals	1	4	5	1	--	10	3	5	--

A = Migmatic gneiss

B = Older muscovite-biotite granite

C = Melanocratic syenite

D = Leucocratic syenite

E = Granite porphyry

F = Olivine basalt

G = Dolerite

H = Calcite basalt

I = Amphibolite

APPENDIX III

PRINCIPAL PARAMETERS OF GRAVITY STATIONS

Station Number	Elevation ASL (M)	Latitude Deg. & Min. (N)	Longitude Deg. & Min. (E)	Observed Gravity (gu)	Freeair Anomaly (gu)	Bouguer Anomaly (gu)
9002	720.16	10° 13.18'	9° 24.19'	9779935.2	214	-590
9003	748.50	10° 13.18'	9° 27.47'	9779880.2	246	-589
10001	741.47	10° 13.49'	9° 27.59'	9779895.7	238	-589
10002	724.98	10° 14.03'	9° 27.81'	9779925.2	214	-595
10003	708.82	10° 14.54'	9° 28.00'	9779949.6	186	-605
10004	717.95	10° 15.06'	9° 28.17'	9779936.6	198	-602
10005	723.40	10° 15.55'	9° 28.27'	9779924.2	200	-607
10006	724.28	10° 16.11'	9° 28.41'	9779919.0	195	-613
10007	706.28	10° 16.58'	9° 28.53'	9779970.1	188	-600
10008	708.70	10° 17.14'	9° 28.58'	9779976.0	198	-592
9004	711.86	10° 17.68'	9° 28.62'	9779973.1	202	-592
9005	708.89	10° 18.23'	9° 28.70'	9779994.9	212	-579
10009	702.71	10° 18.81'	9° 28.86'	9780009.9	205	-579
10010	691.66	10° 19.05'	9° 29.30'	9780057.0	217	-555
10011	675.74	10° 19.21'	9° 29.83'	9780093.0	203	-551
10012	684.01	10° 19.48'	9° 30.30'	9780094.5	228	-535
10013	695.04	10° 19.93'	9° 30.67'	9780051.9	217	-558
10014	713.13	10° 20.49	9° 30.58'	9780043.0	261	-534
9006	696.15	10° 21.00'	9° 30.51'	9780068.1	233	-544
10015	710.27	10° 17.67'	9° 29.22'	9779989.4	214	-578
10016	705.47	10° 17.72'	9° 29.81'	9779995.4	205	-582
10017	713.47	10° 17.94'	9° 30.22'	9779988.3	221	-575
10018	702.26	10° 18.42'	9° 30.64'	9780014.9	211	-573
10019	689.46	10° 18.39'	9° 31.22'	9780039.3	196	-574
9007	673.30	10° 18.50'	9° 32.11'	9780055.4	161	-590
9008	677.62	10° 16.69'	9° 30.68'	9780044.6	171	-585
10020	727.38	10° 15.53'	9° 28.50'	9779931.8	220	-591
10021	713.94	10° 15.56'	9° 29.05'	9779935.6	183	-614
10022	714.59	10° 15.56'	9° 29.64'	9779978.2	227	-570
10023	686.57	10° 15.56'	9° 30.19'	978008.4	171	-595
9009	684.74	10° 15.56'	9° 30.78'	9780031.9	189	-575
10024	745.30	10° 13.07'	9° 28.04	9779904.4	261	-570
10025	739.78	10° 13.20'	9° 28.61'	9779920.0	259	-566
10026	745.54	10° 13.35'	9° 29.15'	9779895.3	254	-579
10027	731.35	10° 13.51'	9° 29.58'	9779927.2	239	-577
10028	720.80	10° 13.50'	9° 30.15'	9779936.2	215	-599
9010	718.09	10° 13.57'	9° 30.63'	9779944.8	215	-586
10029	708.49	10° 14.03'	9° 30.93	9779967.5	206	-585
10030	693.56	10° 14.32'	9° 31.43'	9780004.8	195	-579
10031	691.28	10° 14.53'	9° 31.94	9780027.4	210	-562
10032	676.65	10° 14.64'	9° 32.44'	9780060.5	197	-558
9011	681.98	10° 14.94'	9° 32.84'	9780051.8	203	-558
10033	654.23	10° 15.49'	9° 33.00'	9780106.9	170	-560
10034	666.10	10° 16.48'	9° 33.00	9780081.3	175	-570
10035	654.82	10° 16.95	9° 33.32'	9780118.8	176	-545
10036	682.54	10° 17.50'	9° 33.61'	9780047.9	188	-558

APPENDIX III (Cont'd)

Station Number	Elevation ASL (M)	Latitude Deg. & Min. (N)	Longitude Deg. & Min. (E)	Observed Gravity (gu)	Freeair Anomaly (gu)	Bouguer Anomaly (gu)
9012	628.64	10° 17.44'	9° 33.94'	9780115.5	93	-565
10037	715.35	10° 13.50'	9° 31.33'	9779989.4	252	-546
10038	700.95	10° 13.35'	9° 31.87'	9780021.6	240	-542
10039	705.92	10° 13.27'	9° 32.40'	9780029.9	264	-524
10040	701.50	10° 13.33'	9° 32.98'	9780058.0	278	-504
10041	696.00	10° 13.54'	9° 33.49'	9780076.7	279	-478
10042	702.26	10° 13.54'	9° 34.06'	9780076.1	298	-486
9013	679.08	10° 13.46'	9° 34.65'	9780071.6	222	-536
10043	677.54	10° 12.97'	9° 34.75'	9780075.0	223	-533
10044	667.76	10° 12.38'	9° 34.77'	9780097.7	219	-526
10045	659.67	10° 11.87'	9° 34.72'	9780111.1	210	-526
10046	646.50	10° 11.34'	9° 34.53'	9780133.9	195	-526
9014	636.64	10° 11.05	9° 34.31'	9780148.5	180	-530
9015	685.44	10° 13.38'	9° 34.99'	9780059.2	227	-537
10047	687.97	10° 13.46'	9° 35.61'	9780053.5	231	-536
10048	686.88	10° 13.66'	9° 36.17	9780074.6	247	-518
9016	668.04	10° 13.92'	9° 36.69'	9780060.1	174	-571
10049	682.58	10° 13.84'	9° 35.22'	9780080.0	239	-522
10050	678.28	10° 14.14'	9° 35.72'	9780090.4	235	-522
10051	689.62	10° 14.51'	9° 36.13'	9780098.7	276	-493
10052	678.70	10° 15.00'	9° 36.40'	9780118.3	259	-470
9017	700.88	10° 15.43'	9° 36.64'	9780010.4	218	-564
10053	680.91	10° 13.32'	9° 35.19'	9780067.0	224	-536
10054	662.24	10° 13.05'	9° 35.68'	9780100.6	201	-538
10055	676.04	10° 12.73'	9° 36.03'	9780097.5	242	-512
10056	661.50	10° 13.38'	9° 37.00'	9780073.7	170	-568
9018	646.39	10° 13.05'	9° 37.42'	9780104.5	156	-565
10057	660.08	10° 14.01'	9° 37.17'	9780080.7	169	-567
10058	663.06	10° 14.32'	9° 37.67'	9780079.6	176	-564
9019	670.18	10° 14.48'	9° 38.19'	9780116.1	234	-514
10059	671.78	10° 15.06'	9° 38.46'	9780116.5	236	-514
10060	758.98	10° 15.33'	9° 38.67'	9780134.5	212	-523
10061	670.18	10° 16.00'	9° 38.73'	9780115.7	225	-522
10062	668.58	10° 16.56'	9° 38.74'	9780157.0	259	-487
10063	658.98	10° 17.17'	9° 38.82'	9780144.2	213	-522
10064	655.78	10° 17.76'	9° 38.92'	9780155.8	212	-560
9020	642.89	10° 18.03	9° 39.21	9780177.2	195	-520
10065	636.49	10° 18.40'	9° 38.73'	9780195.9	189	-521
10066	631.49	10° 18.76'	9° 38.26'	9780191.7	167	-537
10067	639.69	10° 19.27'	9° 38.08'	9780187.0	185	-529
10068	658.89	10° 19.81'	9° 37.97'	9780165.9	220	-515
10069	655.69	10° 20.37'	9° 37.97'	9780172.5	214	-517
10070	649.59	10° 20.82'	9° 38.56'	9780198.4	219	-506
9021	633.61	10° 21.27'	9° 38.53'	9780208.2	177	-530
10071	640.01	10° 21.82'	9° 38.61'	9780230.0	216	-498
10072	630.23	10° 22.27'	9° 38.86'	9780261.6	215	-488

Station Number	Elevation ASL (M)	Latitude Deg. & Min. (N)	Longitude Deg. & Min. (E)	Observed Gravity (gu)	Freeair Anomaly (gu)	Bouguer Anomaly (gu)
10073	619.21	10° 22.87'	9° 38.92'	9780299.6	215	-475
10074	611.21	10° 23.39'	9° 38.88'	9780316.5	205	-477
9022	608.46	10° 24.00'	9° 38.94'	9780341.3	218	-461
10075	641.29	10° 18.03'	9° 38.64'	9780128.5	138	-560
10076	686.09	10° 18.33'	9° 38.17'	9780111.1	257	-499
9023	722.02	10° 18.22'	9° 37.64'	9780017.8	275	-517
10077	642.89	10° 16.84'	9° 38.39'	9780128.6	149	-565
10078	745.30	10° 16.61'	9° 38.35'	9779935.3	273	-552
9024	657.29	10° 17.00'	9° 38.00'	9780127.9	192	-535
10079	638.09	10° 18.28'	9° 40.31	9780190.8	189	-523
9025	635.85	10° 18.36'	9° 40.56'	9780223.4	193	-505
9026	673.38	10° 16.31	9° 38.74'	9780119.8	238	-513
10080	658.34	10° 16.28'	9° 38.50'	9780112.9	184	-550
10081	664.50	10° 16.20'	9° 38.30'	9780042.3	133	-577
10082	675.90	10° 16.20'	9° 37.72'	9780026.5	136	-608
10083	678.18	10° 15.75'	9° 37.72'	9780099.9	235	-512
9027	707.14	10° 15.50'	9° 37.70'	9780020.6	247	-534
10084	759.55	10° 16.31'	9° 37.42'	9779950.3	334	-485
10085	920.49	10° 16.42'	9° 37.15'	9779624.9	505	-506
9028	671.25	10° 15.92'	9° 37.80'	9780117.0	230	-490
9029	1076.23	10° 16.60'	9° 37.00'	9779303.5	663	-526
10086	657.92	10° 15.05'	9° 36.19'	9780103.0	180	-538
10087	644.60	10° 15.19'	9° 36.17'	9780125.2	160	-543
10088	640.35	10° 15.39'	9° 35.64'	9780132.1	153	-545
10089	627.52	10° 15.67'	9° 35.70'	9780145.9	125	-559
10090	624.48	10° 15.97'	9° 34.72'	9780142.2	111	-566
10091	613.51	10° 15.27'	9° 34.47'	9780160.2	93	-563
9030	620.71	10° 16.81'	9° 34.19'	9780141.1	94	-571
10092	621.33	10° 17.14'	9° 34.00'	9780136.8	89	-568
10093	633.22	10° 17.92'	9° 33.86'	9780125.9	111	-559
10094	609.52	10° 18.00'	9° 34.42'	9780173.5	85	-559
10095	595.12	10° 18.25'	9° 34.78'	9780212.7	77	-559
10096	613.68	10° 19.19'	9° 35.69'	9780187.4	106	-563
10097	614.64	10° 19.33	9° 36.25'	9780197.9	118	-563
9031	637.99	10° 19.53'	9° 37.19'	9780180.1	172	-538
10098	627.32	10° 19.36'	9° 36.56'	9780192.6	152	-545
10099	623.77	10° 19.26'	9° 36.00'	9780192.6	142	-552
10100	650.80	10° 19.36'	9° 37.67'	9780163.4	195	-528
9032	687.91	10° 18.68'	9° 36.00'	9780014.7	165	-586
10101	631.90	10° 19.84'	9° 36.70'	9780197.3	168	-537
10102	626.73	10° 19.92	9° 36.16'	9780230.6	185	-514
10103	617.68	10° 20.19'	9° 35.70'	9780263.0	186	-503
10104	593.83	10° 20.46'	9° 35.22'	9780291.0	142	-522
9033	609.35	10° 20.73'	9° 34.73'	9780260.3	157	-523
10105	738.69	10° 18.63'	9° 36.63'	9779920.8	228	-560
9034	1017.71	10° 18.28'	9° 36.31'	9779326.5	496	-600
10106	1153.85	10° 17.81'	9° 36.19'	9779045.8	638	-603

Station Number	Elevation ASL (M)	Latitude Deg. & Min. (N)	Longitude Deg. & Min. (E)	Observed Gravity (gu)	Freeair Anomaly (gu)	Bouguer Anomaly (gu)
9035	1227.40	10° 17.55'	9° 36.08'	9778898.5	719	-600
10107	1227.40	10° 17.33'	9° 36.26'	9778898.9	721	-576
9036	1031.24	10° 17.14'	9° 37.03'	9779384.7	602	-518
10108	782.45	10° 17.19'	9° 37.58'	9779876.7	326	-518
10109	662.62	10° 17.33'	9° 38.13'	9780171.2	250	-472
10110	666.77	10° 14.17'	9° 38.39'	9780130.1	239	-505
10111	672.43	10° 13.75'	9° 38.79'	9780113.5	242	-508
9037	682.94	10° 13.30'	9° 39.14'	9780090.6	254	-508
10112	627.44	10° 17.36'	9° 34.36'	9780133.7	104	-569
9038	598.23	10° 17.36'	9° 34.54'	9780178.8	59	-575
10113	813.34	10° 17.33'	9° 35.12'	9779716.8	267	-607
9039	1007.42	10° 17.30'	9° 35.65'	9779331.5	475	-602
9040	1283.67	10° 17.05'	9° 35.78'	9778764.6	762	-600
10114	1317.33	10° 16.61'	9° 35.83'	9778691.2	795	-597
10115	1173.63	10° 16.22'	9° 35.93'	9779088.2	750	-552
10116	903.98	10° 15.75'	9° 36.05'	9779695.9	528	-450
9041	678.69	10° 15.25'	9° 36.14'	9780104.5	244	-485
10117	704.18	10° 14.61'	9° 36.67'	9780082.8	304	-475
10118	694.61	10° 14.33'	9° 36.17'	9780101.6	295	-480
10119	657.38	10° 14.32'	9° 38.72'	9780145.4	224	-509
10120	657.58	10° 14.58'	9° 39.24'	9780149.5	219	-507
10121	654.18	10° 14.87'	9° 39.72	9780159.3	225	-505
10122	654.18	10° 15.34'	9° 40.17'	9780169.5	233	-497
10123	657.38	10° 15.47'	9° 40.63'	9780168.1	241	-493
10124	663.78	10° 15.81'	9° 41.06'	9780168.8	250	-481
10125	660.58	10° 16.00'	9° 41.56'	9780191.4	271	-467
10126	654.45	10° 16.33'	9° 41.91'	9780224.9	284	-446
9042	655.11	10° 16.70'	9° 42.28'	9780233.0	292	-439
10127	685.80	10° 15.45'	9° 38.00'	9780125.6	286	-479
9043	670.56	10° 15.91'	9° 37.70'	9780101.8	213	-535
10128	651.91	10° 16.67'	9° 41.81'	9780228.6	278	-449
10129	651.91	10° 16.89'	9° 41.42'	9780225.9	274	-453
10130	644.87	10° 17.17'	9° 41.05'	9780237.4	272	-448
10131	634.95	10° 17.61	9° 41.19'	9780263.4	256	-453
9044	641.11	10° 18.00'	9° 40.83'	9780243.7	253	-462
10132	658.16	10° 16.55'	9° 42.89'	9780232.0	302	-433
10133	652.41	10° 16.22'	9° 42.55'	9780194.9	248	-479
10134	644.49	10° 15.57'	9° 42.58'	9780215.9	248	-471
10135	627.88	10° 15.19'	9° 42.78'	9780242.0	210	-490
10136	623.00	10° 14.76'	9° 43.04'	9780262.8	233	-462
10137	612.03	10° 14.32'	9° 43.31'	9780255.1	194	-489
10138	599.23	10° 13.85'	9° 43.52'	9780270.1	172	-497
10139	593.57	10° 13.52'	9° 44.00'	9780292.3	179	-484
9045	585.05	10° 13.44'	9° 44.14'	9780287.6	148	-505
10140	583.97	10° 12.94'	9° 43.61'	9780287.5	147	-506
10141	581.57	10° 12.46'	9° 43.47'	9780284.3	139	-510
10142	582.87	10° 12.04'	9° 43.19'	9780283.0	144	-506

Station Number	Elevation ASL (M)	Latitude Deg. & Min. (N)	Longitude Deg. & Min. (E)	Observed Gravity (gu)	Freeair Anomaly (gu)	Bouguer Anomaly (gu)
10143	577.12	10° 11.55'	9° 42.96'	9780292.6	138	-505
10144	579.65	10° 11.22'	9° 42.55'	9780289.0	144	-502
10145	580.30	10° 10.63'	9° 42.19	9780288.0	148	-499
10146	588.00	10° 10.33'	9° 41.84'	9780280.0	166	-490
10147	590.48	10° 9.82'	9° 41.55'	9780288.0	183	-476
10148	591.14	10° 9.49'	9° 41.19'	9780292.2	192	-528
9046	578.68	10° 9.22'	9° 41.00'	9780297.4	160	-486

REFERENCES

Ajakaiye, D.E.; 1968. A gravity investigation of the Liruei Younger Granite ring complex of northern Nigeria. Geol. Mag; 105, 256-263.

_____ 1970. Gravity measurements over the Nigerian Younger Granite province. Nature, 225, 50-52.

_____ 1974. A gravity profile across the Banke ring complex, Nigeria. Geoexploration, 12, 59-60.

_____ 1975. Densities of rocks in the Nigerian Younger Granite province. Jour. Min. Geol., 11, 34-43.

_____ 1976. Negative gravity anomalies in the Younger Granites of northern Nigeria. Geology of Nigeria, C.A. Kogbe (Ed.), 207-224.

_____ 1981. Aeromagnetic anomalies across the Nigerian Younger Granite province. Unpublished paper, first ISCMA, Kenya.

Ajakaiye, D.E. & Burke, K., 1973. A Bouguer gravity map of Nigeria. Tectonophysics, 16, 103-115.

Ajakaiye, D.E. & Sweeney, J.F., 1974. Three dimensional gravity interpretation of the Dutsen-Wai complex, Nigerian Younger Granite province. Tectonophysics, 24, 331-344.

Allan, A.L., Hollwey, J.R. & Maynes, J.B.H., 1971. Practical Surveying and Computations. William Heinemann Publ. Coy., 204-218.

Anderson, E.M., 1936. The dynamics of the formation of cone sheets, ring-dykes and cauldron subsidences. Proc. Roy. Soc. Edin., 56, 128-157.

Bancroft, A.M., 1960. Gravity anomalies over buried step. Jour. Geoph. Res., 65, 1630-1631.

Barth, T.F.W. & Smithson, S.B., 1967. The Precambrian Holum granite, South Norway. Repr. Norsk Geologisk Tiasskrft, 47(1), 21-35.

Billings, M.P., 1945. Mechanisms of igneous intrusives in New Hampshire. Am. Jour. Sc., (5th Ser.), 43, 40-68.

Blockley, J.G., 1980. Tin deposits in W. Australia. Bull. Geol. Svy. W. Australia (ed) (12), 1-205.

Bott, M.H.P., 1953. Negative gravity anomalies over acid intrusions and their relation to the structure of the Earth's crust. Geol. Mag. 110, 257-267.

_____ 1967. Gravity investigations of subsurface shape and mass distributions of granite batholiths. Bull. Geol. Soc. Am., 78, 859-878.

_____ 1973. Deep structures beneath the Tertiary volcanic regions of Skye, Mull and Ardnamurchan, N. W. Scotland. Repr. Natural Physical Sci., 242(121), 114-116.

Bowden, P. & Turner, D.C., 1974. Peralkaline and associated ring complexes in the Niger-Nigeria province, W. Africa. In "The Alkaline Rocks", Srensen, H. (ed). J. Wiley & Co., 330-351.

Bowden, P., Bennette, J.N., Kinnard, J.A., Witley, J.E., Abba, S.I. & Hadzigeorgiou-Stavrakis, P.K., 1981. Urainium in the Niger-Nigeria Younger Granite province. Min. Mag., 44, 379-389.

Buchanan, M.S., Macleod, W.N., Turner, D.C., Berridge, N.G., & Black, R., 1971. The geology of the Jos Plateau: vol. 2, Younger Granite complexes. Bull. Geol. Svy. Nigeria, 32, 1-190.

Chapman, R.W., 1935. Percy ring dyke complex. Am. Jour. Sc. (5th Ser.), 30(17), 401-431.

Cox, K., 1976. Composition of igneous rocks. Understanding the earth, I.G. Gas (ed.), M.I.T. Press, 13-39.

Cratchley, C.R. & Jones, G.P., 1965. An interpretation of the geology and gravity anomalies of the Benue valley, Nigeria. Overseas Geol. Svy., Lond. Geoph. Paper 1, 7-26.

Dobrin, M.D., 1976. Introduction to geophysical prospecting. McGraw-Hill Coy. New York. 390-475.

Falconer, M.A. & Raeburn, C., 1923. The Northern Nigerian Tinfields of Bauchi province. Bull. Geol. Svy. Nigeria, 4, 1-70.

Gustaf, L., 1967. Gravity measurements over the Bohus granite in Sweeden. Repr. Geologiska Foreningens: Stockholm Forhanolingar, 88, 542-548.

Hammer, S., 1939. Terrain corrections for gravimeter stations. Geophysics, 4, 184-194.

Lahee, F.H., 1931. "Field Geology", McGraw-Hill Coy. New York. 789.

Mason, R., 1978. Petrology of metamorphic rocks. George Allen and Unwin Thomas Coy. 25-150.

Moorhouse, W.W., 1959. The study of rocks in thin section. Harper and Row. New York, 20-596.

Nagy, D., 1964. The gravitational attraction of a two-dmensional polygonal body of arbitrary cross-section. Publ. Grav. Div., Ottawa.

Nettleton, L.L., 1971. Elementary gravity and magnetics for geologists and seismologists. S.E.G. monograph series, No. 1, 1-121.

Okezie, C.N., 1964. Discussion on ring structures in the Sara Fier Younger Granite complex, Northern Nigeria. Quat. Jour. Geol. Soc. Lond. 120, 125.

Olade, M.A., 1978. Geochemistry of the Banke complex, Northern Nigeria. Jour. Min. Geol., 15(2), 97-107.

_____ 1979. The Abakaliki pyroclastics of southern Benue trough, Nigeria. Their petrology and tectonic significance. Jour. Min. Geol., 16(1), 17-25.

Onyeagocha, C.A., 1979. Mallam Tanko serpentinite. Petrology and economic implications. Jour. Min. Geol. 16(1), 37-40.

Oyawoye, M.O. 1968. The geology of the Zaranda ring complex, Northern Nigeria. Jour. Min. Geol., 3, 33-47.

Pettijohn, F.J., 1975. Sedimentary Rocks. Harper and Row Publ. Coy. New York. 256.

Ragan, D.M., 1973. Structural geology. An introduction to geometrical techniques. John Wiley & Sons., New York, 91-112.

Rahaman, M.A., 1976. Review of basement geology of S.W. Nigeria. Geology of Nigeria, C.A. Kogbe (ed.), 41-48.

Sandberg, C.H., 1958. Terrain corrections for an inclined plane in gravity computations. Geophysics, 23, 701-711.

Sissons, B.A., 1981. Density determination from subsurface gravity measurements. Geophysics, 46, 1568-1571.

Soliman, M.M., 1982. Chemical and physical properties of beryl and cassiterite ores, Southern Desert, Egypt. Applied Science, 91, 17-26.

Telford, W.M., Geldart, L.P., Sheriff, R.E. & Keys, D.A., 1976. Applied Geophysics. Cambridge Un. Press.

Turner, D.C., 1976. Structure and petrology of the Younger Granite complexes. Geology of Nigeria. C.A. Kogbe (ed.), Elizabeth Publ. Coy. Lagos, 134-158.

Turner, F.J., 1968. Metamorphic Petrology. McGraw-Hill Company. New York, 265-281.

Van Overmeeren, R.A., 1981. A combination of electrical resistivity and seismic refraction exploration in Sudan. Geophysics, 46, 1304-1313.

Verheijen, P.J.T. & Ajakaiye, D.E., 1980. Analysis of errors in barometric elevations in Northern Nigeria. Geophysics,45, 1144-1152.

Wright, J.B., 1976. Volcanic rocks in Nigeria. Geology of Nigeria. C.A. Kogbe (ed.), Elizabeth Publ. Coy. Lagos, 93-142.